WEATHER IN A BOTTLE: TOWARDS A NORTH AUSTRALIAN HYDRO CLIMATE RECORD

Costijn Zwart

Submitted for the degree of

Doctor of Philosophy

In the College of Science, Technology and Engineering
within the

Division of Tropical Environments and Societies

James Cook University

Supervisors: Michael I. Bird, Niels C. Munksgaard, Jonathan Nott
and Naoyuki Kurita

October 2021

Statement on the contributions of others

A specific contributions statement is given at the beginning of each Chapter. The table below summarises the contributions of my supervisors, collaborators and financial assistance I received towards this thesis.

	Contribution	Name
Intellectual support	Editorial support	Michael Bird[1,2] Niels Munksgaard[1,2,3] Naoyuki Kurita[4] Jordahna Haig[1,2]
	Laboratory access and analysis	Michael Bird Niels Munksgaard Christopher Wurster[1,2] Jennifer Whan[5] Dirk Sachse[6]
	Data access and analysis	Alain Protat[7] Naoyuki Kurita
Financial support	Stipend	Australian Postgraduate Award
	Laureate fund LE130100159 to Michael Bird	Australian Research Council

[1] Centre for Tropical Environmental and Sustainability Science, College of Science, Technology and Engineering, James Cook University, P.O. Box 6811, Cairns, Australia.
[2]ARC Centre of Excellence for Australian Biodiversity and Heritage.
[3] Research Institute for the Environment and Livelihoods, Charles Darwin University, Darwin, Australia.
[4] Graduate School of Environmental Studies, Nagoya University, Nagoya, Japan.
[5] Advanced Analytical Centre, James Cook University, Cairns, Australia.
[6] German Research Centre for Geosciences (GFZ), Potsdam, Germany.
[7] Australian Bureau of Meteorology.

Acknowledgments

I would like to thank my supervisors for their enthusiasm, intellectual support and giving me the freedom to make this project my own. A big thanks to my wife Jordahna Haig for her endless patience and general support and my friends and family that always remained optimistic and kept motivating me to finish this thesis.

I gratefully acknowledge the sampling volunteers:
Tropical Cyclones: A. Campbell, D. Buckle, D. Lambrinidis, A. Padovan, F. Foti, H. Stone, N. Shoobridge, E. Garcia, W. Smith, M. Lauva, M. Sandery, H. Seneviratne, K. O'Donnell, B. Royal, F. Downing, S. Carthew, J&D. Prescott. Julie Toft, Emily Wiltshire, Damian Goodwin, Rob Callin, Amy Bevan, Miriam Goosem, Steven Goosem, Steve Turton, Emmerson Marcello, Paul Nelson, Bradley Smith, Brian Muirhead, Peter Valentine, Mirko Karan, Stephen Lewis, David Roberts, Annette Ryan, Nathan English, Ian Tuart, Anna Jaques, Yolanda Angel, Lynn Willis, Yoko Ishida, Lawrence Di Bella, Sam Sellick and Ash Benson. Emma Vestergaard is thanked for analytical assistance.

Daily rainfall samples Rangers Chillagoe, BoM staff Willis Island, D.Lambrinidis, Rainy Comly, Jen Whan, Jordahna Haig.

Leaves & Lake water: Michael Brand (Charles Darwin University)

Furthermore I would like to thank my colleagues that provided support and fruitful discussions during the meetings of the IAEA Coordinated Research Project entitled: *'Stable isotopes in precipitation and paleoclimatic archives in tropical areas to improve regional hydrological and climatic impact models'*.

Abstract

The aim of this PhD project was to provide and/or refine an interpretive framework for water stable isotope proxy records in north Australia and elsewhere. This involved an extensive measurement campaign, aimed at capturing the isotopic signature of modern rainfall, including extreme weather events such as Tropical Cyclones (TCs) which will be presented here. These results contribute to the reconstruction of a hydro-climate record spanning the last 11000 years BP. Until now, rainfall water isotopic composition has often been interpreted as a simple wet-dry proxy. However, the results of this project show that rainfall isotopic composition is strongly associated with weather-, cloud- and rainfall-type rather than simply rainfall amount. This has important implications for climate reconstructions and for other fields that use water stable isotopes. In addition to the monsoon rainfall measurements, four TCs were sampled for their rainfall and vapour isotopic content. The data indicates that TC rainfall stable isotopic composition strongly correlates with distance from the eye wall and that TCs passing further away than ≈100 km will most likely not be distinguished from regular monsoon rainfall in a stable isotope proxy record. This suggests that TC activity may potentially be under-estimated in the pre-historic record. Furthermore the first, leaf wax hydrogen-isotope record from north Australia is presented. These results are compared to the aquatic pollen record from Girraween Lagoon, and other published records of hydro climate change. This marks an important step towards the reconstruction of hydro climate in this region and will ultimately contribute to unravelling the natural and human drivers of change in northern Australia's climate and biodiversity.

Contents

Chapter 1

Introduction

The Tropics are expected to house ≈50% of the worlds population and close to 60% of the worlds children by 2050. While containing 54% of the world's renewable water resources, half its population is considered vulnerable to water stress [1]. A thorough understanding of tropical environmental change and associated climate dynamics, across a range of spatial and temporal timescales, is therefore important. However, past- and present environmental change in the Tropics remain under-researched because, amongst other reasons, logistical challenges and degradation of environmental records [2].

Climate over much of the tropics is characterised by monsoons, defined by an annual reversal of surface winds and associated differences in rainfall amounts during summer (wet) and winter (dry) seasons [3]. The Indonesian-Australian summer monsoon (IASM) represents an extensive Southern hemisphere monsoon system. It is anchored in the south by the Australian continent, coupled through the maritime continent and Indo-Pacific Warm Pool (IPWP) to the Northern Hemisphere East Asian Summer Monsoon (EASM) [4, 3]. The regions under the influence of the IASM currently experience strong seasonality in rainfall with a well defined wet season from December to March associated with the inflow of moist air from the northwest and a prolonged dry season from April to November dominated by trade winds from the southeast [5]. Interannual rainfall variability is tightly coupled to monsoon 'burst' and 'break' periods, modulated by wider atmospheric phenomena that vary on a range of timescales [6]. The Madden-Julian Oscillation (MJO) and cyclogenesis impact rainfall amount on intra-annual timescales while the El Niño-Southern Oscillation (ENSO) and Indian Ocean Dipole (IOD) currently exert significant control over total rainfall amount of inter-annual timescales [7]. In addition to annual rainfall amount, the distribution of rainfall in the pre- and post-monsoon seasons also exhibits significant ENSO-related variability. Up to 30% of annual rainfall can fall in the transitional period before the monsoon, and this is critical to the timing of ecological processes such as leaf flush/fall and grass growth in the wet-dry tropical savannas of northern Australia [5].

In northern Australia, as in other parts of the world influenced by strongly monsoonal climates [8, 3], rainfall variability associated with interactions between the monsoon circulation and other atmospheric phenomena, including ENSO and cyclogenesis, leads to episodic extreme drought and flood events [9, 10]. These represent a key risk to agriculture, infrastructure and, more broadly, to sustainable ecosystem function across northern Australia [11]. As climate changes in the future in response to anthropogenic forcing, it is also likely that rainfall variability and the incidence of extreme events will also change across the region, although the direction and magnitude of change are less well known than the trends in future temperature [11]. In northern Australia this is because it is not clear how the phase, amplitude and intensity of ENSO will interact with the monsoon and other sources of climate variability in the future [7].

Climate has varied substantially in the past and this variability is recorded in a variety of natural archives that can be used to calibrate climate models and improve our understanding of future climate scenarios. In tropical monsoon regions, these archives potentially provide insight into the range of past hydroclimate variability and an understanding of the processes driving monsoon hydroclimate.

This thesis focusses on processes controlling the (water) isotopic [1] composition of natural archives in tropical Australia. Water isotope ratios provide a means to reconstruct past hydroclimate as they are affected by evaporation and rainfall dynamics. Leaf litter in lake sediments for example or calcium carbonate in stalag-

[1] The atomic nuclei of an element containing different numbers of neutrons are called isotopes [12]. Molecules made up of different isotopes have slightly different chemical properties, resulting in for example heavy water. Water isotopic composition acts as a unique fingerprint and can be used to identify waterbodies and their hydrological history. Examples of this environmental tracing are testing for authenticity of bottled water or mapping pathways of rainwater into of ground water reservoirs in water resource management.

mites, record the isotopic fingerprint of water at the time of growth/formation. This makes water isotopes useful to reconstruct past hydrological conditions and thereby draw inferences regarding past climate.

The climatic inferences drawn from interpretation of these proxy records rely on a thorough understanding of processes driving rainfall isotopic composition. This in turn requires isotopic analysis of modern meteoric water samples under a range of different conditions, locations and timescales in order to fully capture the processes that drive climate and meteorological variability.

Early work in the 1950s showed correlations between rainfall isotopic composition and rainfall amount in tropical areas and this general relationship has since been the benchmark for the interpretation of the isotope record. Periods of high/low abundance of the heavier isotopes (commonly referred to as 'enriched'/'depleted') are interpreted as times of low and high rainfall amounts respectively.

A considerable amount of additional meteoric water isotope data is collected by the Global Network of Isotopes in Precipitation (GNIP)[2] and through individual studies. While the so called 'amount effect' is often present, the data exhibits strong scatter and the existence of an 'amount effect' has often been challenged, particularly on shorter sampling timescales where it is very weak or entirely absent. This ambiguity of the 'amount effect' interpretation can lead to opposing interpretations of climate records at the most basic level, e.g. wet versus dry, and unrealistic conclusions about the operation of the climate system in the past [13]. The first objective of is thesis is therefore to determine the drivers of rainfall isotopic variation in tropical north Australia, beyond the amount effect, in order to provide a comprehensive interpretational framework for paleo climatic records from this region and elsewhere.

The main source of the water that becomes incorporated into an isotope proxy record in this region is (summer) monsoon- and TC rainfall. Beside strong seasonality, monsoon rainfall in north Australia exhibits significant inter- and intra annual variability. Chapters 3 and 4 report rainfall isotopic composition across multiple

[2] A monthly precipitation collection network, initiated in 1960 by the International Atomic Energy Agency (IAEA) and World Meteorological Organisation (WMO)

seasons and demonstrate a strong connection between meteorological processes on multiple spatial scales and variability in rainfall isotopic composition. The results of these chapters have important implications for the interpretation of proxy records relying ultimately on water isotopes, in Australia and elsewhere.

Large areas of the (sub)tropics are affected by the periodic destructive passage of TCs, a thorough understanding of past TC activity enables better predictions and risk/impact mitigation for these events under a future changing climate. Reconstruction of TC activity from proxy records is based on the premise that TCs leave an isotopic trace in the soil water that feeds, for example, a cave drip water system. While several of these proxy records have been developed from within the Australian region, until now, no isotopic composition of TC rainfall has been reported. Chapter 5 fills this knowledge gap by reporting the continuous monitoring of vapour and rainfall isotopic composition during destructive TC Ita. Chapter 6 further expands on this topic by examining the rainfall isotopic signatures of four TCs relative to the regular monsoon rainfall isotopic composition and addresses questions such as 'Does the proxy record fully captures past TC activity?', and, 'is here an isotopic distinction between the monsoon and TCs?'.

The hydrogen isotope composition of plant waxes have shown considerable potential for reconstruction of changes in tropical hydroclimate [e.g. 14]. Despite this potential, there are few n-alkane hydrogen-isotope records from the Australian Indonesian Summer Monsoon (AISM) region and none from northern Australia. Chapter 7 presents the first *n*-alkane hydrogen-isotope record from north Australia. The results are compared to the aquatic pollen record from Girraween Lagoon, and other published record of hydroclimate change. This marks an important step towards the reconstruction of hydroclimate in this region and will ultimately contribute to unravel natural and human drivers of change in northern Australia's climate and biodiversity.

Chapter 2

Review of the literature

Michael I. Bird[1,2], Jordahna Haig[1,2], Xennephone Hadeen[1,2], Maria Rivera-Araya[1,2], Christopher M. Wurster[1,2], Costijn Zwart[1,2]

[a]*ARC Centre of Excellence for Australian Biodiversity and Heritage, James Cook University, PO Box 6811, Cairns, Queensland, 4870, Australia.*
[b] *College of Science and Engineering, James Cook University, PO Box 6811, Cairns, Queensland, 4870, Australia.*

Published as section 4.1 in:"Stable isotope proxy records in tropical terrestrial environments", *Palaeogeography, Palaeoclimatology, Palaeoecology* (2020): 109445

Abstract

The first step in interpreting a water stable isotope record is to determine the isotopic composition of its meteoric source water and variability under different meteorological conditions. In the tropics, this is not straightforward due to complex meteorology and the absence of a clear temperature effect such as found at high latitudes. The so called 'amount effect', a negative correlation between rainfall amount and δ values, has long been the benchmark of interpreting variation in tropical rainfall isotopic composition. However, in recent years, many studies have reported weak correlations, or data that contradicts the 'amount effect'. This suggests that using δ values as a simple wet-dry proxy may lead to unrealistic interpretations of stable isotope records. While explanations underlying the 'amount effect' such as isotopic exchange, sub-cloud evaporation and progressive lowering of condensation temperatures during larger rainfall events cannot be ignored, additional processes, such as moisture convergence, precipitation history, and cloud/rainfall type have been proposed to strongly influence tropical rainfall isotopic composition. This potentially leads to a refined interpretation of stable isotope proxy records. Information on meteoric water source dynamics and evaporative conditions can also be retrieved from stable isotope records that contain both hydrogen and oxygen isotope compositions through the d-excess parameter. Furthermore, recent triple oxygen datasets have shown promising as a complementary tracer of airmass history.

Author contributions

C. Zwart wrote and and M.I. Bird edited the manuscript. All authors provided critical feedback and commented on the manuscript.

Interpreting a water stable isotope record requires the determination of its meteoric source water isotopic composition and variability under different meteorological conditions. Observational networks are relatively sparse in tropical regions compared to the higher latitudes. This, and the very complex nature of tropical meteorology makes understanding the processes that determine rainfall isotopic composition in the tropics a complex task. Globally, patterns of $\delta^{18}O$ and $\delta^{2}H$ values in precipitation are correlated broadly with temperature, with low values characteristic of high latitudes and altitudes [15], Fig. 3; see Bowen et al. [16] for a recent review). This correlation with temperature is observable in mountainous regions of the tropics, with a reduction in $\delta^{18}O$ value of 0.14–0.24‰ per 100 m increase in altitude [17]. Modern patterns in $\delta^{18}O$ and $\delta^{2}H$ values also tend to decrease with increasing distance from the coast. All of these processes are the result of the condensation of the heavy isotopes into precipitation by Rayleigh distillation, commonly referred to as rainout effects.

Tropical $\delta^{18}O$ rainfall and palaeo-records are often interpreted using the classical 'amount effect'. This is a negative correlation observed between monthly rainfall amount and rainfall $\delta^{18}O$ at coastal and island stations in the tropics [15, 18]. Dansgaard [15] proposed "qualitatively several possible, and probably contributing reasons for the amount effect": (1) Rayleigh distillation; the progressively lowering of rainfall $\delta^{18}O$ as clouds cool and rainfall amount increases, partly linked in the tropics to increasing elevation of condensation (2) Isotopic exchange between rain drops and surrounding evaporatively enriched vapour leading to higher $\delta^{18}O$ values, this effect being strongest during light rains and, (3) kinetic fractionation during evaporation that increase $\delta^{18}O$; this latter effect is also most pronounced during light rains as humidity below cloud base is relatively low.

The bulk microphysical framework described above has been the basis for modern rainfall isotope predictions (see Figure 2.1) and many interpretations of tropical $\delta^{18}O$ palaeo-records over the last decades. However, many modern rainfall studies have found that the 'amount effect' is often not significant and also weaker over land at

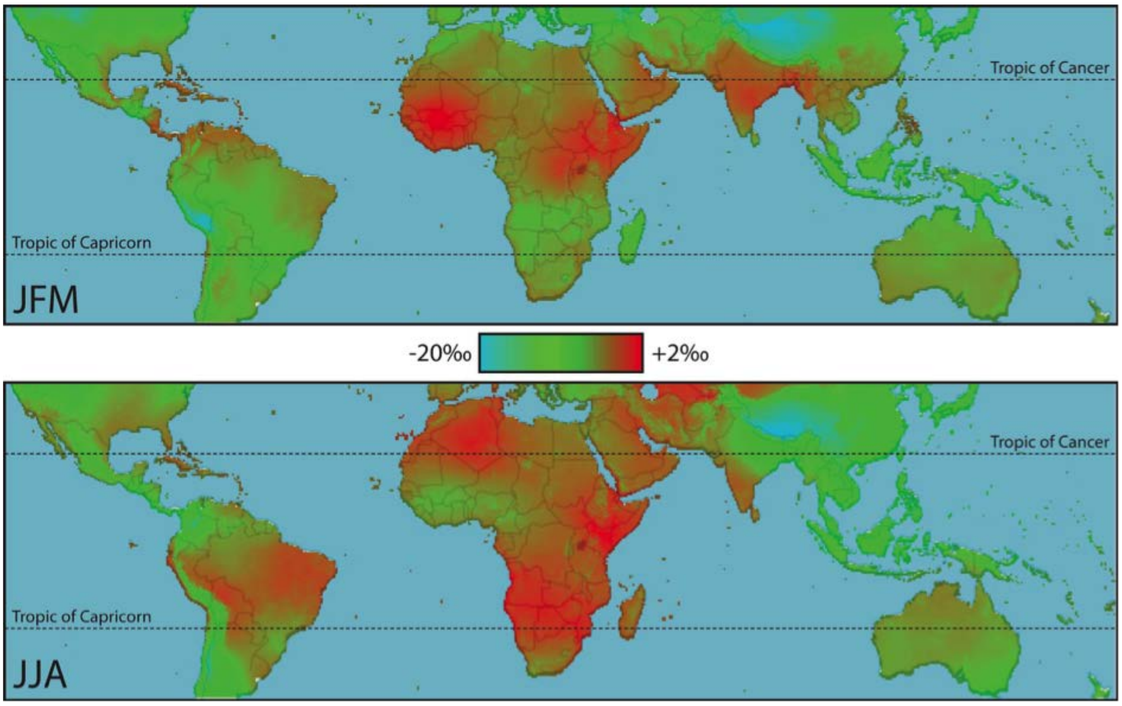

Figure 2.1: Seasonal IsoMap (`https://isomap-prod.rcac.purdue.edu/isomap/`) predictions of rainfall oxygen isotope isotope composition for tropical regions in the periods January-March (JFM) and June to August (JJA) based on regressions against precipitation and elevation for 942 GNIP stations sampling between 1961 and 2009.

tropical stations (see for example [18, 19] or on shorter timescales [e.g. 20, 21, 22, 23].

Furthermore, [24] and [25] for example, have pointed out that Rayleigh distillation is only valid for an idealised closed system while heavy tropical precipitation at a station requires convergence of additional moisture from elsewhere. Conflicting results regarding the 'amount effect' have not only been reported by modern rainfall studies, but also by several proxy records [26, 27, 28]. Recent studies stress that using $\delta^{18}O$ as a direct representation of local rainfall may lead to unrealistic conclusions about the climate system [e.g. 13].

Comprehensive analysis of regional atmospheric conditions and its relationship with rainfall and vapour $\delta^{18}O$ have now emerged from the development of large meteorological datasets and advanced meteorological models. Rainfall $\delta^{18}O$ variability has been attributed to convergence of isotopically distinct vapour and different air-mass trajectories [29, 30, 24, 22] and strong relationships have been found between $\delta^{18}O$, regional convective activity and associated regional rainfall in upwind regions [31, 32, 33, 34, 23, 35, 36]. Local convective activity has also been found to provide the dominant control on isotope variations in mountainous streams rather than the traditional altitude effect [37].

Although the link between regional convective activity and $\delta^{18}O$ variability is now generally accepted, the underlying processes and their relative contribution to the 'amount effect' are still the subject of debate. Risi et al. [38] proposed that isotopically light vapour from high altitudes is injected into the lower atmosphere by downdrafts and meso-scale subsidence and reused, producing precipitation with low $\delta^{18}O$ values. This was further explored by Kurita [19] who demonstrated a strong relationship between $\delta^{18}O$ and degree of convective organisation, and associated stratiform rainfall fraction. Rain- and cloud-type was found to be the dominant driver of $\delta^{18}O$ variability by Gedzelman et al. [39], Coplen et al. [40], Aggarwal et al. [41] and Zwart et al. [42] on short (30-min events, daily) and longer (monthly) sampling timescales respectively, using ground and satellite-based radar data.

Relative contributions to the 'amount effect' of the different processes described above may not be uniform across the tropics. Konecky et al. [13] showed that cloud-type is a dominant driver in regions where stratiform rainfall is abundant, however, along the tropical rainbelt perimeters and inland areas of Africa, local meteorology can inhibit the sustained presence of stratiform rain and moisture source may play a more dominant role.

$\delta^{18}O$ and δ^2H values in rainfall tend to co-vary along the so-called Global Meteoric Water Line (GMWL); $\delta^2H= 8 \times \delta^{18}O + d$ [15, 43] with d≈10‰ (see Figure 2.2 for a local MWL in northern Australia). The intercept, d (or d-excess), represents the relative abundance of the heavy isotopologues of oxygen ($H_2{}^{18}O$) and Hydrogen ($^1H^2H^{16}O$). Deviations from d = 10‰ indicate that water has been subject to non-equilibrium processes such as, for example, evaporation (Figure 2.2). This makes d-excess a useful independent tracer of moisture history. d-excess is closely related to evaporative conditions (SST, wind, relative humidity) in the moisture source region and altered by mixing of air masses on trajectories towards the precipitation site [44, 45, 46].

The interpretation of d-excess for continental stations is complex due to continental recycling and sub-cloud evaporation in a relatively dry atmosphere [48, 49]. Furthermore, analytical uncertainty can be relatively high compared to its natural range of variability [50]. Despite these drawbacks, d- excess has been successfully used to, for example, calibrate general circulation models [51], examine moisture source regions and ENSO dynamics in South America [52] and provide insights in to tropical cyclone dynamics [53]. Recently, analytical improvements enabled the development of triple oxygen datasets for meteoric waters, which has resulted in the development of an ^{17}O excess parameter that can be used as a complementary tracer of airmass history [see for example 54, 55].

For some proxy materials including some tree ring records and speleothems, the connection between rainfall and proxy is rapid and relatively direct. For many others the rainfall remains in a terrestrial reservoir for a significant period and can be subject to further modification before incorporation into a proxy. Evaporation,

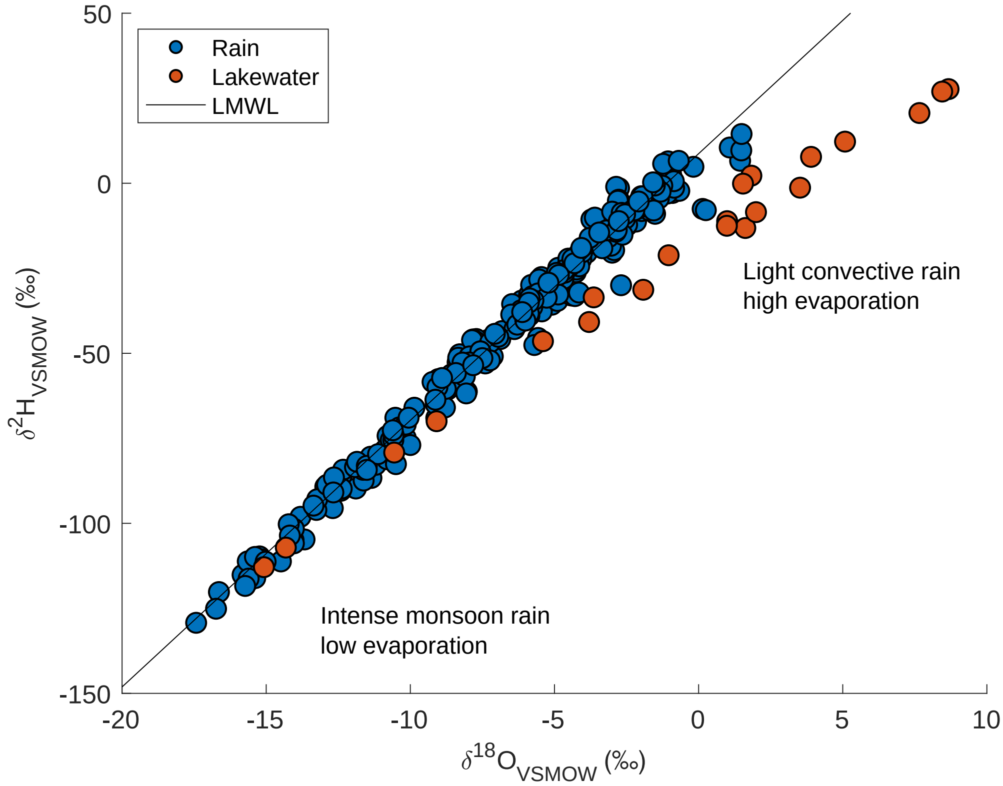

Figure 2.2: Variation in 300 rainfall and lake water stable isotope compositions from the 'Top end' of the Northern Territory, Australia. Rainfall data represent individual 12 hourly samplings of rain from January to April of 2013. Lake waters represent samples opportunistically collected from lakes in the region in the April to November period from 2011 to 2013. Lake sites are as described in [47]. Intense monsoonal rain has low δ^{18}O and δ^2H, light convective rain has high δ^{18}O and δ^2H. Lake waters recently refilled by intense monsoonal rain have low δ^{18}O and δ^2H values, evaporative loss of water through the dry season progressively leads to higher δ^{18}O and δ^2H values.

from standing water bodies and from the soil surface, leads to enrichment in the $\delta^{18}O$ and $\delta^{2}H$ values of the remaining water, generally along a line with a slope less than the meteoric water line (Figure 2.2). The degree to which the water isotope composition departs from the meteoric water is dependent on the conditions under which evaporation occurs and the proportion of evaporation relative to the size of the reservoir. Gibson et al. [56] found that whereas the slope of the local evaporation line for lakes in high latitudes is 5–8, the slope for lakes in tropical regions is 4–5, and for soil water is 2–3. Groundwater can also have a variable residence time and its isotope composition may [57] or may not [58] reflect current environmental conditions. In the seasonal tropics in particular, recharge of groundwater tends to occur mainly from high rainfall events that have an isotope composition that is lower than that of average rainfall [59].

For these reasons, observed trends in the isotope composition of many tropical proxy records tend to be interpretable only as relative changes in precipitation. This is possible because, at the general level, wetter periods (with less relative evaporative potential) tend to result in lower isotope values, whereas drier periods (with more relative evaporative potential) tend to result in higher isotope values. The caveat to this general statement is that recent work has demonstrated that some significant changes in the stable isotope composition of average precipitation are driven by factors such as changes in cloud type and vapour source region [13].

Chapter 3

Stable Isotopic signature of Australian Monsoon controlled by regional convection

C.Zwart[1,2] N.C. Munksgaard[1,2,3] N. Kurita[4] M.I. Bird[1,2]

[1] *Centre for Tropical Environmental and Sustainability Science, School of Earth and Environmental Science, James Cook University, Cairns, 4870 QLD, Australia.*
[2] *ARC Centre of Excellence for Australian Biodiversity and Heritage*
[3] *Research Institute for the Environment and Livelihoods, Charles Darwin University, Darwin, Australia*
[4] *Graduate School of Environmental Studies, Nagoya University, Nagoya, Japan*

Published in: *Zwart, C., et al. Quaternary Science Reviews 151 (2016): 228-235.*

Abstract

The aim of this study was to identify the main meteorological drivers of rainfall isotopic variation in north Australia in order to improve the interpretation of isotopic proxy records in this region. An intense monitoring program was conducted during two monsoonal events that showed significant and systematic isotopic change over time. The results showed a close link between isotopic variation in precipitation and variability in monsoon conditions, associated with the presence of large convective envelopes propagating through the study site. The largest negative amplitudes in the isotopic signal were observed when eastward and westward moving precipitation systems within the convective envelope merged over the measurement site. This suggests that the amplitude of the isotopic signal is related to the size and activity of the convective envelope. The strong correlation between rainfall isotopic variation, regional outgoing longwave radiation and regional rainfall amount supports this conclusion. This is further strengthened by the strong relationship between isotopic variation and the integrated rainfall history of air masses prior to arriving at the measurement locations. A local amount effect was not significant and these findings support the interpretation of $\delta^{18}O$ as proxy for regional climatic conditions rather than local rainfall amount. Meteorological parameters that characterize intra-seasonal variability of monsoon conditions were also found to be strongly linked to inter-seasonal variability of the monthly based $\delta^{18}O$ values in the GNIP database. This leads to the conclusion that information about the Australian monsoon variability can likely be inferred from the isotopic proxy record in North Australia on short (intra seasonal) and long (inter seasonal or longer) timescales.

Author contributions

C. Zwart wrote the manuscript, analysed and interpreted the data. N. C. Munksgaard developed the research question and performed the laboratory analysis. N. Kurita provided assistance in analysing satellite data and participated in critical discussion on development of the manuscript. M. I. Bird provided facilities for data analysis and participated in critical discussion on development of the manuscript. All authors provided critical feedback and commented on the manuscript.

3.1 Introduction

The AISM dominates the climate of tropical northern Australia. An understanding of AISM variability both past and present is paramount in order to be able to better predict future hydrological conditions under a changing climate. The isotopic composition of rainfall strongly influences the isotopic values preserved in natural archives commonly used to study past hydrological conditions, such as coral deposits, sediment cores, speleothems, molluscan shells and leaf waxes [60, 61, 62, 63, 64, 65]. Monthly mean rainfall isotope composition obtained from local stations shows a strong correlation with local rainfall amounts in tropical regions [15, 18] and this so called 'amount effect' is therefore widely used in palaeoclimate and palaeohydrological studies which reconstruct past monsoon variability [66, 67]. Part of this effect is explained by Rayleigh distillation that progressively depletes ^{18}O and ^{2}H values in the residual water vapour via rainout during successive condensation/evaporation cycles. This amount effect is generally observed in rainfall samples collected over monthly periods and the isotope composition of rainfall on shorter (event-based or daily amounts) timescales can be independent of the local rainfall amount [15, 20, 25].

However, despite a robust 'amount effect' being observed on longer timescales, rainfall isotopic composition is affected by complex atmospheric processes acting on different spatial and temporal scales [68, 38, 33, 21]. In the hydrological cycle, stable isotope ratios measured as the ratio of a heavier- to lighter isotopes (in this study oxygen ($^{18}O/^{16}O$) and hydrogen ($^{2}H/H$) reflect condensation/evaporation processes where the heavier isotopes are preferentially fractionated into the liquid phase and lighter isotopes into the remaining vapour phase. Thus, isotopic ratios provide information about the source, transport and precipitation history of moisture and can be particularly useful as tracers when used in conjunction with data on the prevailing meteorological conditions [68, 69, 22]. For example, vapour becomes progressively depleted in ^{18}O and ^{2}H when traveling through regions of enhanced precipitation [31], recycling of vapour in strong convection events is known to deplete vapour [38], possibly due to the appearance and increase in size of the stratiform fraction of the convective system [32, 41]. and moisture source and trajectories have been linked to variability in rainfall isotopic composition [70]. Furthermore, enrichment of rain droplets occurs below the cloud base when droplets evaporate [71, 48, 72, 21]. These processes should be considered when interpreting isotope proxy records.

In the tropics, several studies have reported a relationship between rainfall isotopic composition and large scale convective activity associated with intra seasonal variability (ISV) rather than precipitation amount [31, 32, 33, 34]. Risi et al. [38] proposed downdraft recycling as an explanation for isotopic variation over these shorter time scales, independently of local rainfall amount. In this explanation, isotopically-depleted vapour from higher levels is injected into the lower atmosphere via downdrafts and reused for precipitation. Kurita [19] examined the role of the mesoscale downdraft recycling mechanism proposed by Risi et al. [38] using surface vapour and precipitation data collected in the Western Pacific and Indian Ocean. They indicated that low isotope ratios are associated with Mesoscale Convective Systems (MCS) that develop large stratiform rain areas whilst relatively high isotope ratios are associated with smaller-scale disorganised convection. A recent study by Aggarwal et al. [41] based on monthly timescales proposed that isotopic variation in precipitation is mainly the result of a difference in growth conditions of the condensation particles between convective and stratiform rain, with convective and stratiform rain producing high, and low, isotope ratios, respectively.

Recently, the stable isotopic composition of rainfall has been reported to vary on time scales as short as minutes [53] to hours [73, 70] and this variability has been connected to characteristics of meso-scale atmospheric processes such as the MJO [32]. In this study, aimed at improving our understanding of the influence of the AISM on the tropical Australian isotope record we identify the atmospheric processes that drive isotopic variation in rainfall in north Australia on short (event-based) time scales and then we examine the relationship between AISM ISV and inter-seasonal isotopic variation. The objectives of this study were to (i) elucidate the main drivers of isotopic variation on 12 hourly timescales during two monsoonal events over Darwin, Australia that exhibited strongly divergent isotopic trajectories over time and (ii) investigate whether the same drivers can also explain the variation observed in the long term 23 year monthly Darwin GNIP record.

3.2 Methodology

As adopted in previous studies [20, 34] we use the term 'local' to refer to phenomena within a few kilometers to the measurement site and 'regional' when referring to the area within a bounding box ($10° \times 5°$ in this study) around the site.

3.2.1 Site description

Darwin is located on the Northern Territory coastline, adjacent to the Beagle Gulf which connects the Timor and Arafura Sea these linked to the Indian Ocean and Coral Sea respectively (see Fig. 3.1a). The region experiences a monsoonal climate with a pronounced wet season from November until April (during which time 90 % of annual rain falls) and dry season from May to October. Low level westerly winds and high rainfall amounts dominate in the wet season, while southeasterly trade winds and low rainfall totals are typical of the dry season [6]. Onset of the monsoon occurs when the monsoon trough (a band of low pressure and convergence) moves over the area, associated with moisture laden westerly winds and widespread rainfall. ISV of the AISM was recognized by [74], who identified active 'burst' and 'break' periods. [75] reported that bursts were associated with large scale envelopes of enhanced convective activity propagating either eastward or westward. Burst and break periods are each characterized by different types of convection. Active periods (bursts) are associated with large-scale organized convective areas with mesoscale stratiform decks while convection during break periods is more isolated yet more intense [6]. The dominating mode in ISV of the AISM is the MJO, defined an eastward moving large-scale convective envelope. Strong phases of the MJO result in enhanced convection and more rainfall. The passage of this area of moisture convergence is characterized by a zonal wind shift in the lower atmosphere from east

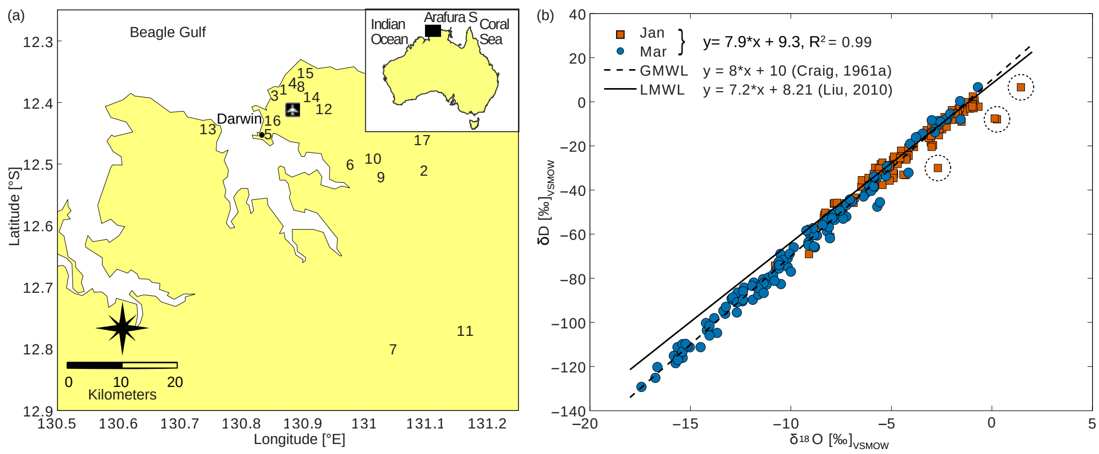

Figure 3.1: (a) Location map of Darwin and the 17 sample stations and BoM station Darwin Airport. (b) Non-weighted δ^2H plotted versus δ^{18}O for both events in January (vermilion squares) and March (blue circles). Outliers are indicated with dashed black circles. GMWL: Global Meteoric Water Line, LMWL: Local Meteoric Water Line reported by [76].

to west and often coincides with the onset of the monsoon. Other modes include westward moving Equatorial Rossby waves, tropical cyclones that can significantly increase rainfall amounts over short periods of time and eastward moving Kelvin waves [6].

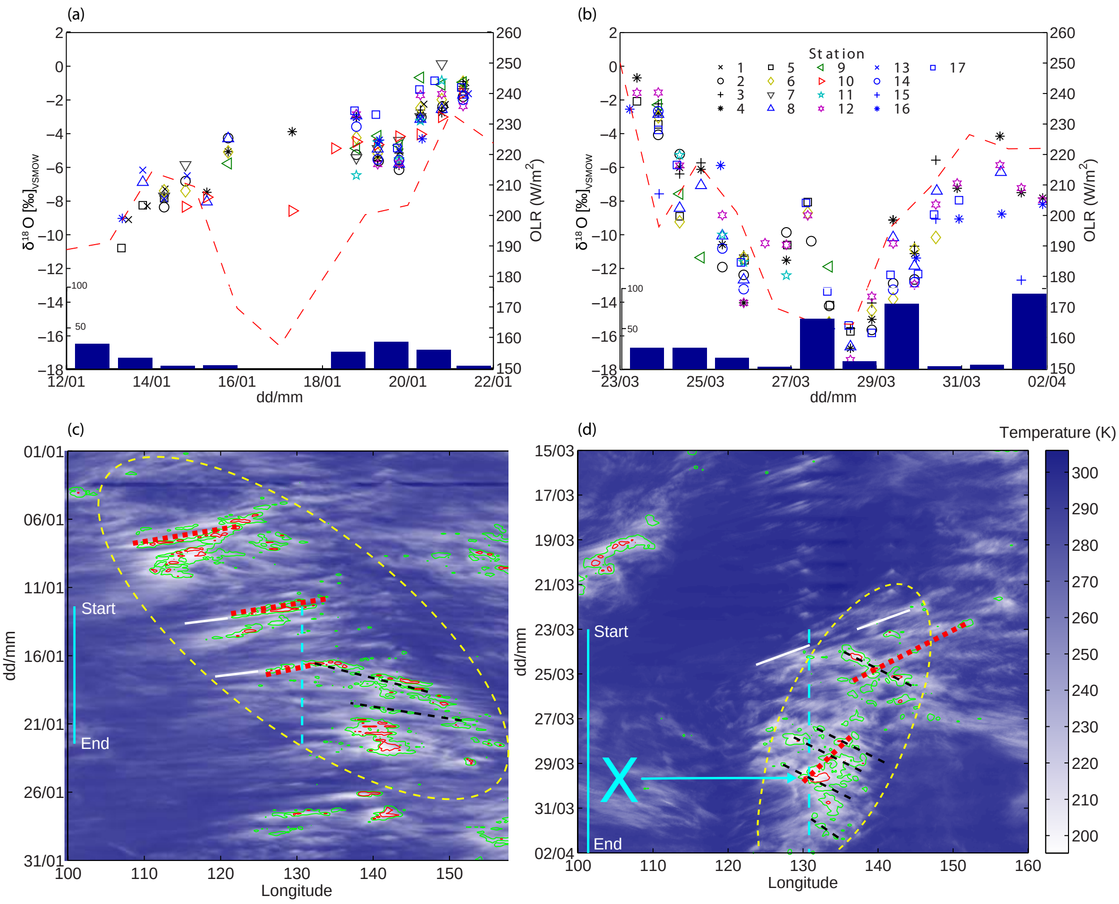

Figure 3.2: (a,b):δ^{18}O values measured during two events; January and March respectively. Markers represent the different measurement stations and the red dashed line = regional average OLR. n=225 Blue bars represent daily rainfall [mm] at Darwin Airport. (c,d): Hovmöller plots showing 5 degree latitude averaged MT-Sat, IR1 cloud top temperatures. Green and red contour lines represent TRMM 1 and 5 mm hr^{-1} respectively. The yellow dashed lines enclose the identified MJO (c) and ER cloud envelope (d). The red and black dashed lines indicate westward and eastward propagating precipitation systems respectively. Solid straight white lines show examples of westward trailing cloud shields. The cyan dashed line indicates longitude Darwin and measurement period (solid). The cyan X marks the intersection between eastward and westward propagating systems. Precipitation systems and cloud envelopes were identified using Hovmöller plots of TRMM 3B42-v7 [77] and archived imagery made available by CICS-NC, (see https://ncics.org/portfolio/monitor/mjo/) respectively.

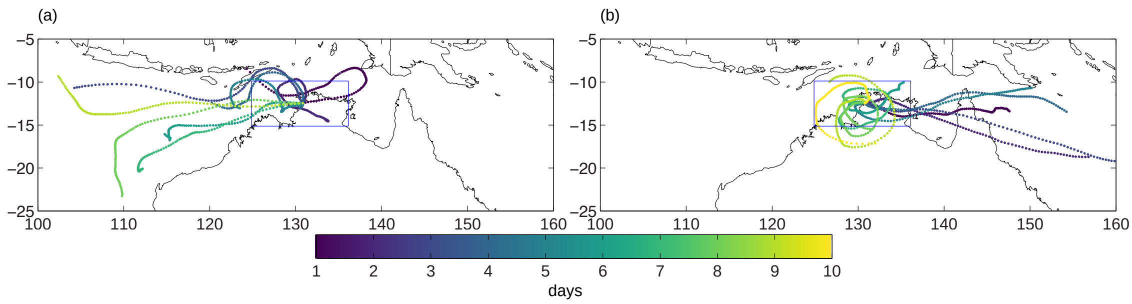

Figure 3.3: Hysplit 96 hr air mass back trajectories arriving in Darwin at 850 hPa (a) January and (b) March/April. Color bar indicates starttime of trajectory (days into event). Blue rectangle represents 10°×5° bounding box over Darwin as a reference.

3.2.2 Sampling and analysis

Two major wet season rainfall events were sampled in January and March of 2013 respectively. A total of 228 rainfall samples were collected during these rainfall events by volunteers on 17 different stations covering 2000 km^2 around Darwin, see Fig. 3.1a. Another rainfall event occurred in February 2013, however, this event could not be sampled for logistical reasons. Sampling times were coordinated for all stations from 7am–7pm and 7pm–7am. Accumulated 12 hourly rainfall was collected from open vessels on open ground at each station directly at the end of each measurement period and capped to minimize evaporation and risk of isotopic exchange with the surrounding vapour. The δ^{18}O and δ^{2}H values of all samples were determined using a diffusion sampler and Picarro L2120-I WS-CRDS system described by [30] coupled to an autosampler and are reported in the standard δ notation (‰), i.e $\delta^{18}\text{O} = [(^{18}O/^{16}O_{sample} -^{18} O/^{16}O_{standard})/^{18}O/^{16}O_{standard}] \times 10^3$. The isotopic values are reported relative to the VSMOW scale and were calibrated using three secondary standards; Lake Eacham Water (δ^{18}O = +1.51 ‰ ;δ^{2}H = +4.09 ‰), Cairns Tapwater (δ^{18}O = -4.37; δ^{2}H = -26.47) and Evian water (δ^{18}O = -10.20 ‰ ;δ^{2}H = -72.84 ‰). The secondary standards were calibrated against the IAEA reference waters VSMOW, GISP and SLAP. Typical precision for samples and standards was $\pm$0.2 ‰ for δ^{18}O

and $\pm$0.6 ‰ for δ^{2}H.

Meteorological data

Precipitation radar images and local 30 minute and daily averaged meteorological data (temperature, relative humidity, dew point, and precipitation) were obtained from the Australian Bureau of Meteorology (hereafter referred to as BoM, station id= 014015; name= Darwin airport; latitude=12.42°S; longitude=130.89°E, see Fig. 3.1a; height=30.4 m). Satellite images (MT-Sat, IR1), used to examine cloud top temperatures, were provided by the Center for Environmental Remote

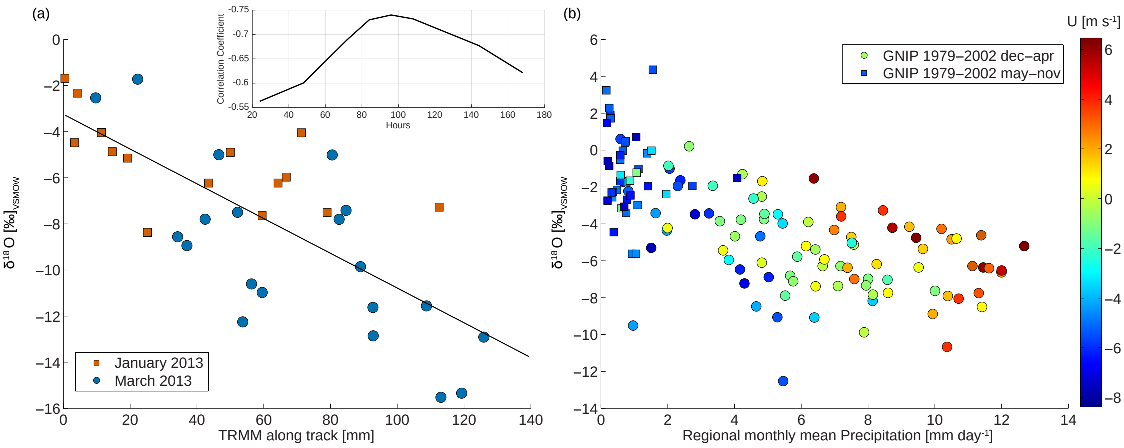

Figure 3.4: (a) δ^{18}O against accumulated TRMM rainfall along track [mm]. (b) Monthly GNIP δ^{18}O versus regional averaged GPCP n=148, Dec-Apr (circles) and May-Nov (squares). Colorbar indicates strength of zonal wind [m s^{-1}], positive values represent westerly and negative values easterly wind direction. Inset shows correlation against length of trajectory (hours)

Sensing (CEReS), Chiba University, Japan. Interpolated Outgoing Longwave Radiation (OLR) data were obtained from NOAA and is described by [78]. Regional average daily OLR values were calculated by averaging daily OLR values over a bounding box of 10°(EW)×5°(NS), centered over Darwin airport. Monthly and daily regional average precipitation amounts were computed using the Global Precipitation Climatology Project (GPCP, version 2.2) dataset [79] and Tropical Rainfall Measuring Mission 3B42-v7 [TRMM 77] respectively. Mean regional rainfall (daily) rainfall was computed by averaging over a bounding box of 10°(EW)×5°(NS), centered over Darwin airport. Monthly-based isotopic records of precipitation at the Darwin station archived in the GNIP database were used for months overlapping with the GPCP and OLR data (n=149).

Air mass back trajectories were computed using the Hybrid Single-Particle Lagrangian Integrated Trajectory HYSPLIT) model version 4.0 [80]. The Global Assimilation Data set (GDAS-1) provided by the United States National Centers for Environmental Prediction (NCEP) was used as input for the wind fields. HYSPLIT back trajectories were computed in isobaric mode with different runtimes (24-168 hours) and the height selected was 850 hPa. Total rainfall along HYSPLIT trajectories (P_{tr}) was calculated as the sum of the closest gridpoints in the 0.25° TRMM 3B42-v7 3-hourly dataset to the trajectory positions using:

$$P_{tr} = \sum_{t=0}^{t=n} P(t)_{xy}, \tag{3.1}$$

where t is the time (hours) back from starting point, n is total track length (hours), x and y are longitude and latitude respectively and $P(t)_{yx}$ is the precipitation rate (mm/hour) in the TRMM dataset at the position closest to the HYSPLIT track location at time t. Starting points of back trajectories were set at 12-hour intervals corresponding to sample collection times. MJO and ER cloud envelopes were identified using archived imagery made available by the Cooperative Institute for Climate and Satellites, North Carolina (CICS-NC, see https://ncics.org/portfolio/monitor/mjo/). Long term monthly averaged (1984-2010) equivalent potential temperature (θ_e) was

Table 3.1: Pearson ρ correlation coefficients and p-values between $\delta^{18}O$ values, local, regional and along track precipitation amounts and OLR.

	local [mm]	regional [mm]	along trajectory [mm]	OLR [W m^{-2}]
$\delta^{18}O_{JanuaryMarch}$	-0.21 (<0.3)	-0.70 (<0.05)	-0.74 (<0.05)	0.59 (<0.05)
$\delta^{18}O_{GNIP}$	-0.50 (<0.05)	-0.69 (<0.05)		0.66 (<0.05)

calculated at 850hPa level using

$$\theta_e = T_e \left(\frac{P_0}{P}\right)^{\frac{R_d}{C_{pd}}}, \tag{3.2}$$

where $T_e = T + (\frac{Lv}{Cpd})r$, with $P_0 = 1000$ hPa, $P = 850$ hPa, $Rd = 287.04$ J/(Kg K), $C_{pd} = 1004$ J/(Kg K), $Lv = 2400$ J/Kg, T is temperature (K) and r the mixing ratio (Kg/Kg) . NCEP/NCAR reanalysis temperature and mixing ratio fields were used for T and r respectively (see ftp.cdc.noaa.gov).

3.3 Results

The relationship between δ^2H and δ^{18}O of rainfall samples collected during both events is presented in Fig. 3.1b. A least square regression analysis resulted in a highly significant (Pearson rho = 0.99, $p < 0.05$) meteoric water line (MWL) for both events: δ^2H= 7.9× δ^{18}O + 9.3 ($R^2 = 0.99$) which is similar to the GMWL determined by Craig [81]. Three out of the 228 samples were collected when rainfall amounts were very small (<2 mm) and plotted off the MWL, it is therefore most likely that these evaporated, resulting in isotopic change while awaiting sample collection and have therefore been discarded. As the O and H isotope results are highly correlated with each other, results will be discussed in terms of δ^{18}O only.

3.3.1 January 2013

The MJO moved across SE Asia in early January and into the western Pacific by the end of the same month. The monsoon trough lingered over Darwin on the 13th and moved further south on the 15th, producing significant rainfall over Darwin during the measurement period. This event marks the official onset of the Northern Australian Monsoon on the 17th of January [82]. The total rainfall measured at Dawin Airport BoM site for this event was 129.2 mm. Figure 3.2a shows 12 hourly δ^{18}O values measured during this rainfall event in January. The δ^{18}O values varied from -10.8 ‰ to +0.14 ‰ and showed an overall trend towards heavy isotope enrichment as the event progressed. The rainfall-weighted average δ^{18}O value of the January event was -5.8 ‰ with most stations showing a similar trend in δ^{18}O values over the course of the event. Soundings [83] above Darwin showed that easterly winds were present in the lower and upper atmosphere during the start of the event and winds in the lower atmosphere shifted to westerly on the 16th and 17th while the upper air easterlies weakened. Easterly winds were present again above Darwin in the mid- and upper levels around the 20th while westerly winds persisted near the surface. This shift in zonal winds corresponded to the passage of an area of convergence in the lower atmosphere, associated with the passage of the MJO. Figure 3.2c shows a large scale convective envelope, identified as the MJO moving eastward over the course of the month. Westward trailing cloudshields and rain areas developed successively off the main envelope from the 11th to the 15th (shown as purple dashed and solid straight red lines in Figure 3.2c). The lowest δ^{18}O values in January coincide with the passage of westward moving precipitation systems over Darwin around the 13th. The westward moving systems stopped developing around the 17th and started to move in a southeasterly direction thereafter.

The upwind region became clear of large precipitation areas and large convective envelopes were positioned well downwind (East) of Darwin for the remainder of the measurement period. Regional averaged OLR and δ^{18}O values follow a similar increasing trend for the event in January, except for a dip in OLR on the 17th. A westward trailing cloudshield was located over Darwin around the 17th, resulting in low regionally averaged OLR values of approximately 160 W m^{-2}. Darwin was on the western edge of an eastward moving precipitation system (shown as black dashed line in Figure 3.2c) that developed from this cloudshield, precipitation amounts at the sampling stations were therefore very small resulting in sample collection at only two stations, Darwin Airport reported no rain for that period. This explains the relatively weak response of δ^{18}O values to the large negative excursion in OLR values between January 14th and 18th. Enriched δ^{18}O values were associated with higher OLR values after January 18th (i.e. less organized convection during break conditions) whereas low isotopic compositions coincided with low OLR values of $\approx$

200 W m^{-2}.

Air mass back trajectories over Darwin at 850 hPa, see Fig. 3.3a, illustrate the arrival of the westerlies at 850 hPa, associated with the onset of the Monsoon. Air masses early in the event (13–14 Jan) exhibited trajectories that were regional (relatively close to the boundaries or within a 10°× 5° bounding box). Trajectories developed a more westerly direction as the event progressed, originating from the Indian Ocean.

3.3.2 March 2013

The second measurement period in March represents the last significant rainfall event of the 2012–2013 wet season. On 23rd March a high pressure area was located over the Tasman Sea, between Australia and New Zealand, extending a ridge of high pressure over eastern Australia. Darwin experienced a monsoon break period while the MJO was positioned over the Pacific and convective activity over northern Australia was low. The monsoon trough re-activated just north of Australia on the 24th and 25th. A low-pressure area developed within this active trough over the Arafura Sea and slowly moved west-southwest to remain stationary just west of Darwin for the remainder of the month and into the beginning of April. This low brought heavy rainfall to northern Australia with 321.8 mm recorded at Darwin Airport during the measurement period.

Data from all measurement stations showed a similar trend throughout the course of the event, (see Fig. 3.2b). The δ^{18}O values were initially relatively enriched during the break conditions (≈ -1 ‰) but became more depleted over the following 5 days to a minimum of -17.4 ‰ during the burst on 28 March, before becoming more enriched again during break conditions towards the end of the sampling period. The rainfall-weighted average δ^{18}O value for the event in March was -10.0 ‰ .

Convective activity developed over Darwin from the 23rd onwards, as westward propagating disturbances identified as an equatorial Rossby (ER) wave moved into the region, (see Fig. 3.2d). Low level easterly winds were observed above Darwin at the start of the event and gradually decreased and shifted to westerly around the 28th

as the convective envelope moved into the region. Eastward trailing cloud shields and rain areas were also identified throughout the measurement period (shown as clack dashed lines in Fig. 3.2d). These convective systems developed further during the event and increased in size (up to ≈500 km diameter), both over Darwin and in the upwind region, spanning across and area of ≈1500 km. Intersections between the westward and eastward propagating systems produced areas of enhanced convective activity (labeled as X in Fig. 3.2d), reaching a peak on the 29th coinciding with the lowest recorded δ^{18}O values, decreasing thereafter. Regionally averaged OLR and δ^{18}O values were strongly correlated. The timing of the minimum δ^{18}O values coincided with the lowest region-averaged OLR values of ≈160 W m^{-2}.

Air mass back trajectory end points, see Fig. 3.3b, were initially located in the Coral Sea (until 28th) and became closer to Darwin from the 29th–31st. Air mass back trajectory end points were located relatively close to Darwin —near the edges of the bounding box—towards the end of the event with air masses travelling over the Timor and Arafura Sea on the 1st and 2nd of April.

3.3.3 ISV of monsoon driving rainfall isotopic composition

Pearson ρ correlation coefficients and corresponding p-values between δ^{18}O values of both events and precipitation amounts (local and regional), regionally averaged OLR and precipitation amount along air mass back trajectories, are provided in Table 3.1. The correlation between δ^{18}O and local precipitation amount was not statistically significant (ρ =-0.21, p-value<0.3), whereas correlation with regional parameters was significant. The relationship between δ^{18}O values for both events and precipitation along the trajectories was evaluated for different trajectory lengths (24-168 hours) and showed the strongest correlation for a 96 hour trajectory duration (ρ =-0.74, p-value <0.05; Fig. 3.4a).

3.3.4 Inter-seasonal variation of monsoon in the Darwin GNIP record

Isotopic variation in precipitation over longer time scales (Darwin 23 year, monthly GNIP record) also showed strong relationships with regional precipitation amount and OLR, see Fig. 3.4b and Table 3.1. In order to further explain these relationships, zonal 850 hPa winds were examined as these are indicators of monsoonal active (bursts) and inactive (break) periods [6]. Three regimes were identified in the data for the available years 1979–2002; (i) low isotopic values and higher regional precipitation accompanied by strong westerlies, with this regime dominant in the monsoon season from December to April, (ii) high isotopic values accompanying relatively low regional rainfall amounts associated with easterly winds in the dry season and (iii) a transition from low to high isotopic values where regional average zonal winds are weak or entirely absent. The significant outlier at point δ^{18}O=-12.52 ‰ represents April 1985 during which time Tropical Cyclone Gretel tracked along the coast near Darwin, with 189.5 mm recorded at Darwin Airport in this month. Cyclonic precipitation is known to result in very low isotope values close to the centre of the cyclone [84, 85, 53].

3.4 Discussion

3.4.1 Intra-seasonal variability

The isotopic evolution of two typical monsoon rainfall events was fully captured during their burst-break cycle. Results of the current study suggests that the isotopic record in tropical Australian rainfall in this study reflects regional (10° ×5° box, centered over Darwin) climatic conditions rather than local rainfall amounts, similar to results that have been reported elsewhere [19, 33, 34].

The ISV of monsoon conditions, caused by different convection types resulted in distinctively different isotopic signatures. This means that high-temporal-resolution isotopic records from archives such as stalagmites, in this region [see for an example elsewhere 84] could be used to reconstruct ISV of the AISM as short term isotopic variations are picked up within the rainfall signal.

The lowest $\delta^{18}O$ values occurred when eastward and westward moving convective systems merged over the measurement location, creating the largest stratiform cloud areas. These merger events were also reported by Kurita et al. [32] and strengthens the hypothesis that the size of the convective active area plays a dominant role in the lowering of $\delta^{18}O$ values. Our results confirm the connection reported by [86] and [41] between the type of convection, relative position of the measurement site (ie upwind/downwind of convective area) and measured $\delta^{18}O$ values.

Merger points between eastward- and westward moving systems provide a favorable environment for the development of MCS. MCS contain large regions of stratiform rainfall and these are responsible for depletion of the δ values in precipitation due to the injection of depleted vapour from high altitudes into the lower altitudes from which the precipitation is derived [19]. Recycling of vapour through successive MCS's results in an amplification of this negative isotopic signal. This is reflected in the strong correlation that we observed between isotope values and integrated rainfall amounts along trajectories. In contrast, enriched isotopic values were associated with periods when convective activity in, or upwind of the measurement region was low, the size of stratiform decks was reduced and recycling through successive MCS's was absent. Higher $\delta^{18}O$ values, associated with oceanic trajectories have also been observed by Treble et al. [87] and Corrales et al. [88] and attributed to entrainment of oceanic moisture. However, since the majority of trajectories had a significant oceanic path and a similar vapour source, we suspect that the absence of large convective areas with associated stratiform fractions and hence less rainfall/moisture recycling along the trajectories prior to arriving at the measurement site led to relatively high $\delta^{18}O$ values.

3.4.2 Connection between intra- and inter-seasonal variability

Long term monthly averaged climatology is summarized in Figure 3.5. There is a clear difference in cloudiness (OLR) between the wet (low) and dry (high) season, accompanied by a shift in 850hPa wind fields bringing in warm moist tropical air in the wet season (characterized by higher θ_e values) and relatively colder dry air in the dry season (low θ_e values). This study found a strong connection between these monsoon characteristics and isotopic variation in the GNIP record. Monsoon 'bursts' —of widespread convection in the wet season accompanied by westerly winds at 850 hPa—produce low δ^{18}O values. High δ^{18}O values are produced during monsoon 'breaks' (when convection is scattered, shorter-lived and 850 hPa easterlies prevail). The strong relationship between short-term meteorological drivers of isotopic variability found during the two events and inter-seasonal/annual variation of δ^{18}O in the GNIP record supports the hypotheses that past monsoon activity can be reconstructed from the isotope record in north Australia. These results demonstrate that the local isotopic record has regional significance and enable a more comprehensive interpretation of past monsoon activity.

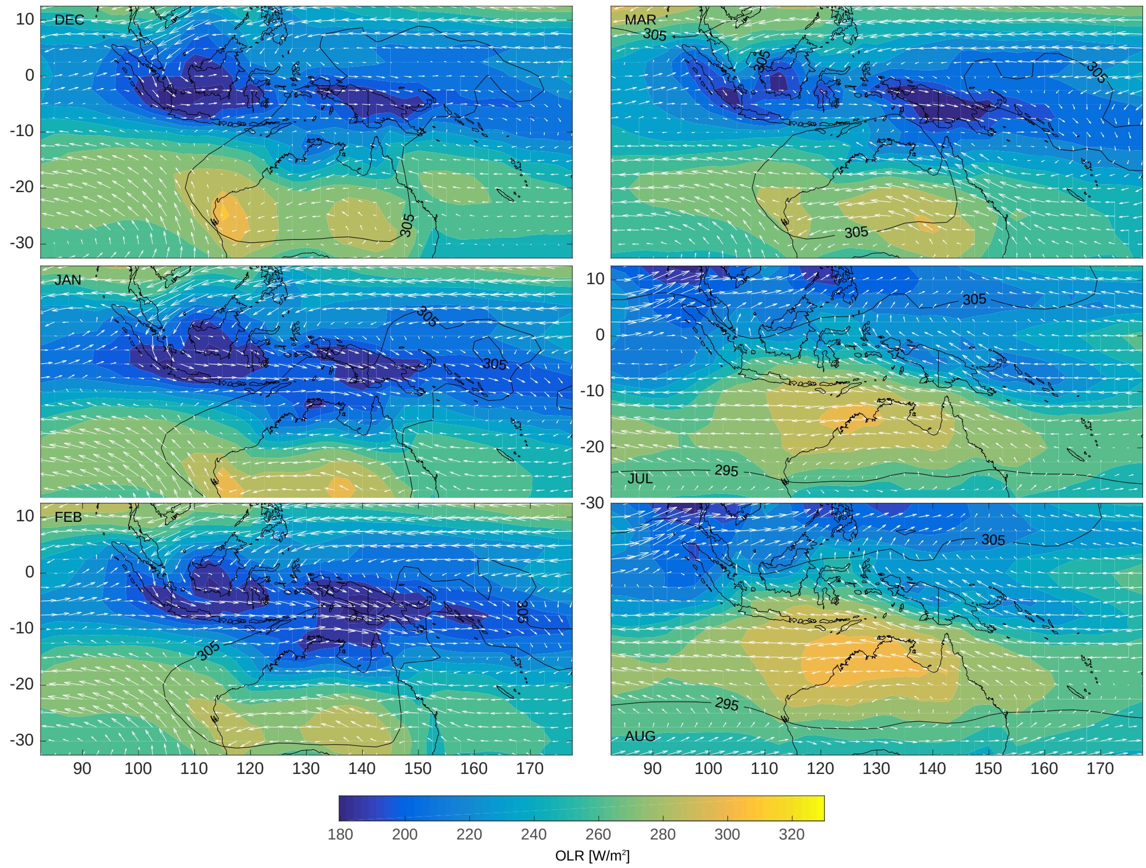

Figure 3.5: Long term (1981-2010) NCEP/NCAR average of 850hPa winds (white arrows), OLR (color) and derived θ_e (black contour lines).

3.5 Conclusions

Low isotopic values in precipitation measured on 12 hourly timescales in Darwin, northern Australia, were associated with large convective areas propagating through the region. The largest negative amplitude in the isotopic signal was observed at the intersection of eastward and westward moving precipitation systems within the convective envelope. The main drivers of isotopic variation in precipitation on these intra-seasonal timescales were found to be (i) integrated precipitation history along air mass trajectories and (ii) the extent and organisation of convective activity in the region. A local amount effect was not statistically significant on 12 hourly timescales.

OLR and regional precipitation amount show strong correlations with observed isotope ratios in rainfall in single events and in monthly GNIP isotope data, supporting the interpretation that rainfall isotopic variation on longer time scales is driven by the same meteorological factors that explain short term intra-seasonal monsoon variability. This suggests that information about the variability of the Australian monsoon can likely be inferred from the isotopic proxy records in north Australia on short (intra seasonal; speleothems, molluscan shells and coral records) and long (inter seasonal or longer; leaf waxes, sediment records) timescales.

Chapter 4

Isotopic signature of Monsoon conditions, Cloud modes and Rainfall type

C.Zwart[1,2] N.C. Munksgaard[1,2,3] Alain Protat[4] N. Kurita[5] D. Lambrinidis[3] M.I. Bird[1,2]

[1] *Centre for Tropical Environmental and Sustainability Science, College of Science, Technology and Engineering, James Cook University, P.O. Box 6811, Cairns, Australia*

[2] *ARC Centre of Excellence for Australian Biodiversity and Heritage*

[3] *Research Institute for the Environment and Livelihoods, Charles Darwin University, Darwin, Australia*

[4] *Australian Bureau of Meteorology*

[5] *Graduate School of Environmental Studies, Nagoya University, Nagoya, Japan*

Published in: *Zwart, Costijn, et al. Hydrological processes 32.15 (2018)*: 2296-2303.

Abstract

This work provides a comprehensive physically based framework for the interpretation of the north Australian rainfall stable isotope record (δ^{18}O and δ^{2}H). Until now interpretations mainly relied on statistical relationships between rainfall amount and isotopic values on monthly timescales. Here we use multi-season daily rainfall stable isotope and high resolution (10 min) ground-based C-band polarimetric radar data and show that the five weather types (monsoon regimes) that constitute the Australian wet season each have a characteristic isotope ratio. The data suggests that this is not only due to changes in regional rainfall amount during these regimes but, more importantly, is due to different rain- and cloud-types that are associated with the large scale circulation regimes. Negative (positive) isotope anomalies occurred when stratiform rainfall fractions were large (small) and the horizontal extent of raining areas were largest (smallest). Intense, yet isolated, convective conditions were associated with enriched isotope values whereas more depleted isotope values were observed when convection was widespread but less intense. This means that isotopic proxy records may record the frequency of which these typical wet season regimes occur. Positive anomalies in paleo climatic records are most likely associated with periods where continental convection dominates and convection is sea-breeze forced. Negative anomalies may be interpreted as periods when the monsoon trough is active, convection is of the oceanic type, less electric and stratiform areas are wide spread. This connection between variability of rainfall isotope anomalies and the intrinsic properties of convection and its large-scale environment has important implications for all fields of research that use rainfall stable isotopes.

Author contributions

C. Zwart developed the research question, analysed and interpreted the data and wrote the manuscript. N. C. Munksgaard and D. Lambrinidis performed the laboratory analysis. A. Protat processed the radar data. N. Kurita and M.I. Bird participated in critical discussion on development of the manuscript. All authors provided critical feedback and commented on the manuscript. Acknowledgement of Valentin Louf (Monash University) for the calibration of the CPOL data.

4.1 Introduction

Reconstructions of past monsoon conditions largely depend on the interpretation of the stable isotope proxy records that can be found in, for example, lake sediment deposits, speleothems, corals and tree rings [61, 62, 85, 89].

In tropical areas such as north Australia, the stable isotope record has been interpreted in the frame work of an 'amount effect'; a correlation based on the relationship between rainfall isotope values and amount of precipitation on monthly or longer timescales [18]. However, the timescales of the process involved in determining rainfall isotopic values vary from decades (ocean surface temperature) to seconds (cloud microphysics). Typically the statistically based 'amount effect' becomes weaker or is entirely absent on shorter timescales [see for example 20, 22, 23, 21].

Traditionally, the ISV of north Australian monsoon conditions have been interpreted as the alternating occurrence of so called monsoon 'bursts' -periods of high rainfall over the ocean associated with low-level westerly winds- and 'breaks', periods of high rainfall over land associated with moist low-level easterly winds [74, 90, 6]. More recently, [91] demonstrated that the highly variable north Australian wet season conditions can be divided into five regimes:

- Dry Easterly (DE) trade wind regime. Lower tropospheric winds are southeasterly in this regime and the moisture profile is driest compared to other regimes.

- Deep West (DW) regime, this is the active monsoon regime. Moist lower tropospheric winds (up to ≈400 hPa are westerly and the precipitable water content and humidity are highest during this regime.

- Easterly (E), this is the buildup regime, it represents the transition from tradewind (DE) to the active monsoon (DW) regime. The wind and humidity profile of this regime are similar to the DE regime but weaker/higher respectively.

- Shallow West (SW). This is a mixed inactive/break regime. The eastern part of Australia's monsoon region (see inset Figure 4.2) experiences and active monsoon during this regime but monsoon circulation over Darwin is weaker and westerly winds are shallow. Moisture profiles in the lower troposphere are wetter than the easterly regimes.

- Moist East (ME). This regime corresponds to break monsoon conditions. Zonal winds in the entire troposphere are easterly and relatively weak. Humidity profiles during this regime are higher than DE and E regimes.

Several meteorological studies have used radar reflectivity data and demonstrated that cloud, convective cell and precipitation properties, are closely linked to the above large scale circulation regimes [92, 93, 94].

The aim of this work is to link the variability of rainfall isotope composition to the intrinsic properties of convection and its large-scale environment, with a longer term scope to better interpret the paleo climate archives in north Australia and elsewhere. We use ground based radar reflectivity and climate reanalysis data to evaluate atmospheric conditions and its rainfall isotopic response in a 3.5 year daily rainfall isotope time series. The high temporal resolution of our dataset enables us to examine meteorological conditions in great detail and link cloud and rainfall types to their associated rainfall isotopic composition.

4.2 Methods

4.2.1 Rainfall sampling and isotope analysis

Accumulated 24 hourly rainfall was collected from January 2014–July 2017 near Charles Darwin University (12.37°S 130.86°E). A Palmex rainfall sampler designed to prevent sample evaporation, were used with a 14.5 cm diameter funnel. The minimum volume for sampling was 10 ml (equivalent to $\approx$ 0.5mm rain). Stable isotope analys was carried out using Picarro L2120i and L2130i instruments and autosampler connected to a diffusion sampler device [see 30]. Measurements were scaled relative to the Vienna Standard Mean Ocean Water (VSMOW) scale using 3 secondary water standards whose composition were determined relative to the certified isotope standards VSMOW, Standard Light Antarctic Precipitation (SLAP) and Greenland Ice Sheet Precipitation (GISP) by multiple analyses using Isotope Ratio Infrared Spectrometry (IRIS) and Isotope Ratio Mass Spectrometry (IRMS) at three laboratories. Precision is typically ± 0.1‰ and ± 0.5‰ for δ^2H and δ^{18}O respectively (1σ s.d.). Correlations are reported as Pearson ρ.

4.2.2 Meteorological data

Monsoon burst periods were identified following the definitions of [95] and [96]. According to these definitions a burst occurs when regional daily precipitation rate increases from below to above the long term mean within a seven day period. In their method, regional is defined as the land area covered by the rectangular box (10°-20°S, 120°-150°E, which represents the extent of the Australian summer monsoon [97], see inset of Figure 4.2), however we also included the area over the ocean as this greatly impacts coastal land points. Secondly we analysed lower tropospheric zonal wind as indicator of burst conditions analogous to Drosdowsky [90]. Era Interim reanalysis data and Global Precipitation Measurement mission (GPM) over land and sea was used to calculate regional daily (15 March 2014–28 April 2017) and long-term (1979–2009) precipitation rates.

The mean wind and humidity profiles that characterise different monsoon regimes are easily distinguished [see Figure 2 in 91, 94]. We plotted wind and humidity profiles for each day in our isotope dataset using NCEP reanalysis data. First, profiles were classified as west- or easterly by evaluating the wind direction in the lower- to mid-troposphere (1000–500 hPa). Second, the classification was subdivided into the DW/SW or DE/E/ME regimes. This was done by visually finding the closest match to the mean profiles reported by [91]. Reanalysis data and OLR were downloaded from the NOAA (`https://psl.noaa.gov/data/gridded/`, `https://www.esrl.noaa.gov/psd/`). Regional average daily OLR values were calculated by averaging daily OLR values over the above bounding box of 30°(EW)×10°(NS), centered over Darwin airport. Local rainfall statistics (station identifier 14015) as well as MJO parameters were obtained from the BoM website (`http://www.bom.gov.au/`).

Cloud- and rainfall properties were analysed using C-band radar data. The Darwin C-band-dual-polarization (CPOL) Doppler research radar is located $\approx$ 20 km from the sampling site and has a range of 150 km. The CPOL radar minimum detectable signal is -2 dBZ at 100km for the period used in this paper. The analysis has been restricted to 100km range to make sure we were able to detect 0-dBZ echo top heights at any included range. The existing 17-year radar data set was calibrated using a combination of the Relative Calibration Adjustment technique [98] and statistical comparisons with the NASA TRMM and GPM precipitation radars in space using the technique described in Warren et al. [99]. Rainfall and cloud types were classified using the method described by Kumar et al. [100]. This algorithm by Steiner et al. [101] classifies gridded radar pixels at the 2.5 km level as convective if the reflectivity value is at least 40 dBZ or greater than a threshold on the area-averaged background reflectivity.

All radar pixels above the 2.5 km level were assigned the same classification, this assumption is reasonable during convective wet season conditions in Darwin [100]. Cloud types were determined using the zero-dBZ Echo Top Height (ETH $\leq$ 6.5 km=Cumulus Congestus, 6.5 km$\geq$ ETH $\leq$ 15 km= deep convective and ETH >15 km=overshooting convective, following Kumar et al. [100]. The daily average of classified pixels (convective or stratiform) were calculated by averaging in space (over the radar domain) and time (from start to finish of isotope sampling). The duration that stratiform pixels were present in the radar domain was recorded by setting a counter while stratiform pixels were present in the radar domain and reset once the radar domain was clear.

Spectral analysis was performed on the 10-day running mean δ^{18}O anomaly (3-year mean removed) using a Lomb-Scargle Fourier transform as our data was unevenly spaced. Statistical significance was assessed by generating a red noise spectrum and confidence intervals using the program REDFIT [102].

Sea Surface Temperatures (SST) were downloaded from the Integrated Marine Observing System (IMOS) website (http://imos.org.au/sstproducts.html). Anomalies were calculated by averaging over a rectangular box (10°-15°S×127.5°-132.5°E) and subtracting the summer mean (October–May).

4.3 Results

Results will be discussed in terms of δ^{18}O only as the O and H isotope results were highly correlated (Figure 4.1b). A least square analysis of δ^{18}O and δ^{2}H of the rainfall samples resulted in a significant and strong correlation ($\rho = 0.99$, $p<0.05$). The resulting meteoric water line (MWL) is $\delta^2\mathrm{H} = 7.93\times\delta^{18}\mathrm{O} + 13.25$ ($R^2 = 0.98$ (Figure 4.1b).

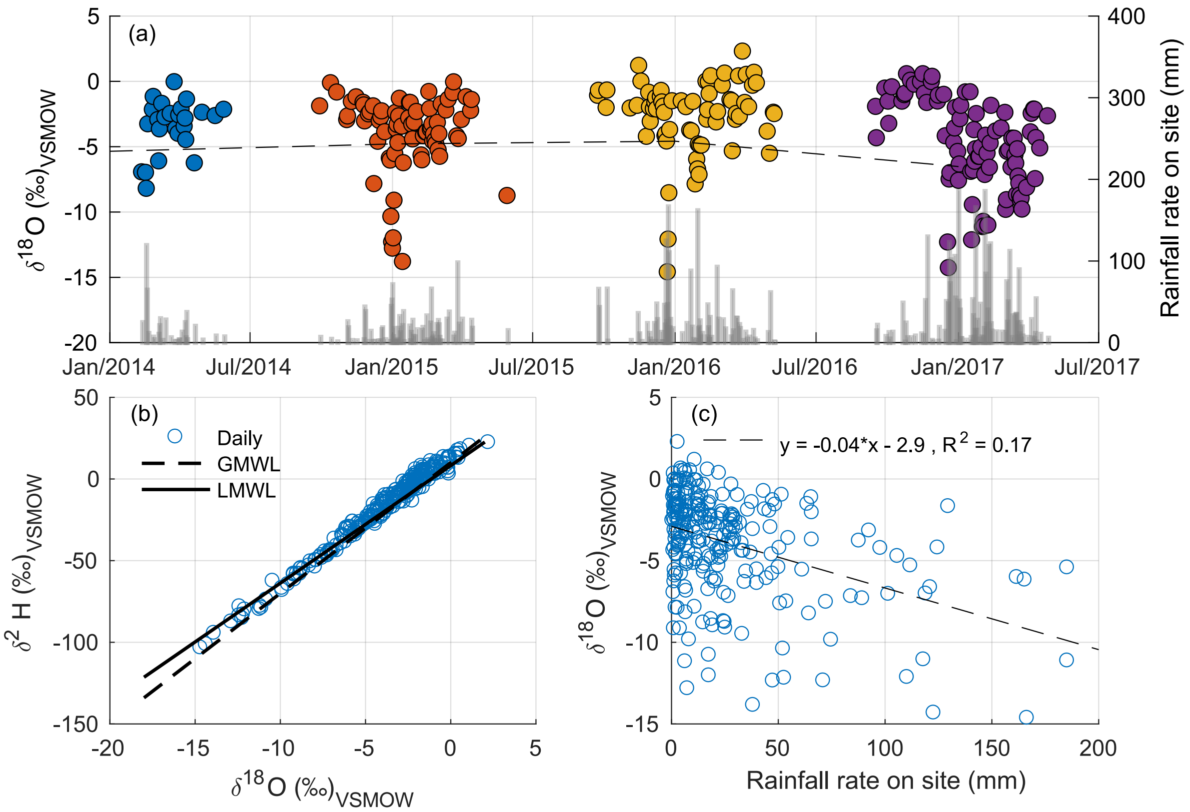

Figure 4.1: (a) Daily time series of δ^{18}O. Blue, Red, Yellow and Purple indicate season 13/14, 2014/2015, 2015/2016 and 2016/2017 respectively. Grey bars show rainfall collected over isotope sample period. Dashed line connects amount weighted seasonal means. (b) δ^2D versus δ^{18}O. Dashed and solid black lines are Global Meteoric [81] and Local [76] Meteoric Water Lines respectively. (c) Daily δ^{18}O versus rainfall collected on site.

4.3.1 Rainfall amount

Rainfall in Darwin and corresponding daily isotope values showed a strong seasonality (Figure 4.1a). Rain days during the months May to September were absent with the exception of one rain event in June 2015. The rainfall isotopic composition throughout seasons 2014/2015 and 2015/2016 and to a lesser extend in season 2016/2017 showed a distinct Y shape with enriched values at the start (September) and end (May) of the season and largest negative excursions around January/February. Minimum $\delta^{18}O$ values of ≈ -15 ‰ were reached around January in every season except for season 2013/2014, however we note that this season was incomplete as sampling only started mid January and low $\delta^{18}O$ events might have occurred earlier. The total rainfall recorded at Darwin Airport during 2014/2015 and 2015/2016 was below the long term (1961–1990) average, with season 2016/2017 showing higher than average rainfall totals [103]. The amount weighted $\delta^{18}O$ values per season remain fairly constant for the first 3 seasons and show a decrease for the 2016/2017 season (dashed line Figure 4.1a and Table 4.1).

Table 4.1: Seasonally amount weighted $\delta^{18}O$ values and accumulated rainfall amounts at the measurement site. Total sample days used for analysis n= 214, amount weighted $\delta^{18}O$ for all measurements = -5.53 [‰], amount weighted standard deviation = 3.43 [‰]. Annual mean values at bottom of table from GNIP 1962–2002, [76] and BoM (1961–1990) respectively [103].

	$\delta^{18}O$ [‰]	Rainfall [mm]	n	nr Bursts
13/14 (partial season only)	-5.35	468	25	
2014/2015	-4.79	1220	73	10
2015/2016	-4.58	1990	69	7
2016/2017	-6.52	3070	90	5
Annual long term mean	-5.27	1770		
DE	-1.86	3.4 %	9.4 %	
DW	-7.39	49.7 %	34.1 %	
E	-1.89	9.3 %	11.2 %	
SW	-3.61	19.4 %	26.6 %	
ME	-4.89	16.8 %	17.2 %	

Several peaks in rainfall coincide with large negative excursions of the isotope ratios, however a scatterplot of rainfall amount at the site (local gauge) against δ^{18}O values shows a large range of δ^{18}O values for a given rainfall amount and only a weak correlation (ρ = -0.40, p<0.05, Figure 4.1c). Regional rainfall amount shows a stronger correlation with δ^{18}O (ρ = -0.58 p <0.05 respectively).

Using the definition of monsoon bursts proposed by [95] we identified 10, 7 and 5 bursts for seasons 2014/2015, 2015/2016 and 2016/2017. Season 13/14 was excluded from this analysis as only the second half of the season was sampled. We note that due to the specifics of [95] description of a burst (see Methods), many burst-like features do not classify as bursts and would be excluded from analysis if only rainfall amount was used in the classification. Large bursts always occurred when the MJO was in phase 5 or 6. Spectral analysis of the 10-day moving average δ^{18}O anomaly shows significant peaks around a period of ≈51 days (see Figure 6.2a) which most likely reflects the influence of the MJO [32]. Other significant peaks occur around the 18- and 15-day period, with these periods attributed by [95] to the passages of extra tropical disturbances and their associated fronts.

4.3.2 Weather types

Next, we analysed the rainfall isotopic compositions of the the five different large scale circulation regimes regimes that occur in Darwin [91]. The five regimes are associated with different wind- and humidity profiles as discussed above. Large peaks in precipitation rate coincided with strong westerly winds, for example January 2015, the end of December 2015, February and March 2016 and mid December 2016 and February 2017 (Figure 4.2). Lower –than seasonal average– δ^{18}O values were observed during burst periods with westerly winds. Positive δ^{18}O anomalies were often observed when easterly winds dominated the lower troposphere.

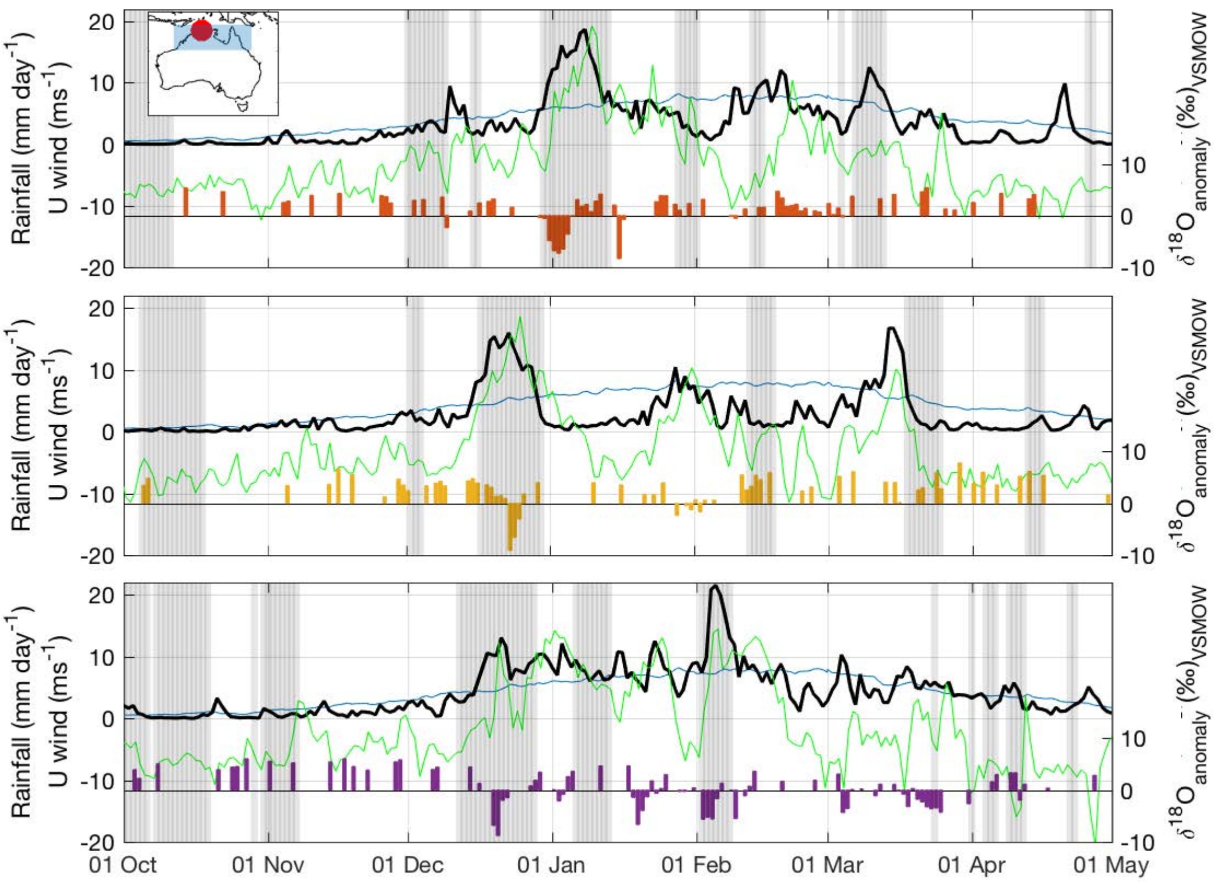

Figure 4.2: Long term climatology and regional daily precipitation rates, analogous to [95, 96]. Top to bottom season 2014/2015, 2015/2016 and 2016/2017, inset top left displays defined region and Darwin (blue shading and red dot respectively). Thin blue line: long term smoothed average (1979–2009) precipitation rate. Black line: Global Precipitation Measurement mission (GPM) regionally averaged daily precipitation rate. Green line: Era-Interim mean 850 hPa zonal wind (positive=westerly and negative=easterly). Vertical coloured (orange, ochre, purple) bars show δ^{18}O anomaly (anomaly defined as δ^{18}O - three-year mean δ^{18}O). Grey bars indicate MJO in phase 5 or 6.

$\delta^{18}O$ values clustered according to these regimes and have different amount-weighted mean $\delta^{18}O$ values (Table 4.1), the largest difference was observed between DE and DW regimes (1.6 * s.d.). $\delta^{18}O$ values also showed a robust relationship with lower to mid-tropospheric relative humidity (ρ = -0.66, $p<0.05$, Figure 4.3b) . The DW regime contributed the most rainfall to our dataset at the measurement site and showed the lowest $\delta^{18}O$ values. Rainfall totals were lowest during DE and E regimes and $\delta^{18}O$ values most enriched. Similar amounts of rainfall were recorded during ME and SW regimes and $\delta^{18}O$ values were similar during those periods and intermediate between DW and DE values. SST during the wet season showed a drop of $\approx$6°C during the transition from break to burst conditions (not shown).

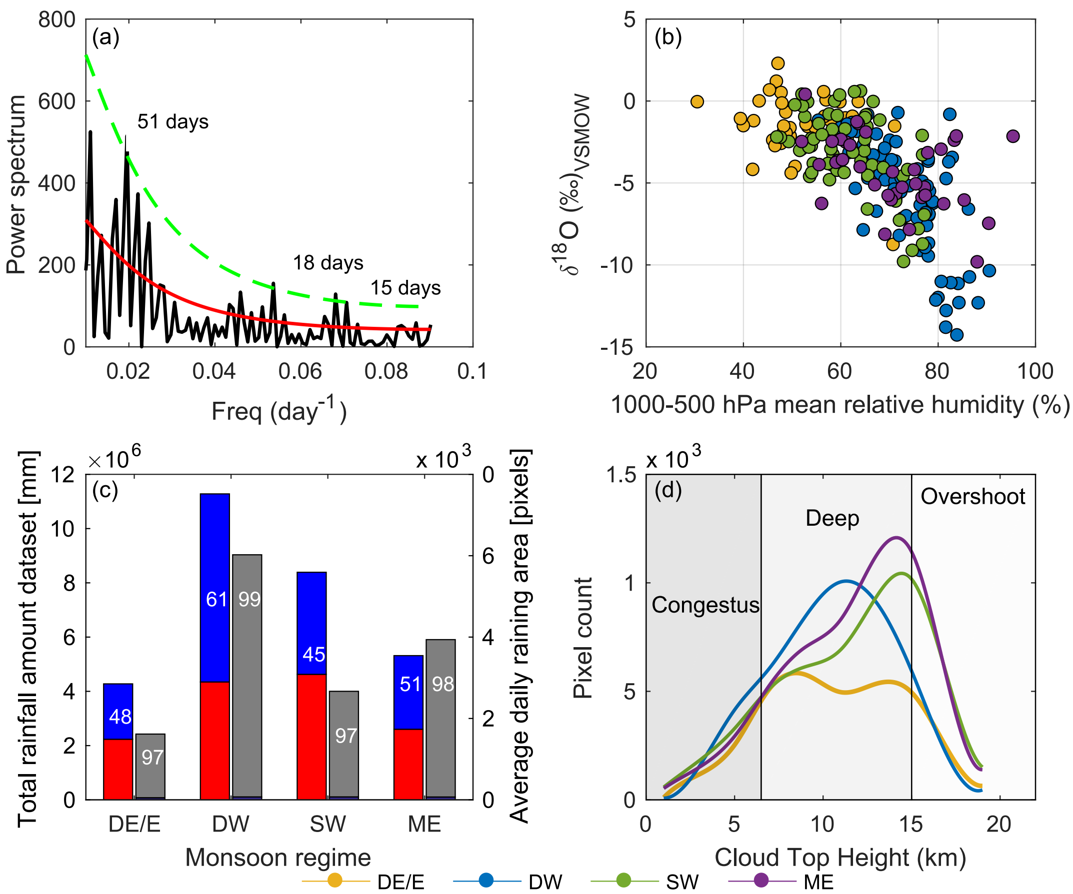

Figure 4.3: (a) Power spectrum of δ^{18}O anomaly (Lomb-Scargle, black line) with Red Noise spectrum and 90% confidence interval (red and green line respectively) generated using REDFIT [102] . (b) δ^{18}O against lower tropospheric relative humidity. Different colors represent monsoon regimes; Dry East and East (yellow), Deep West (blue), Shallow West (green) and Moist East (purple). (c) Rainfall characteristics derived from C-band polarimetric radar for different monsoon regimes. Stratiform (blue) and Convective (red) rainfall totals (whole radar-domain) per regime in dataset (left Y-axis). Black and Grey bars indicate average daily convective and stratiform raining area respectively (right Y-axis). White text indicate stratiform fraction (%).(d) Distribution of Echo Top Heights (ETH) for different monsoon regimes.

Radar derived rainfall amount, stratiform/convective fraction and raining area showed clear differences across monsoon regimes (Figure 4.3c). Our results are similar to Penide et al. [94] that used the same radar in Darwin during two wet seasons (2005/2006 and 2006/2007). We attribute small differences between their and our results to the fact that we only evaluated radar data on days when there was enough rain over our sampling station whereas Penide et al. [94] evaluated all raining days.

The DW regime corresponded to the largest precipitation area and highest rainfall accumulation in the radar domain throughout the dataset. The stratiform rainfall fraction and stratiform fraction of the raining area was also highest, 61% and 99% respectively. Lowest precipitation amount was during the DE regime which also has the lowest stratiform rainfall fraction (43%). The precipitating area of the DE regime was also lowest, however, the stratiform fraction of this area was equal to the E and SW regimes (97%). The precipitating area of the E and SW regime were similar (around 2-3$\times 10^3$ number of pixels), however the SW regime produced more than twice the amount of rain in the dataset than the E regime. Stratiform fractions were lowest for the DE and SW regimes (43 and 45% respectively) and similar for the E and ME regimes (49 and 51% respectively).

Estimated cloud top heights showed different distributions for the different monsoon regimes see Figure 4.3d. DW days show a normal distribution with a mean ETH of $\approx$11 km, reflecting dominance of deep convection in this regime whereas the DE regime shows a double peak at 7 km and 15 km respectively, the shape of the E regime is somewhat similar with a less pronounced secondary peak and higher overall pixel count. Highest counts of overshooting convection were found during SW and ME regimes.

Figure 4.4 further illustrates the different rainfall and cloud properties across the range of δ^{18}O values. δ^{18}O values showed a negative (positive) relationship with stratiform (convective) reflectivity (Figure 4.4a,b). The different regimes were scattered across the range of stratiform reflectivity (Figure 4.4a), however, highest stratiform reflectivity was observed during SW, ME and DW regimes. Increasing convective reflectivity corresponds to an increase in intensity of the convective cells and these intense convective cells were associated with higher $\delta^{18}O$ values (Figure 4.4b) . Days with low convective intensity occurred mainly during the active monsoon regime (DW) and were associated with lowest $\delta^{18}O$ values. Stratiform reflectivity and pixel count was high on these days, and stratiform pixels present in the radar domain for a longer period of time (Figure 4.4c,d). Stratiform pixel count increased exponentially as a function of stratiform reflectivity, indicating a well-developed ice phase in well organised convective systems. It is also in this higher stratiform reflectivity range (dBz > 10) that $\delta^{18}O$ values decrease rapidly.

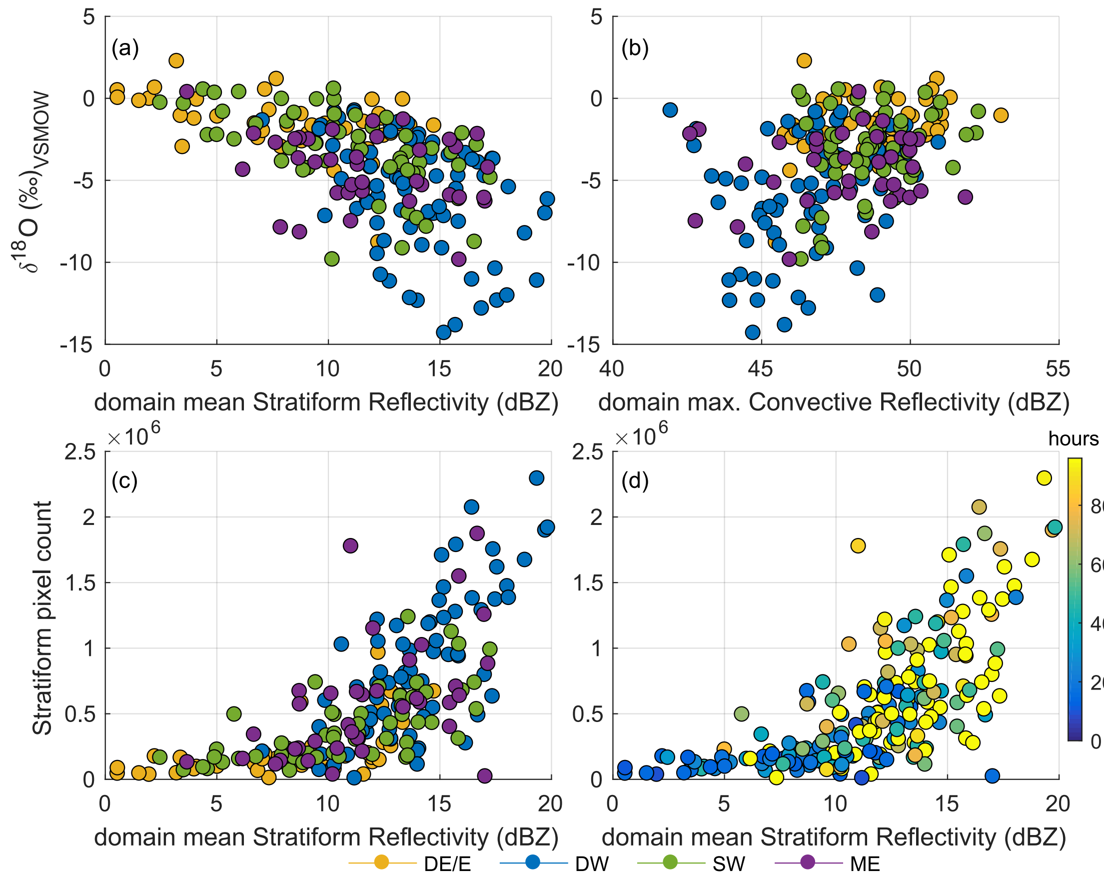

Figure 4.4: Daily $\delta^{18}O$ values against radar-domain-daily-mean stratiform (a) and radar-domain-daily-max convective (b) reflectivities at 2.5 km height. A rainfall isotope sample (coloured circle) appears in both the stratiform and convective panel at a given day. (c) Stratiform pixel count in radar-domain against domain-mean stratiform at 2.5 km, Color indicates Monsoon regime. (d) as (c) but color indicating the duration that stratiform pixels had present in radar domain at time of rainfall sampling.

4.4 Discussion

Regional precipitation amount is significantly correlated with δ^{18}O values (ρ =-0.50 p <0.05) and exhibits similar periodicities. This indicates that they share a common driver and suggests that the stable isotope record can be used as a proxy for inter annual variability of wet season precipitation amount.

The driving forces for sudden increases in regional precipitation amount in this region have been attributed to the MJO [104] and mid-latitude influences such as changes in convective instability, moisture flux and associated changes in circulation, [see 95, 96].

However the correlation between precipitation amount and δ^{18}O here and in many other studies is statistically, not physically based. This is illustrated by the strongly reduced correlation of the amount effect at short timescales as has also been observed for monsoon events in Australia [70, 23] and elsewhere [19, 33].

δ^{18}O values showed a strong link to large scale circulation regimes, indicated by robust correlations between δ^{18}O values and lower tropospheric humidity and regional cloudiness (ρ =-0.66, -0.58 p<0.05 respectively). These regimes have distinct atmospheric wind and moisture profiles [91] and the convective conditions during these regimes have been shown to be of a different kind [93]. Each monsoon regime showed distinct convective/stratiform rainfall fractions, raining area and cloud height distributions.

The influence of these regimes on the rainfall isotopic composition is illustrated by the relatively low isotopic ratios at the end of season 2016/2016. This season was not characterised by the typical 'Y' shape. We attribute this to the presence of DW, SW and ME regimes at the end of the season (from March onward), this resulted in higher than average regional rainfall and types of convection that produced relatively low rainfall isotopic ratios. In contrast, DE and E regimes were present at the end of seasons 2014/2015 and 2015/2016, producing more enriched rainfall isotope compositions.

The link between monsoon regimes and δ^{18}O values is also reflected by the specific range of δ^{18}O values that different monsoon regimes produce. The DW regime produced most rainfall and lowest δ^{18}O values in our data set and also exhibited largest stratiform areas, the DE regime produced little rainfall, highest δ^{18}O values and was associated with smaller convective systems. Similar rainfall characteristics in this region were reported by Penide et al. [94] who analysed two Australian wet seasons (05/06 and 06/07). Our results support the findings of Aggarwal et al. [41] who used monthly TRMM radar data to demonstrate a link between low rainfall isotopic values and large stratiform rainfall fractions and Kurita et al. [32] who found a relationship between low δD values and large stratiform areas.

DE and DW regimes were clearly on opposite sides of the range of isotope values but there was however also still considerable scatter within the different regimes. This scatter indicates the complexity of the interplay between regional scale process and local mechanisms that produce resulting rainfall isotope ratios. The strong depletion of ^{18}O from rain originating from matured convective systems has been attributed to the recycling of depleted vapour from aloft and upstream of the rainfall location Kurita [19] and similar results in Darwin were reported during the merging of large convective envelopes [23].

The interpretation of δ^{18}O was further illustrated by radar reflectivities. Convective cells during the active monsoon regime are often less intense and embedded in large mesoscale stratiform decks [105]. This accords with the relatively lower ETH's during the DW regimes and associated lower convective reflectivities. In general, high convective reflectivities indicate intense convection (strong updrafts and high ETH) and this was associated with smaller stratiform areas and higher δ^{18}O values.

Previous studies have provided possible explanations for the relatively high δ^{18}O values of rain originating from such convective cells: (i) a relatively short life time of these cells, this gives not enough time for a recycling process to take effect [19]. (ii) Cloud microphysics in convective cells producing different δ^{18}O values than stratiform clouds [41]. We currently do not have enough data to provide a comprehensive explanation on this subject.

Rainfall in tropical regions is a mixture of convective and stratiform contributions as stratiform clouds are essentially older convective cells where strong updrafts have ceased to exist [106]. This means that the rainfall isotopic composition that clouds produce is always a mix of these two components and scatter amongst a daily-resolved isotopic ratio. This scatter is evident in the relationship of δ^{18}O and stratiform reflectivity and can be explained as follows: as convective cells grow larger, the sampling site might receive rain from the stratiform area, however for smaller sized systems, the relative convective contribution will be larger.

We observed an increasing amount of scatter in the δ^{18}O values with increasing stratiform reflectivity and an exponential increase in stratiform area with increasing stratiform reflectivity. This illustrates the degree of organisation of the convective cells that have a well developed ice phase; as the convective cells are more developed vertically they live longer and ice particles reside longer and have more chance to aggregate, become larger and yield higher reflectivities than in smaller convective systems.

4.5 Conclusions

Five wet-season weather patterns in Darwin, north Australia showed distinct rainfall isotopic ratios. Rainfall isotopic variability was not related to local rainfall amount but to the properties of convection that are linked to large scale circulation regimes. Positive isotopic anomalies were associated with easterly and shallow westerly regimes when stratiform rainfall fractions were relatively small. The largest negative isotope anomalies were recorded during the active monsoon regime, and were associated with the passage of the MJO.

The data suggest that the isotopic proxy records in north Australia may record the frequency with which these typical wet season regimes occur. This means that positive anomalies in paleo climatic records are most likely associated with periods where continental convection dominates and convection is sea-breeze forced. Negative anomalies may be interpreted as periods when the monsoon trough is active, convection is of the oceanic type, less electric and more wide spread [93].

These results have important implications beyond the application of pelaoclimate research, such as hydrology (groundwater recharge studies) and climate modelling. For example, climate models often fail to predict correctly the variability of rainfall properties [94]. The link between the variability of rainfall properties in its large scale context and isotopic values my be used to improve cloud system parameterisations in isotope-equipped climate models.

Future work will require detailed monitoring of convective cells and the associated rainfall isotopic ratios on short timescales (continuous to minutes) to disentangle the influence of processes such as vapour recycling and cloud microphysics on the resulting rainfall isotopic composition.

Chapter 5

Stable isotope anatomy of tropical cyclone Ita, north-eastern Australia, April 2014

Niels C. Munksgaard[1,2] C. Zwart[2] N. Kurita[3] Adrian Bass[2] Jon Nott[2] M.I. Bird[2]

[1] *Research Institute for the Environment and Livelihoods, Charles Darwin University, Darwin, Northern Territory, Australia*

[2] *Centre for Tropical Environmental and Sustainability Science, College of Science, Technology and Engineering, James Cook University, Cairns, Queensland, Australia*

[3] *Graduate School of Environmental Studies, Nagoya University, Nagoya, Japan*

Published in: *Munksgaard, Niels C., et al. PloS one 10.3 (2015).*

Abstract

The isotope signatures registered in speleothems during TCs provides information about the frequency and intensity of past TCs but the precise relationship between isotopic composition and the meteorology of TCs remain uncertain. Here we present continuous $\delta^{18}O$ and $\delta^{2}H$ data in rainfall and water vapour, as well as in discrete rainfall samples, during the passage of TC Ita and relate the evolution in isotopic compositions to local and synoptic scale meteorological observations. High-resolution data revealed a close relationship between isotopic compositions and cyclonic features such as spiral rainbands, periods of stratiform rainfall and the arrival of subtropical and tropical air masses with changing oceanic and continental moisture sources. The isotopic compositions in discrete rainfall samples were remarkably constant along the $\approx$450 km overland path of the cyclone when taking into account the direction and distance to the eye of the cyclone at each sampling time. Near simultaneous variations in $\delta^{18}O$ and $\delta^{2}H$ values in rainfall and vapour and a near-equilibrium rainfall-vapour isotope fractionation indicates strong isotopic exchange between rainfall and surface inflow of vapour during the approach of the cyclone. In contrast, after the passage of spiral rainbands close to the eye of the cyclone, different moisture sources for rainfall and vapour are reflected in diverging d-excess values. High-resolution isotope studies of modern TCs refine the interpretation of stable isotope signatures found in speleothems and other paleo archives and should aim to further investigate the influence of cyclone intensity and longevity on the isotopic composition of associated rainfall.

Author contributions

Conceived and designed the experiments: NCM CZ AB JN MIB. Performed the experiments: NCM CZ AB JN MIB. Analyzed the data: NCM CZ NK. Contributed reagents/materials/analy- sis tools: NCM CZ NK AB. Wrote the manuscript: NCM CZ NK AB JN MIB.

5.1 Introduction

The use of isotopes to reconstruct long-term, high-resolution records of TCs is a relatively recent advance within the developing field of palaeotempestology. TC rainwater, compared to monsoonal and thunderstorm rain, is typically depleted in $\delta^{18}O$ and $\delta^{2}H$ due to extensive isotopic fractionation of atmospheric moisture flowing towards the TC core. To date, this fingerprint has been used to develop annual records of TCs extending back over 1500 years in Australia [107, 85] and at weekly intervals over a 26 year period in Belize [84] from cave speleothems. These records are registered following the percolation of $\delta^{18}O$ depleted rainwater through the cave roof, dissolving limestone which precipitates as generally seasonal layers of speleothem calcite between 100 and 200μm thick. The same TC isotope fingerprint is also preserved in tree ring cellulose [108] and has been used to generate tree-ring records of past TC activity over the last 200 years in the south-eastern USA [109].

While existing speleothem and tree ring isotope proxy records compare well with historical records of TCs for these regions there still remains uncertainty around the precise relationship between the isotope signature registered by the proxy and meteorological parameters of the TC. These parameters include the TC intensity, longevity of the system, distance from the sampling location to the TC eye or track and distance inland from the coastal crossing location and associated progressive weakening of system intensity and persistence of the isotopic signature within the rainfall.

Following the pioneering work in the Gulf of Mexico [110, 111, 112] there have been relatively few studies examining the isotope values of TC (or ex-TC) rainfall over a substantial portion of the life of a TC system or along the TC track [113, 69]. Of particular relevance are the characteristics of the isotope values after the cyclonic system crosses the coast and begins to weaken, as sampling locations can be some distance inland from the coast. There is also little available data on the relationship between isotope values and various structural aspects of TCs such as spiral bands and zones in between and variations in relative humidity and rainfall rates.

The energy driving the circulation of TCs is provided by the evaporation of moisture from the sea surface and the subsequent release of latent heat upon the condensation of water vapour which also generates precipitation [110]. Moisture is conveyed along the surface towards the TCs low-pressure core and inside a radius of about 100 km from the core moisture inflow is typically 10-fold greater than the moisture flux from the surface within the central area itself [114]. As a consequence, the O and H isotope anatomy of TCs is influenced not only by the physical processes within the cyclone itself but also by the moisture sources and the precipitation histories of the air masses that become entrained in the circulation system [69, 115, 116]

We present here the results of an investigation into the O and H isotope characteristics of rainfall generated during TC Ita, which made landfall in northeast Queensland on April 11th, 2014. After landfall, TC Ita travelled over land parallel to the coast and re-entered the Coral Sea $\approx$ 300 km south of its initial landfall location. Samples of rainfall were collected along the length of this track at a variety of time intervals over a two-day period. The most intense sampling was undertaken near Cairns where, for the first time, two Isotope Ratio Infrared Spectrometers (IRIS) were used to simultaneously obtain continuous real-time $\delta^{18}O$ & $\delta^{2}H$ values of both rainfall and water vapour during the approach and passage of a TC. The results allow us to draw conclusions about the characteristics of the isotope values along the cyclone track and over time after making landfall. Comparisons between isotope values and rainfall rates, relative humidity and moisture source areas were also possible. The results are important for not only understanding the isotope variability within a TC over time but also for testing specific conclusions made about a previously derived $\approx$ 800 year long TC isotope record collected close to the track of this system [85].

5.2 Observations

Tropical Cyclone Ita developed from a tropical low on 1 April 2014 over the Solomon Islands and gradually moved westward. Banding features wrapped around the circulation and deep convection became persistent by 2 April. On 10 April, Ita intensified into a Category 5 system on the Australian Scale (central pressure ≈ 930 hPa), but weakened to a Category 4 prior to landfall at Cape Flattery in North Queensland at 11 April 22:00 Australian Eastern Standard Time (AEST) (Fig. 5.1). Following landfall, Ita weakened rapidly to a Category 1 intensity with a central pressure of approx. 990 hPa and moved in a southerly direction parallel to the coast at ≈ 10 km/h. The system re-entered the Coral Sea north of Townsville early on 13 April and continued moving south-east whilst undergoing extra-tropical transition on 14 April [117, 118]. Meteorological observations, details of Cyclone Ita's track and sampling and analysis of rainfall and water vapour are summarised in Table 5.1.

Microwave and radar imaging by NASA's satellite-borne Tropical Rainfall Measuring Mission [TRMM, see 77]. show that just prior to landfall on April 11 cloud tops approached an altitude of 15 km near the eye and the most intense rainfall occurred in distinct bands up to an altitude of ≈ 6 km [119]. Land-based radar reflectivity images from the WF 100 C Band radar at Cairns [120] show that the cyclone remained relatively well structured with distinct spiral rainbands extending out to a distance of ≈ 200 km over the Coral Sea during its 36 hour transit from Cape Flattery to Townsville (Fig. 5.2). However, rainbands became poorly defined on the western side of the cyclone as it moved south.

5.3 Methods

5.3.1 Continuous sampling

Isotopic $\delta^{18}O$ and $\delta^{2}H$ values of rainfall were measured continuously at Trinity Beach, Cairns (Lat. 16°47.5' S, Long. 145°41.8' E, altitude 20 m above mean sea level (AMSL)) from April 10-13 2014 using Diffusion Sampling - Cavity Ring-down Spectrometry (DS-CRDS) [30] with addition of thermo-electric control of air and water inlet temperature for enhanced suppression of temperature dependent drift. This system continuously converts rain water into water vapour for real-time stable isotope analysis by a Picarro L2120-i CRDS analyser at 30 s intervals. A total of 1612 30 s measurements of rainfall isotopic composition were acquired during the 28 hour period of rainfall associated with Cyclone Ita. Rainfall was collected on a 0.64 m^2 inclined metal sheet connected to a small receptacle (≈15 ml volume) fitted with a float switch which automatically switched between pumped sampling of rainwater from the receptacle (during rainfall) and reference water (between rainfall) [30, 70]. With a sample uptake of 2.5 ml min^{-1} the collection system provides sufficient rainwater for continuous time-based analysis at a constant rainfall of<1 mm $hour^{-1}$. This design ensures that the receptable volume is rapidly exchanged as rainfall in excess of the pump uptake rate flushes the receptable and flows to waste. However, where rainfall is intermittent the rainfall data may be truncated as 5–10 minutes is required for the isotope measurement to stabilise following a switch from reference water to rainfall.

The raw isotope data was downloaded from the analyser as 30 s average values and corrected for drift by referencing each sample value to two bracketing reference water values. To eliminate memory effects between rapidly changing isotopic compositions, data were omitted from the final results where changes between 30 s values exceeded conservative thresholds limits of 0.2‰ for $\delta^{18}O$ or 1‰ for δ^2H which represent the maximum rate of compositional change that can be captured by the DS-CRDS system. Isotopic compositions are given in the standard δ notation, e.g. $\delta^{18}O= [(^{18}O/^{16}O_{sample}$ - $^{18}O/^{16}O_{standard})$ / $^{18}O/^{16}O_{standard}]$ x 10^3. Three water standards were analysed three times during the 60 hour observation period through the rainfall uptake system: Lake Eacham Water ($\delta^{18}O$= +0.88 ‰; δ^2H = +3.7 ‰), Evian Water ($\delta^{18}O$= -10.64 ‰; δ^2H = -71.5 ‰) and Casey Snow Melt ($\delta^{18}O$= -18.36 ‰; δ^2H = -140.4 ‰). The isotopic compositions of these standards were determined by WS-CRDS vaporisation analysis (Picarro L2120-i and A0212) and calibrated against the certified IAEA references waters VSMOW, GISP and SLAP. Isotope data precision at a 30 s integration time was typically <0.2 ‰ for $\delta^{18}O$ and <0.6 ‰ for $\delta^{2}H$ (1SD). Instrumental drift of the L2120i analyser is expected to be < 0.6 ‰ and <1.8 ‰ over a 24-hour period for $\delta^{18}O$ and $\delta^{2}H$, respectively [121]. Rainfall intensity was monitored using an Onset HOBO RG3-M logging rain gauge located at James Cook University 2 km from the Trinity Beach site.

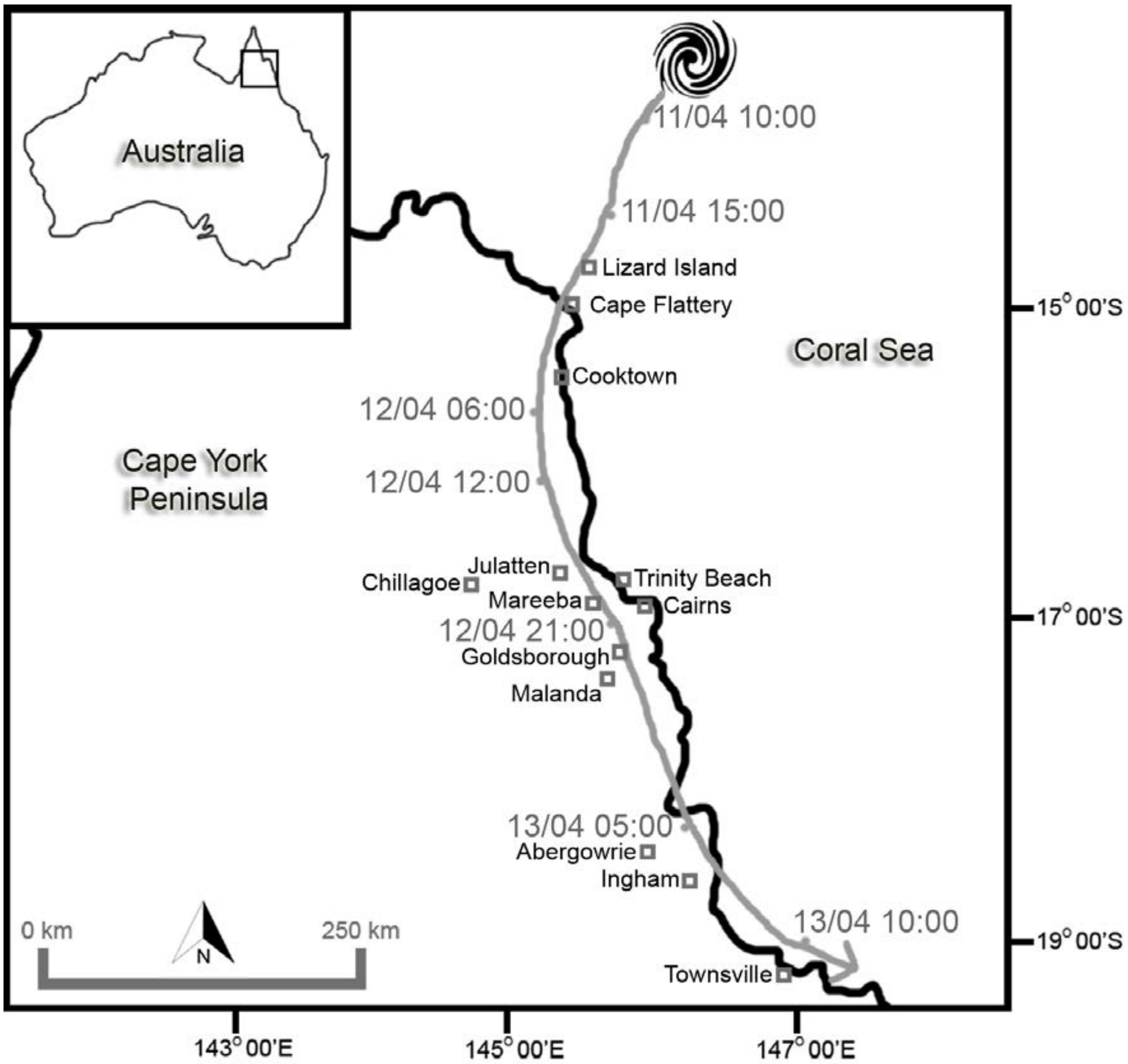

Figure 5.1: Sampling locations and track of TC Ita April 11 to 13, 2014 [117, 118]

Table 5.1: Sampling, analysis and meteorological observations of Cyclone Ita. Data from Bureau of Meteorology [117] with the exception of Lizard Island data [122]. RF and V denotes rainfall and vapour sampling, respectively. *: '-' and '+' indicates land and ocean side of cyclone track, respectively.

Site	Time of closest approach (AEST)	Distance to eye (km)	Minimum pressure at site (hPa)	Movement of cyclone (km/hour, direction)	Sampling and analysis
Lizard Island	11/04/2014 19:00	0 to +5	954	18, SW	none
Cape Flattery	11/04/2014 22:00	0 to +5	963	12, SSW	none
Cooktown	12/04/2014 2:00	0 to +15	975	10, S	RF at 2 sites (n = 15)
Julatten	12/04/2014 16:00	+5 to +10	No data	10, SE	RF at 2 sites (n = 7)
Cairns area	12/04/2014 19:00	+15 to +20	997	10, SSE	Real-time RF and V analysis at 1 site, RF sampling at 8 sites (n = 34)
Mareeba	12/04/2014 19:00	-15	998	10, SSE	RF at 1 site (n = 21)
Goldsborough	12/04/2014 20:00	-10	No data	10, SSE	RF at 1 site (n = 4)
Malanda area	12/04/2014 22:00	-15	No data	15, SSE	RF at 4 sites (n = 17)
Abergowrie	13/04/2014 5:00	-30	No data	18, SE	RF at 1 site (n = 4)
Ingham area	13/04/2014 6:00	-10 to-20	No data	18, SE	RF at 2 sites (n = 10)
Townsville	13/04/2014 10:00	-15 to-30	997	21, SE	RF at 5 sites (n = 23) area

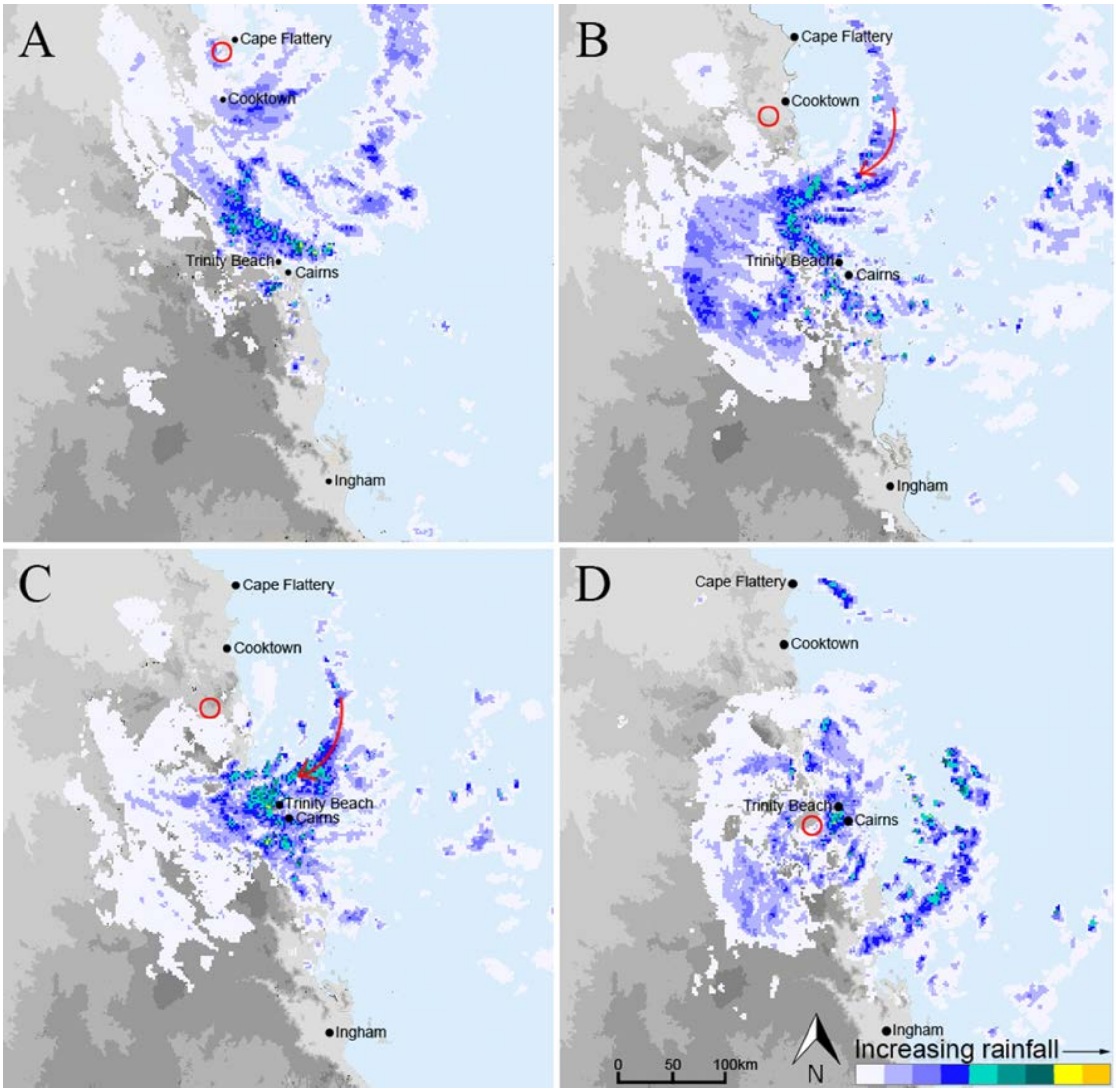

Figure 5.2: Radar images of TC Ita at 11/4 22:10 AEST (A), 12/4 07:20 AEST (B), 12/4 09:50 AEST (C), 12/4 20:00 AEST (D) [18]. Figure is for representative purposes and is similar but not identical to the original image. The approximate position of the eye of the cyclone is indicated by a red circle. The red arrows indicate a spiral rainband with intense rainfall with the most depleted isotopic composition.

Water vapour $\delta^{18}O$ and $\delta^{2}H$ values were measured continuously at Trinity Beach using a Picarro L2130-i WS-CRDS. Water vapour isotopic composition was measured at 1 s intervals during the 59 hour approach and passage of Cyclone Ita. Ambient air was introduced to the instrument via a 6 m length of 3.2 mm internal diameter FEP tubing with the inlet located 3 m above ground level under an elevated building and well shielded from ingress of rain. Raw isotope data was downloaded as 30 s average values and scaled to the Vienna - Standard Mean Ocean Water (V-SMOW) using data for water vapour derived from the same three water standards used for scaling the rain fall data. The water standards were quantitatively converted to water vapour using an LGR Water Vapor Isotope Standard Source (WVISS) [123] connected to the Picarro L2130-i analyser before and after the 60 hour observation period. Isotope data precision when analysing a constant vapour source was typically <0.1 ‰ for $\delta^{18}O$ and <0.2 ‰ for $\delta^{2}H$ (1SD) at a 30 s integration time. Instrumental drift of the L2130i analyser is expected to be < 0.2 ‰ and < 0.8 ‰ over a 24 hour period for $\delta^{18}O$ and $\delta^{2}H$, respectively [121].

5.3.2 Discrete sampling

Discrete samples (n=135) of rainfall were collected by volunteers at 27 sites between Cooktown and Townsville (Table 5.1, Fig. 5.1, S1 Dataset). At some sites rainfall was collected from roof down pipes (i.e. near-instantaneous grab samples) or from accumulated rainfall in buckets placed on open ground and emptied at ≈ 1 hour intervals. At other sites rainfall was accumulated in buckets for ≈ 12 hours with scheduled sampling times at 7am and 7pm (AEST). No rainfall samples were obtained from the sparsely populated area west of the narrow coastal strip along TC Ita's track (Fig. 5.1).

Samples were analysed using the diffusion sampling WS-CRDS system connected to an auto sampler and scaled to VSMOW as described for the continuous rainfall analysis.

5.3.3 Synoptic conditions

The Japanese 55-year reanalysis project (JRA-55) dataset [124] were used to examine synoptic scale weather conditions. The JRA-55 data are on a horizontal 1.25 x 1.25 degree grid with 37 vertical layers from 1000 to 1 hPa. By using this data, we calculated the vertically averaged (925-850 hPa) equivalent potential temperature (θ_e) and vertically integrated (surface to 300 hPa) horizontal water vapor flux (vectors: kg m^{-1} s^{-1}).

5.3.4 Air-mass trajectories

Synoptic scale back-trajectories of air-masses at an altitude of 500 m AMSL were calculated at 6 hourly intervals using HYSPLIT [80] with Global Data Assimilation System (GDAS1) data [125] Time series of vertical wind and humidity profiles for the Trinity Beach measurement site were also based on data obtained from GDAS1 [125].

5.4 Results and Discussion

5.4.1 Rainfall amount and intensity

The total recorded rainfall associated with Cyclone Ita was 198 mm at Cooktown and 211 mm at Townsville [126]. At Trinity Beach we recorded a total rainfall of 231 mm with a rainfall intensity of 7.4 mm $hour^{-1}$ for the continuous rain period from April 11 17:11 to April 13 0:39 (AEST). This intensity slightly exceeds the maximum intensity of 7 mm $hour^{-1}$ recorded for category 1-2 cyclones in a microwave imaging survey of 260 TCs globally [127]. The peak rainfall intensity, recorded during the passage of an inner spiral rainband, was $\approx$ 13 mm per 10 minutes at Trinity Beach.

5.4.2 Rainfall isotopes - spatial distribution

The systematic distribution of isotope compositions of rain and vapour within TCs and the direct link between isotope compositions and the physical processes of evaporation and condensation enables O and H isotope compositions to be used as tracers of the dynamics and structural evolution of TCs [110, 69]. Rainfall associated with TCs is usually characterised by $\delta^{18}O$ and $\delta^{2}H$ values that are distinctly lower than other tropical rain systems and the isotopic values generally decrease inward towards the core of the cyclone [110, 113, 115]. For example, $\delta^{18}O$ values in discrete rainfall samples from five TCs in the western Gulf of Mexico ranged from -3.9 to -14.3 ‰ and all samples taken within 100 km of the cyclone eye had $\delta^{18}O$ values $<$ - 8.7 ‰ [110]. In the Western Pacific, Typhoon Shansan yielded $\delta^{18}O$ values from $\approx$ -4 to -14 ‰ and $\delta^{2}H$ values from $\approx$ -20 to -100 ‰ with the lowest values recorded in close proximity to the advancing eye wall of the cyclone [113]. Airborne sampling of TCs has also yielded low isotope ratios in both rain and vapour at altitude [115, 128]. However, in very intense cyclones, the lowest isotope ratios in rain occurred between 50 and 250 km from the eye while isotope ratios were higher in the eye wall due to the incorporation of vapour derived from sea spray [115].

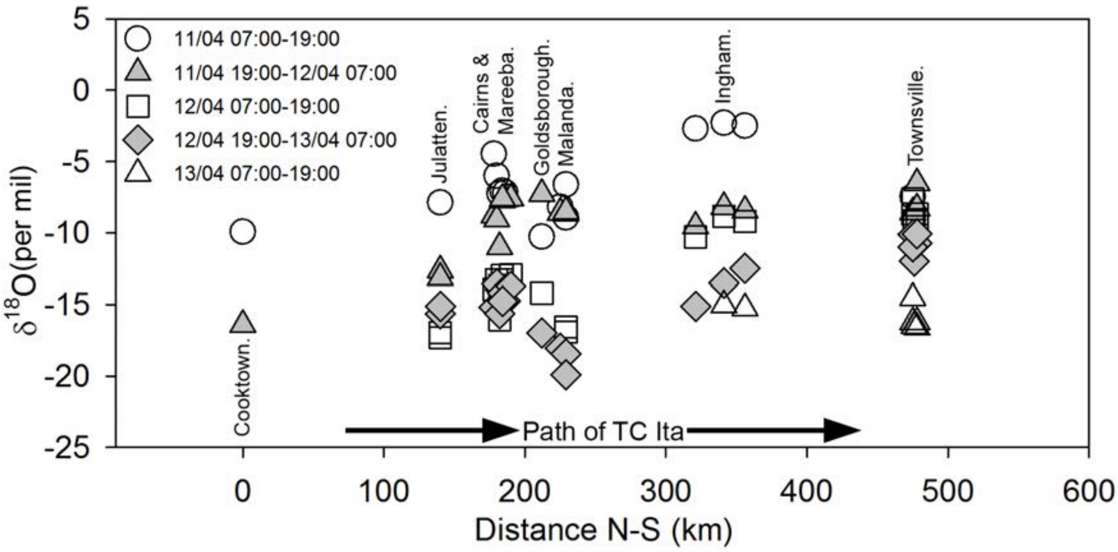

Figure 5.3: $\delta^{18}O$ values in discrete 12 hour rainfall samples (n=85) collected from 27 sites during the north to south passage of TC Ita from April 11–13, 2014.

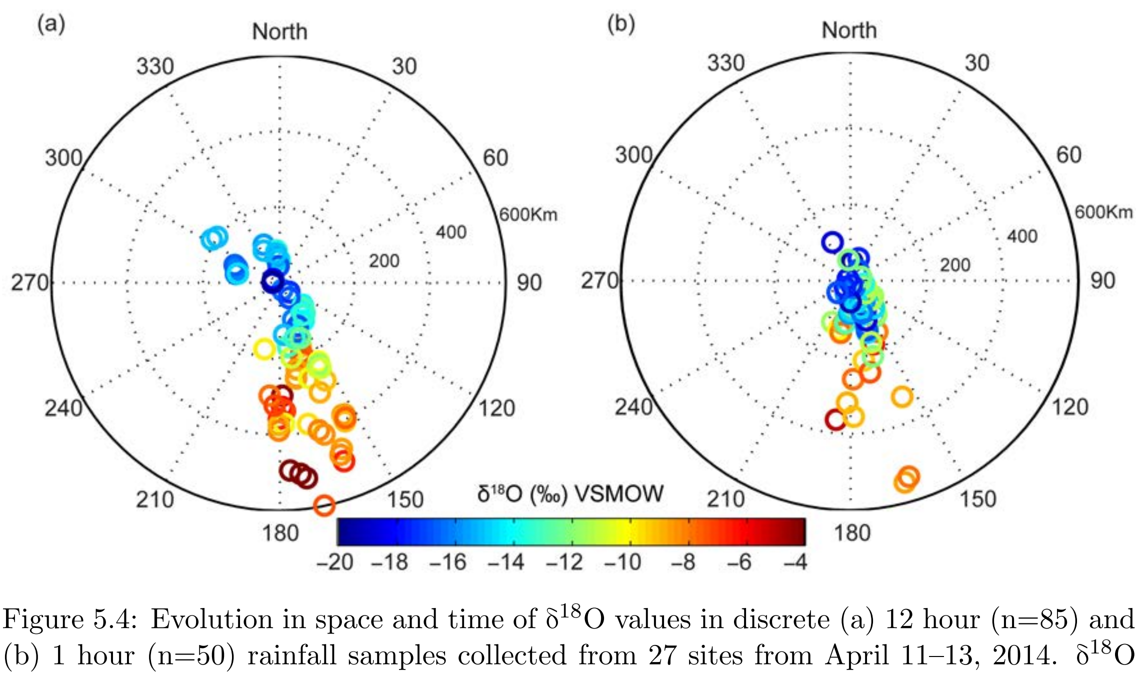

Figure 5.4: Evolution in space and time of $\delta^{18}O$ values in discrete (a) 12 hour (n=85) and (b) 1 hour (n=50) rainfall samples collected from 27 sites from April 11–13, 2014. $\delta^{18}O$ values of samples taken at different times are shown as a function of distance and direction from the eye of TC Ita (at centre of plot) at the time of sampling. Some plot positions were moved slightly in order to separate overlapping data.

In cyclone Ita the amount-weighted mean isotopic compositions of rainfall at the continuous measurement site at Trinity Beach were δ^{18}O= -10.2 ‰ δ^{2}H = -67 ‰ (n = 1612) in a total rainfall of 231 mm. The range of isotopic values in rainfall was -4.8 to -20.2 ‰ for δ^{18}O and -25.4 to -142 ‰ for δ^{2}H whilst the lowest values recorded for a 12 hour cumulative sample were δ^{18}O= -19.9 ‰ and δ^{2}H = -147 ‰ at Malanda. Due to the high condensation efficiency of the converging surface inflow of moist air masses in TCs the mean isotopic values of TC rainfall can be expected to approach the surface vapour values [110]. This is borne out by the mean δ^{18}O and δ^{2}H values in TC Ita rainfall which was only slightly higher than the inter-quartile ranges of δ^{18}O and δ^{2}H values ($\approx$ -11 to -13 ‰ and -75 to -90 ‰ respectively) of western Pacific Ocean surface vapour at latitudes of 5 to 25°S [19].

While the mean and minimum δ^{18}O and δ^{2}H values in rainfall during TC Ita are amongst the lowest recorded for a range of different weather systems passing Cairns, a previous convective rainfall event (43 mm total rainfall) associated with the over-land migration of the monsoon trough (Inter-Tropical Convergence Zone) produced mean isotopic values of δ^{18}O = -13.8 and δ^{2}H = -97 [70] However, large rainfall amounts (e.g. > 100 mm) with relatively low, but variable, isotopic values are likely to be uniquely associated with TCs [110].

The distribution of δ^{18}O and δ^{2}H values in discrete rainfall samples from TC Ita are strongly correlated along the Global and Local Meteoric Water Lines (S1 Dataset); the data will be discussed with reference to δ^{18}O values only. The evolution in space and time of δ^{18}O values in the 12-hour discrete rainfall samples collected at 27 sites along the path of TC Ita is shown in Fig. 5.3. The sampling sites covered a distance of approx. 450 km between Cooktown and Townsville and all were within $\approx$ 30 km of the track of the eye of the cyclone (Table 5.1). It is seen that the range, and progression with time, of isotopic values were similar at all sites as the cyclone approached and passed each site. However, lower minimum δ^{18}O values were recorded at the sites at highest altitude (Malanda at $\approx$750 m AMSL $\approx$ -18 to -20 ‰) compared to sites near sea level (Cairns, Ingham and Townsville $\approx$ 16 to -17

‰. The clear radial distribution of $\delta^{18}O$ values with $\delta^{18}O < -12$ ‰ in all samples collected within 150 km of the eye and, with two exceptions, all $\delta^{18}O$ values < -8 ‰ within a distance of 400 km from the eye is shown in Fig. 5.4. Three samples collected more than 500 km to the south of the eye of the cyclone had $\delta^{18}O$ values > -4 ‰ and represent rainfall prior to the influence of the cyclone. Deuterium excess values ($d = \delta^2H - 8 * \delta^{18}O$, S1 Dataset) varied between +6.5 ‰ and +20.8 ‰ (mean = +14.7 ‰) in the discrete rainfall samples but did not vary systematically with distance to the eye of the cyclone.

The data presented in Figs. 5.3 and 5.4 demonstrate the similarity in the evolution of the isotopic composition of rainfall at all sampling sites as they were approached and passed by TC Ita and indicate that the structure of the cyclone, its moisture and energy sources remained relatively constant during its 30 hour passage over land. It is likely that the proximity of the track to the coast (< 50 km inland) allowed sufficient inflow of warm and moist oceanic air masses to sustain the energy requirement of the cyclone. This is supported by the cyclone's intact circular structure as revealed by radar reflectivity maps (Fig. 5.2a-d) with distinct rainbands on the ocean-ward side as it tracked south whilst the landward side was relatively poorly defined.

5.4.3 Continuous measurement of rainfall and water vapour isotopes

The high resolution isotope data for rainfall and vapour obtained at Trinity Beach enabled the various influences on the stable isotope evolution of TC Ita to be distinguished.

Rainfall intensity, $\delta^{18}O$, δ^2H and deuterium excess values are shown in Fig. 5.5 which also shows the air pressure recorded at nearby Cairns Airport [126]. The data set is provided in S2 Dataset. In addition, the isotope data is interpreted with reference to radar images (Fig. 5.2) and time series of modelled GDAS-1 wind and moisture profiles at Trinity Beach (S1 Fig.). Furthermore, regional scale airmass movements were derived using 48 hour HYSPLIT air-mass back-trajectories (S2 Fig.), and JRA-55 regional maps of equivalent potential temperature (θ_e) and vapour flux (S3 Fig.). It is noted that the 1.25 degrees grid resolution of JRA-55 and GDAS-1 data precludes a reliable analysis of air-mass trajectories close to the cyclone core. Fig. 5.5 includes isotopic values in 1 hourly accumulated rainfall samples collected at Trinity Beach during part of the measurement period for comparison to the continuous monitoring data.

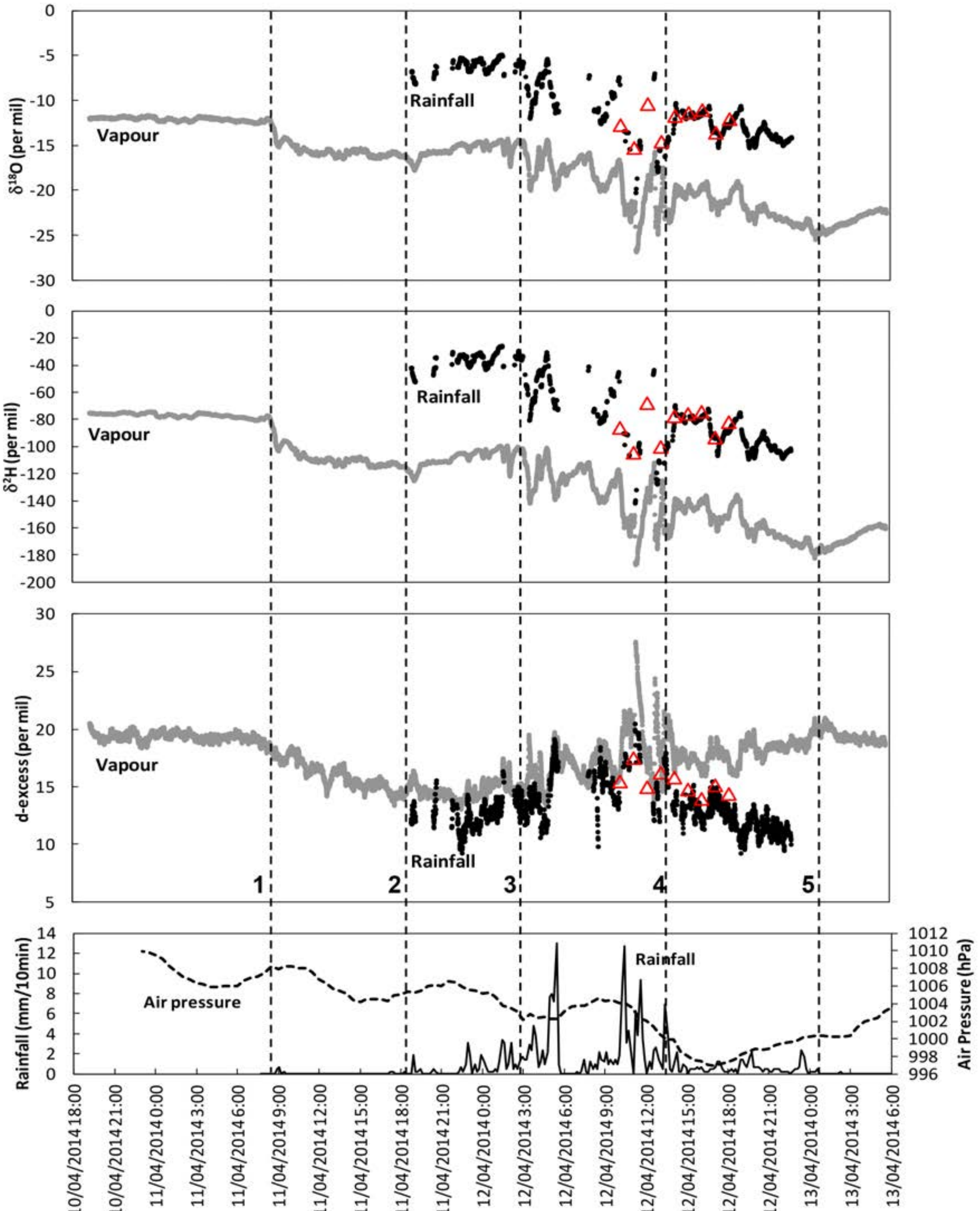

Figure 5.5: $\delta^{18}O$, $\delta^{2}H$ (30 s interval) and d-excess (moving average of five 30 s data points) in water vapour and rainfall and air pressure and rainfall intensity at Trinity Beach. Red triangles indicate values of discrete 1 hour rainfall samples from Trinity Beach. Time markers: 1: First influence of cyclonic circulation; 2: Start of main rain event; 3 to 4: Spiral rain band activity; 5: End of rain event.

The most notable features of the continuous vapour and rainfall isotope data associated with TC Ita are (numbered list corresponds to markers '1' to '5' in Fig. 5.5):

1. A rapid decrease of the vapour δ^{18}O and δ^{2}H values and the commencement of a gradual decrease in vapour d value commenced at ≈ 9:00 AEST on April 11 coinciding with a short rainfall event (insufficient amount for isotope analysis of rain). The eye of the cyclone was located ≈ 370 km to the north over the ocean at this time. HYSPLIT back trajectories show the commencement around this time of an anti-clockwise shift in the source area of air-masses arriving at Trinity Beach. θ_e and vapour flux maps show that warm, moist air mass arrived from the northeast around this time.

2. The commencement of the main rainfall event (and the start of rainfall isotope measurement) at ≈ 18:00 AEST on April 11. The vapour δ^{18}O, δ^{2}H and d values were relatively constant for several hours around this time. The eye of the cyclone was close to the coastline (Fig. 5.2a). Air-mass back trajectories show that the air-mass source area continued to move anti-clockwise over the Coral Sea.

3. The commencement at ≈ 3:00 AEST on April 12 of the arrival of inner spiral rainbands marked by rapid decreases in δ^{18}O and δ^{2}H values in both rainfall and vapour and coinciding with intensifications of rainfall (Fig. 5.2c). d values in both vapour and rainfall started to increase around this time. The eye of the cyclone was located ≈ 150 km to the northwest over land. Wind speed and relative humidity increased significantly above a height of ≈ 950 hPa. The area of highest θ_e was centred north of the Trinity Beach measurement site and air-mass back trajectories show air in-flow from this region of highest θ_e values.

4. The cessation of rainband activity at ≈ 14:00 AEST on April 12. At this time δ^{18}O and δ^{2}H values rose rapidly in rainfall but not in water vapour and a

divergence of d values in vapour (continuing to increase) and rainfall (starting to decrease) commenced. The eye of the cyclone was located ≈ 60 km to the north-west over land at this time. Within the following 2-3 hours the minimum air pressure (997 hPa) was recorded at Trinity Beach and the wind direction changed towards north-westerly as the eye of the cyclone passed ≈ 20 km to the west at ≈ 18:00 AEST (Fig. 5.2d). Moisture levels decreased and arriving air-masses were now tracking over the landmass of Cape York Peninsula.

5. The cessation of rainfall associated with the cyclone at ≈ 00:00 AEST on April 13. This was marked by the commencement of rising vapour δ^{18}O and δ^{2}H values. The eye of the cyclone was located ≈ 80 km to the south at this time. Consequently, wind direction gradually changed towards westerly with air masses tracking clockwise over the coastal ranges to the south before descending from the land side towards the Trinity Beach measurement site.

The pronounced parallel tracking of isotopic values in rainfall and vapour in TC Ita during much of the period of rainfall in the advancing front of the cyclone is reflected in strong correlations between δ^{18}O and δ^{2}H values in rainfall and vapour ($R^2 = 0.97$ for both δ^{18}O and δ^{2}H). This correlation reflects a highly efficient isotopic exchange between rainfall and vapour in a saturated atmosphere. It is notable that vapour isotopic composition prior to the commencement of rainfall remained almost unchanged after rainfall commenced and during the first 8-9 hours of rainfall (Fig. 5.5 markers '1' to '3'). This suggests that the vapour isotopic values measured at ground level until ≈ 3:00 AEST on April 12 were broadly representative of the surface layer inflow. During this period the mean difference in isotopic composition of rainfall (δ^{18}O = -6.0 ‰ δ^{2}H = -36 ‰) and water vapour (δ^{18}O = -15.3 ‰ δ^{2}H = -108 ‰), i.e. $\delta^{18}O_{rain-vapour}$ = 9.3 ‰ $\delta^{2}H_{rain-vapour}$ = 72 ‰ corresponded closely to the equilibrium liquid-vapour fractionation ($10^3\ln\alpha_{l-v}(^{18}O)$ = 9.2– 9.4, $10^3\ln\alpha_{l-v}(^{2}H)$ = 74–77 [129] within the range of surface temperature observed at Trinity Beach during TC Ita (24.5–26.5 °C).

The rapid decrease of vapour δ^{18}O and δ^{2}H values ≈ 9:00 AEST on April 11

(Fig. 5.5, marker '1') coincided with the arrival of a tropical air mass with high θ_e value. The decrease of $\delta^{18}O$ and $\delta^{2}H$ values in this tropical air mass is consistent with previous isotope data collected along 20 oceanic transects over a 4-year period which showed that isotopic values of surface vapour in the tropics is significantly lower than those in the subtropics [19].

The rapid decrease in $\delta^{18}O$ and $\delta^{2}H$ values of both rainfall and vapour from $\approx$ 3:00 to 14:00 AEST on April 12 (Fig. 5.5, markers '3'-'4') were associated with the arrival of an inner spiral rainband. This rainband was sustained for several hours and included several convection cells with anvil stratiform rainfall regions expanded towards the outside of the core by the tangential winds (see radar reflectivity maps in Figs. 5.2b and 5.2c). It has previously been shown that stratiform rain in hurricanes (cyclones) has significantly lower isotope ratios than convective rain as a result of its higher mean altitude of condensation and larger percentage of precipitation derived from great heights [115]. In the inner spiral rainbands of cyclones there is a successive cycling of moisture through subsidence under stratiform rainfall and transport of isotopically depleted vapour into the lower troposphere and towards the TC center where it is reused in subsequent convective condensation-precipitation cycles [19, 48, 32]. Consequently, the isotopic composition of precipitation becomes gradually depleted towards the TC center as the contribution of recycled water increases along the rainband. As the eye of the cyclone approached the Trinity Beach measurement site, the cycling of moisture through successive rainfall events along the upstream region of the spiral band ceased and thus the $\delta^{18}O$ and $\delta^{2}H$ values in rainfall rapidly increased (just prior to marker '4' in Fig. 5.5). In contrast, this rapid increase was not seen in vapour.

The general trends of $\delta^{18}O$ and $\delta^{2}H$ values in rainfall and vapour continued to decrease after the main rainband passed Trinity Beach $\approx$ 14:00 AEST on April 12 (Fig. 5.5, markers '4' to '5') and after the passage of the core of TC Ita to the west (marked by the minimum recorded air pressure, Fig. 5). As the TC moved further south the air mass reaching Trinity Beach after 14:00 AEST on April 12 passed over the coastal ranges to the south in a clockwise rotational motion over the landmass of Cape York Peninsula. This low-level flow passed through the upstream region of the spiral rain band (positioned to the south of Trinity Beach at this time, Fig. 5.2d) and may have transported moisture with low δ values and high d value derived from the air mass subsidence under stratiform rainfall regions. An additional contributing factor to the observed lowering of δ values may have been the addition of land-derived moisture which was derived from earlier low-δ precipitation in the advancing front of TC Ita itself.

5.4.4 Deuterium-excess

The d value in water vapour is often used as a tracer of moisture origin because the d value of moisture evaporated from the oceanic surface depends on surface humidity, temperature and wind speed [116, 44, 130] with humidity the most important factor. The d value decreases with increased relative humidity over the ocean and with decreasing temperature of the ocean surface. In the tropics, increases in surface vapour d values may also indicate subsidence of air from the upper troposphere [19, 32]. The production of precipitation from water vapour essentially conserves the d value [18] although falling raindrops may partially evaporate or re-equilibrate isotopically with surrounding vapour during descent [131, 132].

The decrease in d values (Fig. 5.5 markers '1' to '2') in vapour at Trinity Beach as the outer circulation envelope of TC Ita approached can be attributed to the accelerating inflow of moisture derived from evaporation of surface waters at high relative humidity and temperature as indicated by high θ_e values (S3 Fig.). However, as TC Ita approached the measurement site rainfall intensified and d values in both vapour and rainfall increased (Fig. 5.5, markers '3' to '4'). Previous simulations of the isotopic evolution of hurricanes (cyclones) have shown that d values in rainfall increase near the eye although the simulated d values were lower than observed during TC Ita [115]. In addition, similar increases in d values, accompanied by decreasing $\delta^{18}O$ and $\delta^{2}H$ values has been observed during the active convective phase of MJO in the tropical atmosphere [32]. They highlight the role of vapour recycling due to the subsidence of air masses from stratiform clouds. Because the lowest δ^{18}O and δ^{2}H values during TC Ita corresponded to the successive linked convective-stratiform rainfall events (Fig. 5.2b-c and Fig. 5.5), the large increase of d values may be attributed to downward moisture transport above the boundary layer.

A marked divergence in the d values of vapour and rain occurred from $\approx$ 14:00 AEST on April 12 (Fig. 5.5 marker '4') and continued after the passage of the eye of TC Ita. The divergence in d values indicates that moisture sources were different for precipitation and surface vapour. As described above air masses that arrived after 14:00 AEST ascended the coastal mountain range south of the measurement location, travelled in a clockwise direction across the hinterland and descended the ranges towards the Trinity Beach measurement site. We surmise that the low-level air flow through the upstream region of the spiral rain band (positioned to the south of Trinity Beach at this time, Fig. 5.2d) supplied surface moisture with low δ values and high d values whereas precipitation from higher levels was becoming less depleted and had relatively low d values as it was no longer derived from successive rainband activity.

Enhanced sub-cloud evaporation may also have played a limited role in decreasing d values of falling rain as the measurement site at Trinity Beach is located on a narrow coastal strip adjacent to an elevated hinterland. Observed dewpoints at Mareeba on the hinterland were nearly 5 °C lower than at the coast during this period [126]. It appears that orographic rain south of Trinity Beach dried out the air mass as it moved clockwise over the elevated ranges in that region. Once this relatively dry air mass descended the range it dried further, thereby enhancing sub-cloud evaporation and decreasing the d values of falling rain.

5.4.5 Relevance to speleothem isotope records

There has been uncertainty about the relative importance of various parameters in a tropical cyclone such as intensity, longevity and distance to the eye in terms of the isotope signal recorded in palaeo-archives. Previous research [107] compared these parameters to annual isotope signals recorded in a stalagmite over the past ≈100 years and showed that the strongest relationship was between TC intensity divided by the distance of the cyclone to the sample site and the isotope signal. The isotope values measured during TC Ita also suggest that distance was an important factor. Although the central pressure of TC Ita increased considerably shortly after crossing the coast, the spatial pattern of rainfall $\delta^{18}O$ and $\delta^{2}H$ values surrounding the cyclone as it approached and passed a measurement site remained remarkably constant along a 450 km long path over land (Fig. 5.4). It remains uncertain whether this relationship was a function of distance alone or in combination with decreasing air pressure as TC Ita approached and passed each site. However, it is clear that distance (and likely intensity) is important in determining the isotope values in TC rainfall and the isotopic signal imparted in speleothem limestone deposits. Similar studies of future TCs of varying intensity, longevity and coastal crossing locations should help refine the tempestological interpretation of stable isotope signatures found in speleothems and other palaeo-archives.

5.5 Conclusions

Continuous measurement in real time of $\delta^{18}O$ and $\delta^{2}H$ values in both rainfall and water at a single site coupled with measurement of discrete rainfall samples from multiple sites provided a detailed characterisation of the stable isotope anatomy of TC Ita. In conjunction with local and synoptic meteorological observations the stable isotope values could be linked to specific features of the cyclone such as the passage of convective spiral rainbands, stratiform rainfall and the arrival of a succession of subtropical and tropical air masses with changing oceanic and continental moisture sources.

This study demonstrates that the stable isotope anatomy of TCs can be linked to the detailed physical evolution of the cyclone as well as to their synoptic-scale meteorological setting. At the continuous measurement site the near-simultaneous variations in $\delta^{18}O$ and $\delta^{2}H$ values in rainfall and water vapour and an approach to liquid-vapour isotope fractionation equilibrium indicated isotopic exchange between rainfall and vapour during the approach of TC Ita. Following the passage of spiral rainbands and the cyclone eye, different moisture sources for rainfall and vapour were reflected in diverging d-excess values.

The delineation of the magnitude, spatial scale and longevity of the isotope anomaly associated with TC Ita confirms previous assertions that intense, isotopically depleted rainfall from TC's is likely to impart a detectable isotope signal in a range of environmental proxies over a significant area.

Stable isotope data acquired at high temporal resolution will also provide detailed insights into the hydrological cycle of TCs.

Chapter 6

Tropical Cyclone occurrence may be underestimated in the historical record

C.Zwart[1,2] Jon Nott[1] N.C. Munksgaard[1,2] M.I. Bird[1,2]

[1] *Centre for Tropical Environmental and Sustainability Science, School of Earth and Environmental Science, James Cook University, Cairns, 4870 QLD, Australia.*
[2] *ARC Centre of Excellence for Australian Biodiversity and Heritage*

Prepared for submission to: *TBA*.

Abstract

This chapter presents a multi-year, modern daily rainfall isotope data set and provides an interpretational framework to support the interpretation of existing and future proxy records of climate change and variability, including TCs. We established a modern day precipitation stable isotope record (3.5 years of daily rainfall isotopic compositions) to determine the factors driving rainfall isotopic variation in this region. The data shows a strong correlation between daily rainfall stable isotope composition, regional rainfall amount and OLR. Strong depletion of the heavy isotopes ^{2}H and ^{18}O correspond to (i) the presence of the monsoon trough and coincided with negative excursions in OLR, indicating the presence of large convective areas in the region and (ii) the passage of TCs. We found that the isotopic composition of TC rainfall can be similar to monsoonal rainfall, depending on proximity to the sampling site. High resolution rainfall and vapour data during four TC events showed a strong relationship between rainfall isotopic composition and distance to the TC eye wall (Pearson ρ=0.70, $p<0.05$, n=264). Furthermore, the impact of TC rain on a potential proxy record was evaluated using a mixing relationship which indicates that the 'isotopic impact' of TC rain was spatially quite limited ($\approx$100 km). One out of four observed TC's would most likely go undetected in a proxy record at a site more than 80 km away from the eye wall of a TC. This may imply that the currently available historical TC record for northern Australia is a conservative estimate of TC occurrence in this region.

Conceived and designed the experiments: CZ JN. Performed the experiments: CZ NCM JN MIB. Analysed the data: CZ NCM NK. Performed laboratory analysis: CZ NCM. Wrote the paper: CZ JN NCM MIB.

6.1 Introduction

Monsoon activity and TCs have a major social and economic impact on north Australia and TC intensity is expected to increase under a changing climate (IPCC 2018). Predicting change in TC activity is difficult given the short temporal length of the instrumental TC record (less than 50 years), resulting in low confidence predictions [85]. Climate reconstructions and associated TC activity beyond the instrumental record using stable isotope proxy records can be used to calibrate hydrological and climate models and ultimately lead to improvements in TC predictions [85].

Climate reconstructions use stable isotopes of water, retrieved from natural archives such as, tree rings [133], ocean sediments [134], lake deposits [135] as a proxy for temperature and rainfall amount. In addition, oxygen stable isotopes, retrieved from speleothems, have proven useful to assess past Tropical Cyclone activity in Australia [107, 85] and elsewhere [84]. An important step in interpreting these reconstructions is the translation from the isotopic proxy signal to the climate parameters and/or TC activity. This translation requires a thorough understanding of the factors driving modern day rainfall isotopic variability, across all seasons and also during extreme weather events such as TCs.

The isotopic composition of TC rain is commonly observed to be strongly depleted of the heavy oxygen isotopes (^{18}O) compared to regular rainfall [112, 53]. The isotopic composition of drip water that, for example, becomes the basis for a speleothem proxy record is a mix of soil and TC rain water. In this case, the depletion in soil water isotopic composition caused by TC rain translates in a corresponding depletion in the isotope composition of the speleothem carbonate [115]. Nott et al. [107] was able to reconstruct 800 years of TC activity and found that negative excursions larger than 2.5 ‰ in the detrended calcite δ^{18}O time series indicate a moderate to severe hazard impact at their study site.

While strong depletion in the heavy isotopes in modern rainfall during a TC in north Australia has been reported by [53], no modern multi season baseline isotopic rainfall data or interpretational framework for rainfall isotopic variation during extreme weather events and regular monsoon conditions exists for this region. Until now, interpretations have relied on (interpolated) isotope data from GNIP stations more than 800 km away in very different climatic zones. Furthermore, the meteorological processes driving rainfall isotopic variation during monsoon bursts operate on much smaller timescales (hours to days) than monthly GNIP data. This highlights the need for a multi season modern monsoon rainfall isotopic record that will enable a better interpretation of variability in isotopic proxy records in this region. Examining the isotopic signature of TC rainfall in relation to the regular monsoon rainfall will also provide better insight into the interpretation of extreme weather events in isotopic proxy records.

The goal of this study is therefore twofold; (i) provide a baseline for rainfall isotopic variability observed in north-east Queensland and determine the drivers of rainfall isotopic variation in this area. (ii) tease out the isotopic signature of modern day TCs against this monsoon baseline. First we establish a modern day monsoon rainfall isotope record using four monsoon seasons of daily isotopic measurements and investigate the drivers for isotopic variation in this record. We then compare the isotopic signature of four TCs in relation to the monsoon rainfall isotopic composition. In addition we explore the potential 'isotopic impact' of the TCs on potential stable isotope proxy records by evaluating different mixing scenarios between TC rain and soil water.

6.2 Methodology

6.2.1 Site description

The coastal strip of far north Queensland is unique in north Australia as it experiences orographic rain all year round due to the presence of the Great Dividing range (see Fig. 6.1). Local meteorology in winter (April–October) is dominated by SE trade winds and a daily sea breeze cycle. These moisture laden trade winds rainout over the eastern side of the range, resulting in tropical rainforests on the seaward side. The western slopes of the range experiences a more pronounced wet/dry cycle

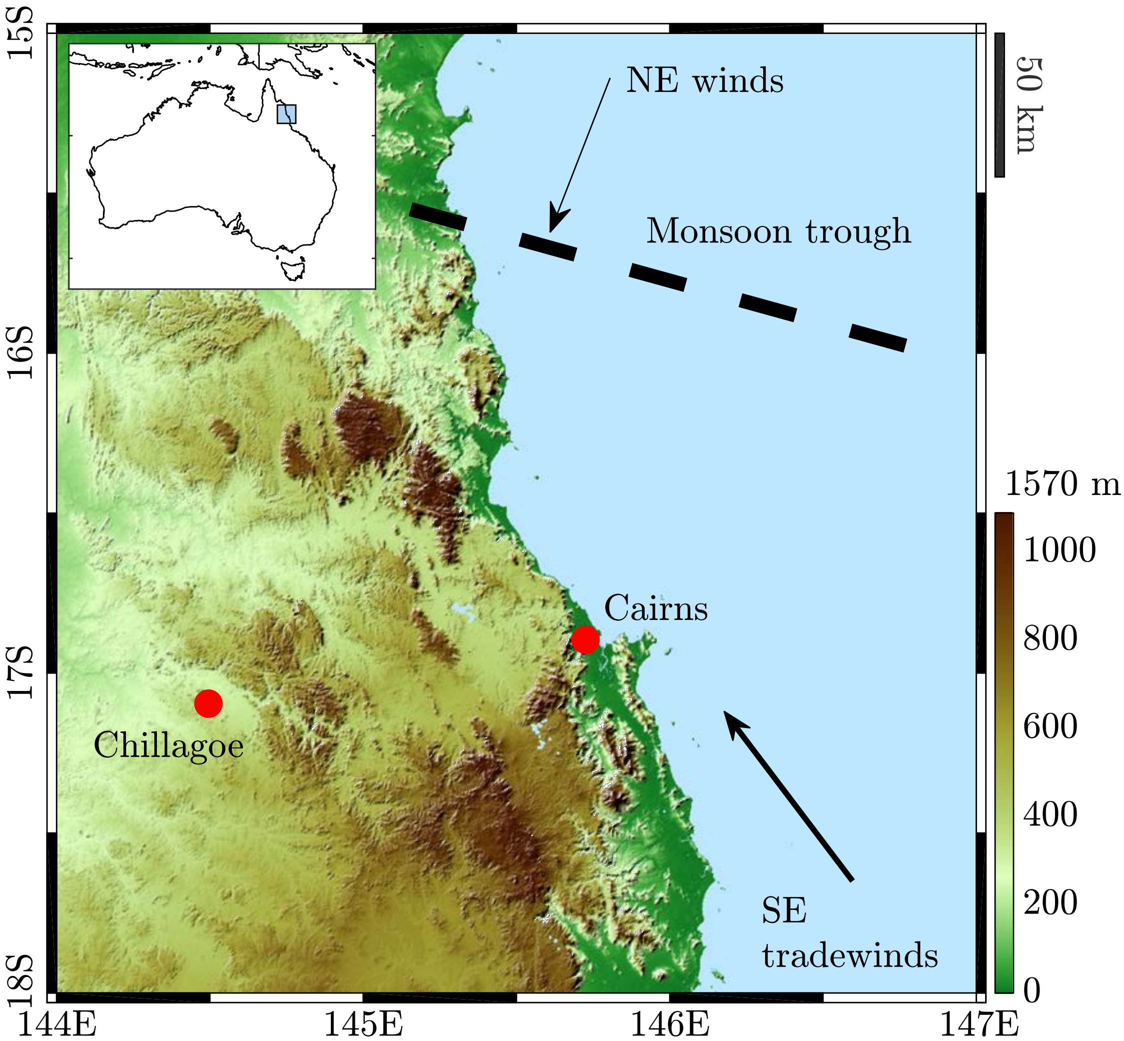

Figure 6.1: Overview of location of rainfall sampling (Cairns) and Chillagoe. Prevailing South-easterly trade winds (thick arrow), Monsoon trough (thick dashed line) and associated North-north-easterly winds (thin black arrow). Colorbar shows elevation (metres).

as found in other areas of north Australia. The Austral summer (November–March) is characterised by frequent changes in flow direction, caused by southern incursions of the monsoon trough. Northerly winds bring equatorial airmass at these times to the region with associated prolonged periods of convective driven rain.

In addition to the typical sea-breeze-forced orographic precipitation in winter and monsoon rains in winter, large –but infrequent– rainfall events occur during the passage of upper level troughs that trigger instability in the lower atmosphere. These troughs pass through the region from west to east.

Speleothems are found in karst-caves near Chillagoe [107, 85], see Fig. 6.1). Chillagoe is located in the rain shadow of the Great Dividing Range and experiences a more distinct wet-dry season although rains do occur in the dry season. Rainfall averages are lower than coastal locations (for example, monthly summer average Cairns 357.6 mm, Chillagoe 181.3 mm) and large rainfall events only occur during active monsoon phases, extreme events such as TCs, or when upper level troughs slowly move eastward across the continent.

6.2.2 Sampling and analysis

Rainfall samples (n=405) were collected at a daily basis at the James Cook University Campus in Cairns (16.81°S 145.68°, see Fig. 6.1). An IAEA recommended rainfall sampler designed to prevent evaporation (Palmex) was used with a 14.5 cm diameter funnel. Samples with volumes below 10 ml were discarded because of suspected evaporation in the collection vessel. A Picarro 2130i instrument was used to analyse the samples for their isotopic compositions via a diffusion sampler device, see Munksgaard et al. [30] and analysis was carried out as described in Zwart et al. [23]: Three in-house water standards were used to scale the measurements to the Vienna Standard Mean Ocean Water (VSMOW) scale. The isotopic compositions of the in-house standards were determined relative to the certified isotope standards VSMOW, Standards Light Antarctic Precipitation (SLAP) and Greenland Ice Sheet Precipitation (GISP) by multiple analysis using Isotope Ration Infrared Spectrometry (IRIS) and Isotope Ratio Mass Spectrometry (IRMS) at three laboratories.

The $\delta^{18}O$ and δ^2H values are reported in the standard δ notation (‰), i.e $\delta^{18}O = [({}^{18}O/{}^{16}O_{sample} - {}^{18}O/{}^{16}O_{standard})/{}^{18}O/{}^{16}O_{standard}] \times 10^3$. Precision was typically ± 0.1 ‰ and ± 0.5 ‰ for δ^2H and δ^{18}O, respectively (1σ s.d.).

A network of volunteers and a 4wd car fitted with isotope measuring equipment collected a total of 134 discrete rainfall samples from TCs Nathan (March 2015), Debbie (March 2017) and Marcus (March 2018). Continuous rainfall and water vapour isotopic composition was measured for TC Ita (April 2014) and continuous vapour isotopic composition for TC Nathan. Tracks of the different TCs are shown in Figure 6.2.

6.2.3 Meteorological data

TC tracks and metrics were retrieved from the BoM best track database `http://www.bom.gov.au/cyclone/history/`. The tracks were linearly interpolated onto 15 min intervals to match meteorological parameters available for the time of rainfall sampling. Rainfall data was retrieved from the following BoM stations; Bowen (033327), Cairns (031011), Chillagoe (30140), Cooktown (031209) and Darwin (014015). OLR data were obtained from NOAA and is described by Liebmann and Smith [78]. Regional average daily OLR values were calculated by averaging daily OLR values over a bounding box of 10°(EW)×5°(NS), centered over Cairns. Airmass source locations for each daily sample were calculated using HYSPLIT, model version 4.0 [80]. The 2.5° global reanalysis archive provided by the United States National Centers for Environmental Prediction (NCEP) was used as input for the wind fields. HYSPLIT back trajectories were computed in isobaric mode, 72 hrs runtime and selected arrival height was 500 m.

6.2.4 Description of events

Cyclone Ita (5–14 April 2014), a category 5 system on the Australian scale originated from a tropical low near the Solomon Islands and weakened to a category 4 system prior landfall, after which time it further weakened rapidly to a category 1 system while tracking south, parallel to the Australian Coastline. The lowest δ^{18}O value

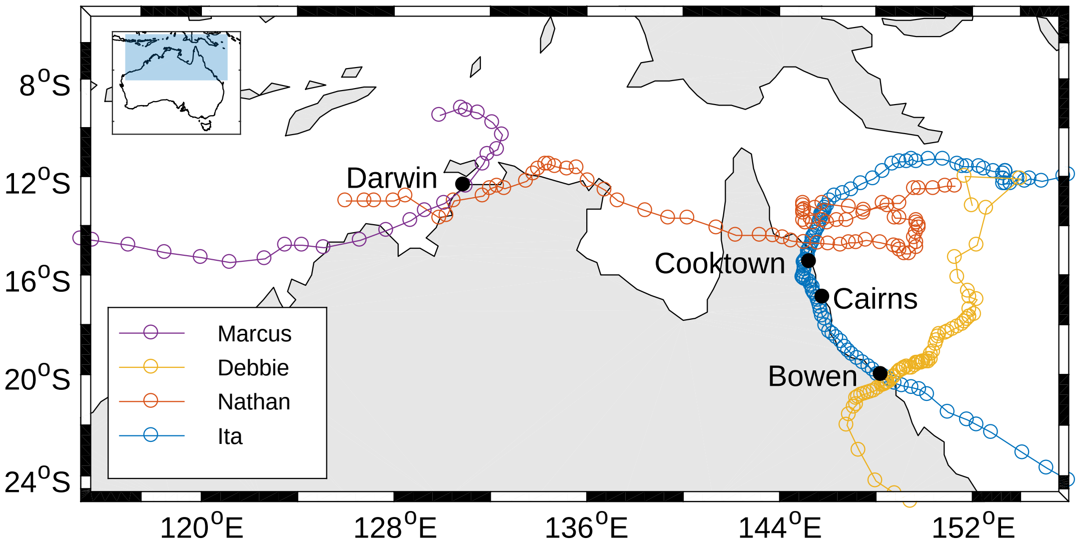

Figure 6.2: Tropical Cyclones that moved through the region during the measurement campaign, Marcus, (March 2018, purple), Debbie (March 2017, yellow), Nathan (March 2015, red) and Ita (April 2014, blue).

recorded was -20.2 ‰, and at this point the cyclone was ≈100 km away from the measurement site in Cairns. A total rainfall of 231 mm was recorded in Cairns (Trinity Beach, Lat. 16°47.5' S, Long. 145°41.8'E, altitude 20 m above mean sea level) and the amount weighted mean isotopic composition of rainfall at this site was δ^{18}O=-10.2 ‰ (n=1612). Refer to Chapter 5 for a detailed description of Ita's development and isotope characteristics.

Cyclone Nathan (10–24 March 2015) developed from a tropical depression in the northern Coral Sea and tracked westward while intensifying to a category 4 system prior to crossing the Cape York Peninsula, north of Cooktown. Nathan weakened to a category 1 system before entering the Gulf of Carpinteria where it re-intensified to a category 3 system while moving west. The lowest δ^{18}O value recorded in Cooktown was δ^{18}O=-10.2 ‰. The mean δ^{18}O value of the discrete rainfall samples taken at 15 minute intervals in Cooktown (n=37) was δ^{18}O=-6.9 ‰, with a total rainfall amount of 81.8 mm.

The isotopic compositions of water vapour (δ^{18}O and δ^{2}H) for this system were monitored at two locations; close to its center (Cooktown ≈80 km from eye of cyclone) and further south (Cairns, ≈ 160 km south of Cooktown, see Figure 6.2). Isotopic compositions of rainfall and water vapour tracked parallel (see Figure 6.3) during the rainfall period, similar to observations made by [53]. Although Nathan was a category 4 cyclone, it did not produce did not produce rainfall in Cairns, and isotopic compositions of water vapour were not greatly affected in that area, ≈ 240 km south of the center of the system, see Fig. 6.3.

Tropical cyclone Debbie (25–29 March 2017) formed in the northern Coral Sea and tracked southwest while intensifying to a category 4 system just before making landfall on the the 28th of March around 11:30 am near Airlie Beach. Debbie subsequently tracked further inland while weakening to a category 1 system and caused widespread flooding along its track. The total amount of rainfall recorded at Bowen airport during the passing of cyclone Debbie was 385.6mm. Lowest rainfall δ^{18}O values in discrete rainfall samples (δ^{18}O=-21.20 ‰) were measured just before

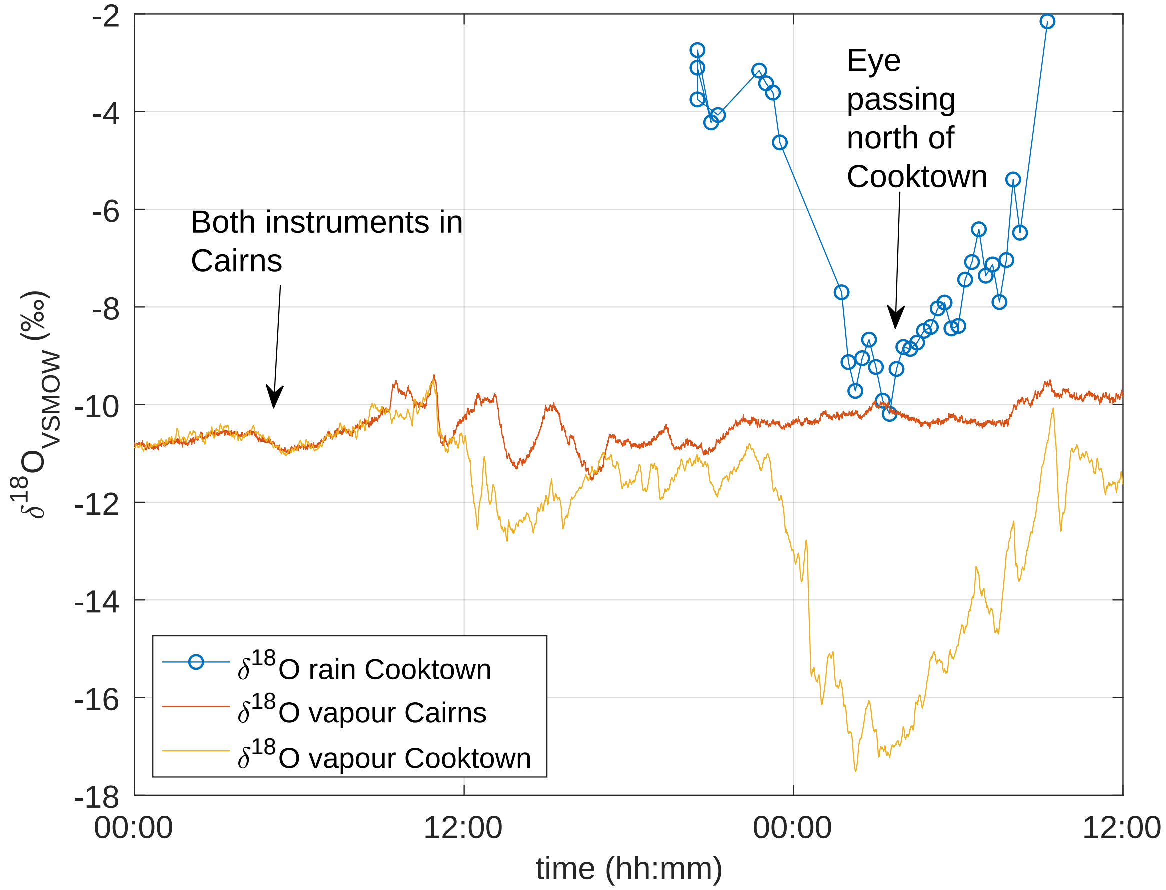

Figure 6.3: Graph showing timeline of δ^{18}O values in rainfall and vapour before and during the passage of TC Nathan. One vapour instrument remained stationary in Cairns (red line), second vapour instrument (yellow line) was transported by road to Cooktown (while measuring continuously) and installed stationary upon arrival. Little influence of cyclone Nathan on isotopic composition of water vapour was observed in Cairns, ≈240 km south. Water vapour δ^{18}O (yellow line) and rainfall δ^{18}O in discrete rainfall samples measured in Cooktown (blue markers) show a large negative amplitude during the passage of Tropical Cyclone Nathan.

cyclone Debbie made landfall, the distance from the measurement location in Bowen to the eye wall was ≈ 30 km at that point.

Tropical Cyclone Marcus (14–25 March 2018) formed in the Arafura Sea as a tropical low on the 15th of March and adopted a Southwesterly track, crossing over Darwin as a category 2 system. It intensified to a category 5 system once over warmer waters off shore Western Australia. Darwin Airport recorded 88.4 mm of rain during the crossing of Marcus, the lowest rainfall δ^{18}O value measured was -18.3 ‰.

6.3 Results and discussion

6.3.1 Isotope record of TCs

The combined data for all four TCs showed a strong relationship between between isotopic values recorded from Tropical Cyclone rain and distance (D) from the eye to the measurement sites (Pearson ρ=0.70, $p<0.05$, n=264, see Fig. 6.4). Minimum δ^{18}O values were recorded ≈25–100 km outside the eyewall rather than closest to the centre, a phenomenon that has also been observed elsewhere [115], attributed to the uptake of (isotopically enriched) seaspray near the eyewall. This strong relationship between TC distance and isotopic composition of rainfall at the measurement site has also been reported by Good et al. [69] and Munksgaard et al. [53]. Studies have linked TC intensity indirectly to low δ^{18}O values of TC rain through the analysis of calcium carbonates derived from speleothems [84, 107]. This seems plausible as one would expect larger, more intense TCs to exhibit larger stratiform decks and stronger moisture recycling and more rainout leading to larger negative anomalies in δ^{18}O values [19].

However, we found no clear relationship (Pearson ρ=-0.16) or discernible patterns between TC mean sea level pressures or maximum sustained winds and TC rainfall δ^{18}O values. On the contrary, we observed low δ^{18}O values (<-15 ‰) across a range of wind speeds, indicative of low Cat. 2 to high Cat. 4 TCs. This suggest that measured δ^{18}O values do not represent TC intensity or that the relationship is too

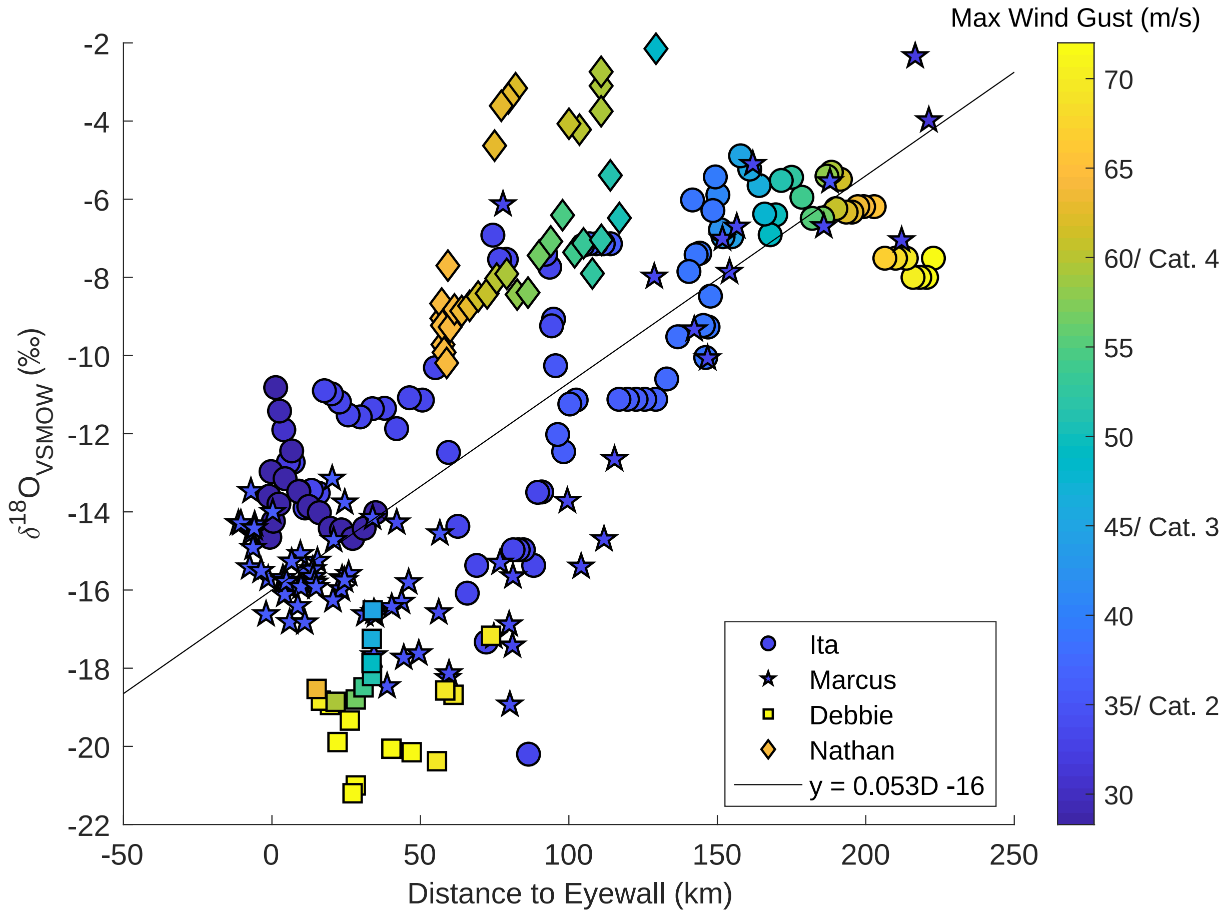

Figure 6.4: Rainfall $\delta^{18}O$ values versus distance to eye D (km), Ita (circles), Nathan (diamonds), Debbie (squares) and Marcus (stars). Positive/negative D indicates approaching/after passage of TC respectively. Color of symbols indicates maximum observed wind gusts (m/s). Black line shows linear regression $\delta^{18}O$ versus Distance to eyewall for combined samples of all TCs. Correlation factor between rainfall $\delta^{18}O$ and D was 0.70, p-value < 0.05 (Pearson ρ).

complex to capture in a linear relationship. A sudden decrease in TC intensity, for example, can lead to a decrease of δ^{18}O values as ice particles from aloft, with low δ^{18}O values, flush out due to ceasing updrafts [112, 115]. Thus, while in some cases, TC intensity may be negatively correlated to δ values, sudden changes in TC intensity can have the opposite effect, resulting in no significant first order statistical relationship.

TC Debbie underwent an eyewall replacement cycle prior to landfall, and the associated drop in intensity and associated flush out of ice particles may have caused relatively low δ^{18}O values. In addition, while making landfall, TCs often also exhibit a sudden decrease in intensity which may result in rapid lowering of δ^{18}O values. After making landfall, as the TC moves over land, it loses its oceanic moisture source and rainout further decreases δ^{18}O rainfall values. This complicates a supposedly relatively simple positive relationship between TC intensity and δ^{18}O values for a speleothem record near the coast.

6.3.2 Daily isotope record

Rainfall and daily δ^{18}O values in Cairns showed a strong seasonality (Fig. 6.5), this suggests that this region is well suited for high resolution environmental proxy records with seasononal resolution. Small rainfall events (<20 mm) comprised ≈80% of the dataset and occurred all year round. This is a very different pattern to that observed at the Darwin GNIP station which has often been used as a 'representative' location for north Australian monsoon rainfall. Approximately 75% of the rainfall samples in Cairns had δ^{18}O values lower than -3‰ and the amount weighted average isotope value from January 2014 to June 2017 was -3.9 ‰. The amount weighted mean δ^{18}O value of the daily wet season (December-January-February-March, djfm) record was -4.3 ‰.

Rainfall amount at the Cairns site was poorly correlated with δ^{18}O values during the wet season (Pearson ρ = -0.29, see Table 6.1) however, large rainfall events (>≈ 50 mm day^{-1} mostly occurred during the wet season and negative excursions in δ^{18}O (below -3‰where δ^{18}O ranged from -14.1–1.2 ‰) were often associated with

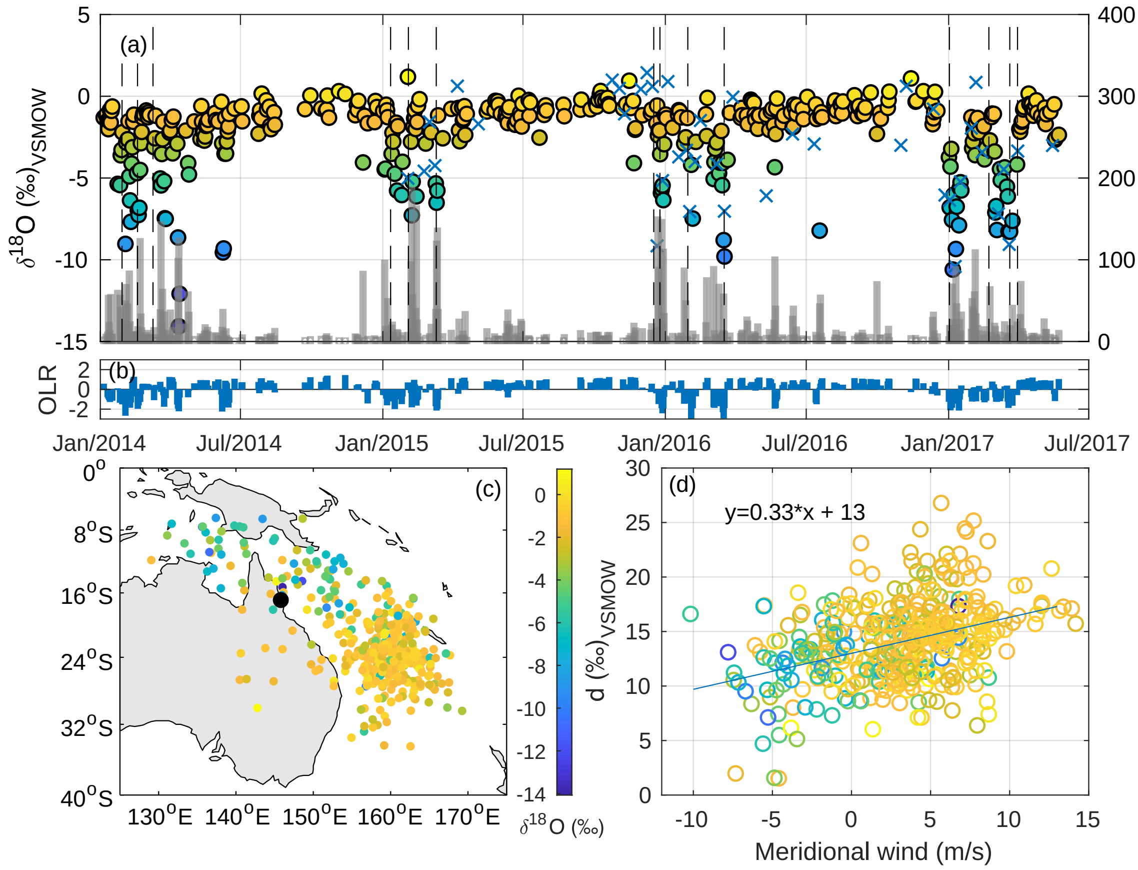

Figure 6.5: (a) δ^{18}O values in daily rainfall samples. Dashed vertical line indicates presence of the monsoon trough over the region. Different ranges of δ^{18}O are given a color for comparison with bottom panels. Grey bars indicates rainfall (local gauge) at the measurement site. Blue 'x' symbol shows weekly average rainfall δ^{18}O values in Chillagoe. (b) OLR anomaly (z-scores). (d) Airmass source (72 hrs back trajectory) locations for sampling days in (a). (e) d-excess versus Meridional (north-south) wind component.

these events. A strong correlation between δ^{18}O values and rainfall amount was observed during the dry season (Pearson ρ =-0.63), suggesting that bulk microphysical processes (Rayleigh distillation, isotopic exchange and kinetic fractionation, see Chapter 2) underlying the 'amount effect' are likely the dominant driver of rainfall δ^{18}O variability in this season [15].

Rainfall isotopic composition at the site was influenced by the amount of convective activity in dry- and wet seasons, illustrated by the strong correlation with cloudiness, (OLR). Larger negative amplitudes of rainfall isotopic ratios (δ^{18}O < -5 ‰) mostly occurred during the presence of the monsoon trough over the area (see Figure 6.5a). This coincided with negative spikes in the daily averaged regional OLR (Figure 6.5b). Low values of OLR indicate the presence of MCS in the region. While relative contributions of processes underlying the link between convection and low δ^{18}O values are still under debate, the link is generally accepted [16]. Kurita [19] explored the vapour recycling hypothesis proposed by [38] and found that rainfall isotopic variability is closely linked to the degree of convective organisation and associated stratiform rainfall fraction. Large scale convective activity was also found to be the dominant driver of isotopic variation in the Bay of Bengal by [34]. Other studies proposed cloud- and rainfall type as determining factors in δ^{18}O variability [41, 42, 40]. Airmass back trajectory analysis showed that airmass source regions for days with relatively low δ^{18}O values (dominated by blue/green in Fig. 6.5) during the wet season originated from sector areas northwest (over north) to the east of Cairns. Air masses with relatively high δ^{18}O values mainly originated from waters south east of Cairns.

This shift in source regions due to the reversal of the seasonal winds was also reflected in the the so called d-excess (defined as d-excess=δ^{2}H-8$\times\delta^{18}$O) values. Winds with a northerly component (meridional wind vector <0, d-excess range 1.5–18.5 ‰) were often below average (d=14.7 ‰) and associated with lower δ^{18}O values (<-4 ‰, indicated by green and blue in Figure 6.5). In contrast, higher d values were more often associated with yellow markers in Figure 6.5, indicating higher δ^{18}O

Table 6.1: Pearson ρ correlation coefficients and p-values between $\delta^{18}O$ in daily rainfall, local and regional rainfall amount, and OLR values.

	rain at site [daily mm]	regional [daily mm]	OLR [W m^{-2}]
$\delta^{18}O_{dry}$ =–3.6 ‰	-0.63	-0.58 (<0.05)	0.46 (<0.05)
$\delta^{18}O_{wet}$ =-4.3 ‰	-0.29	-0.58 (<0.05)	0.56 (<0.05)

Table 6.2: Range, average and standard deviations of TC rainfall $\delta^{18}O$ values.

	$\delta^{18}O$ values (‰)		
TC	range	average	standard deviation
Ita	[-20.2, -4.9]	-10.1	3.4
Nathan	[-10.2, -2.2]	-6.9	2.4
Debbie	[-21.2, -16.5]	-18.9	1.2
Marcus	[-18.9, -2.3]	-14.2	3.7

values and southerly winds (d-excess ranging from 6.1–26.8 ‰, positive meridional wind component). Previous studies have pointed out the relationship between d-excess and moisture source conditions, see for example Pfahl and Sodemann [46]. Airmasses in the wet season (with associated low d-excess values) originate from tropical waters north of latitude ≈16°S and higher d-excess values were associated with subtropical to mid-latitude waters. The difference in Sea Surface Temperature (SST) between these two regions.is on average 6 °C [103]. SST and Relative humidity at the source region are known to be positively and negatively correlated with d-excess respectively [46]. We therefore conclude that d-excess and δ^{18}O values in our dataset indicate the shift between south-easterly trade- and wet season northerly winds. This is also illustrated by the meridional wind vector that shows a positive correlation with d-excess (Figure 6.5d); northerly winds during the wet season bring in airmasses from a region with high SST's and relatively humid conditions, the opposite is true for the winter season.

6.3.3 Potential impact of TC rain on stable isotope proxy records

The stable isotope signal of a TC can be imprinted into a natural archive such as a speleothem if the input of TC rain changes the isotopic composition of a reservoir feeding the speleothem significantly [84]. In Chillagoe, a decrease in δ^{18}O value of 2.5 ‰ below average has been used as a threshold representing the signature of TC rainfall near (<400 km) the observation site [107], meaning that TC rain should lower the δ^{18}O value of the soil water by at least 2.5 ‰.

The TC's in our dataset display a range of rainfall isotopic compositions and associated rainfall amounts which can be compared to the range of variations usually observed during the wet season, see Figure 6.6. The amount weighted mean and standard deviation of the daily wet season record in Cairns was -4.3 ‰ and -4.8 ‰ respectively. The mean δ^{18}O values of TCs varied from -18.9 ‰ (Debbie) to -6.9 ‰ (Nathan), see Figure 6.6. The stable isotope composition of rainfall associated with cyclones Debbie and Marcus differ significantly from the Cairns wet season distribution at the 95% significance level (see also Table 6.2 for an overview of range, average and standard deviation $\delta^{18}O$ values for TC rainfall).

The change in soil water isotopic composition, resulting from the input of low $\delta^{18}O$ rainfall from different TCs was examined through two basic hypothetical volumetric mixing scenarios:(i) average TC $\delta^{18}O$ rainfall values were used as input while the TC rainfall amount varied between 0 and 600 mm, see Fig. 6.7a. (ii) TC rainfall amount was set constant and input TC $\delta^{18}O$ values are varied with distance (D) according to Figure 6.4. For the latter case, TC average $\delta^{18}O$ values were calculated at 25 km intervals.

Scenario 1

First we assume an initial reservoir size equalling one month of wet season rainfall amount in Cairns (≈360 mm, $\delta^{18}O$=-4.25 ‰). This mixing scenario was repeated for a smaller and larger water reservoirs, equalling one month(≈181 mm) and full wet season (djfm, (≈725.3 mm) respectively of average wet season rainfall in Chillagoe, ≈ 130 km inland where previous speleothem isotope studies have been located. The same reservoir initial isotopic composition (Cairns average $\delta^{18}O$=-4.25 ‰) was used for both scenarios as all TC observations were made on coastal locations and a continental effect is likely to change the isotopic composition of both TC and wet season rain in Chillagoe to a similar degree.

The results show that, in this scenario, isotopic mixtures at small rainfall amounts (≈50 mm) fall between the average and critical impact value, meaning that no TC would effect a large enough perturbation in the calcite $\delta^{18}O$ to be detected as TC, see Figure 6.7. Rainfall from Debbie, Marcus and Ita cause a large enough change in soil water $\delta^{18}O$ values from around 75, 100 and 250 mm of rainfall respectively. The isotopic signature of TC Nathan, a category 4 system on the Australian scale, would become imperceptible after when mixing with soil water, either for one month (lower boundary) or a full wet season worth of rainfall (upper boundary) at Chillagoe. TC Debbie is likely to be detected assuming both large and small pre-existing reservoirs

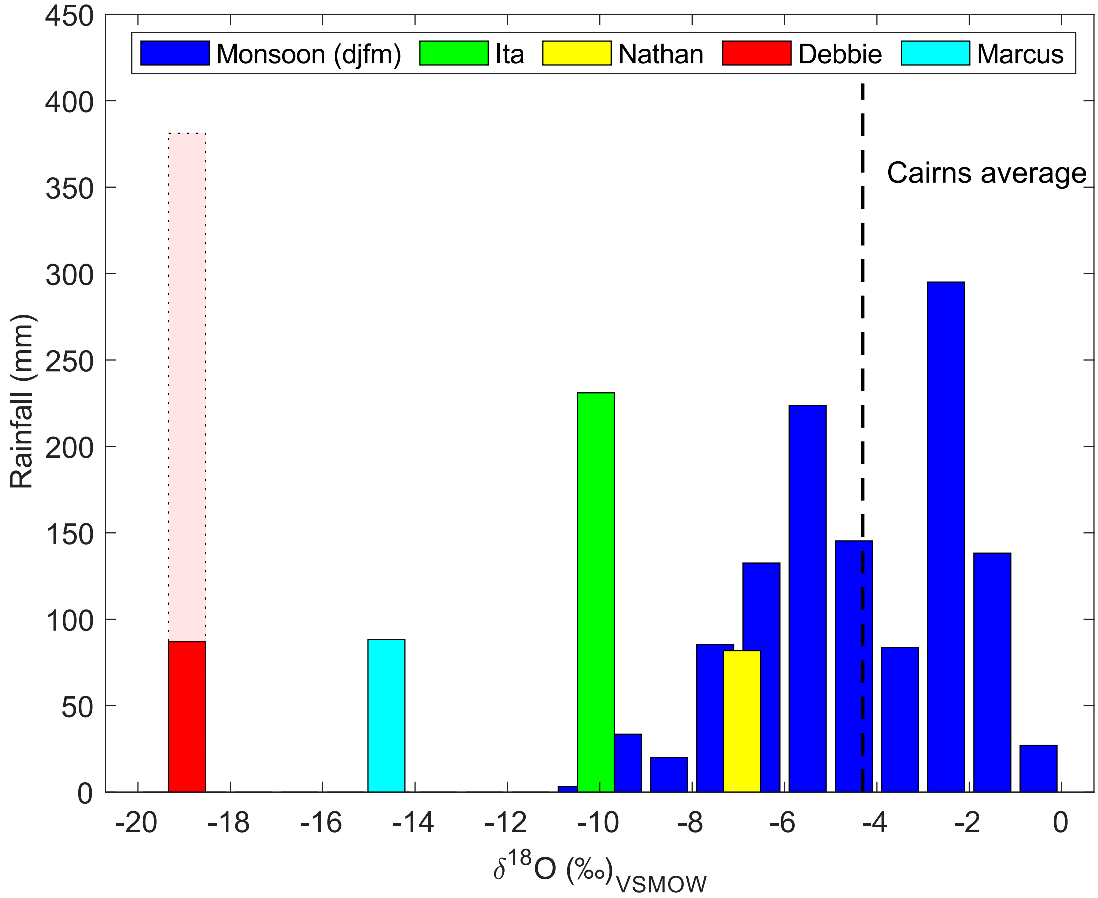

Figure 6.6: Average seasonal rainfall amount versus corresponding $\delta^{18}O$ as measured during 4 wet seasons (blue), dashed lines indicates wet season weighted mean for Cairns (right). Coloured bars show total cyclonic rainfall during measurement and corresponding mean $\delta^{18}O$ for Ita (green) Nathan (yellow) Debbie (red) and Marcus (cyan). Translucent red bar shows total rainfall outside measurement period.

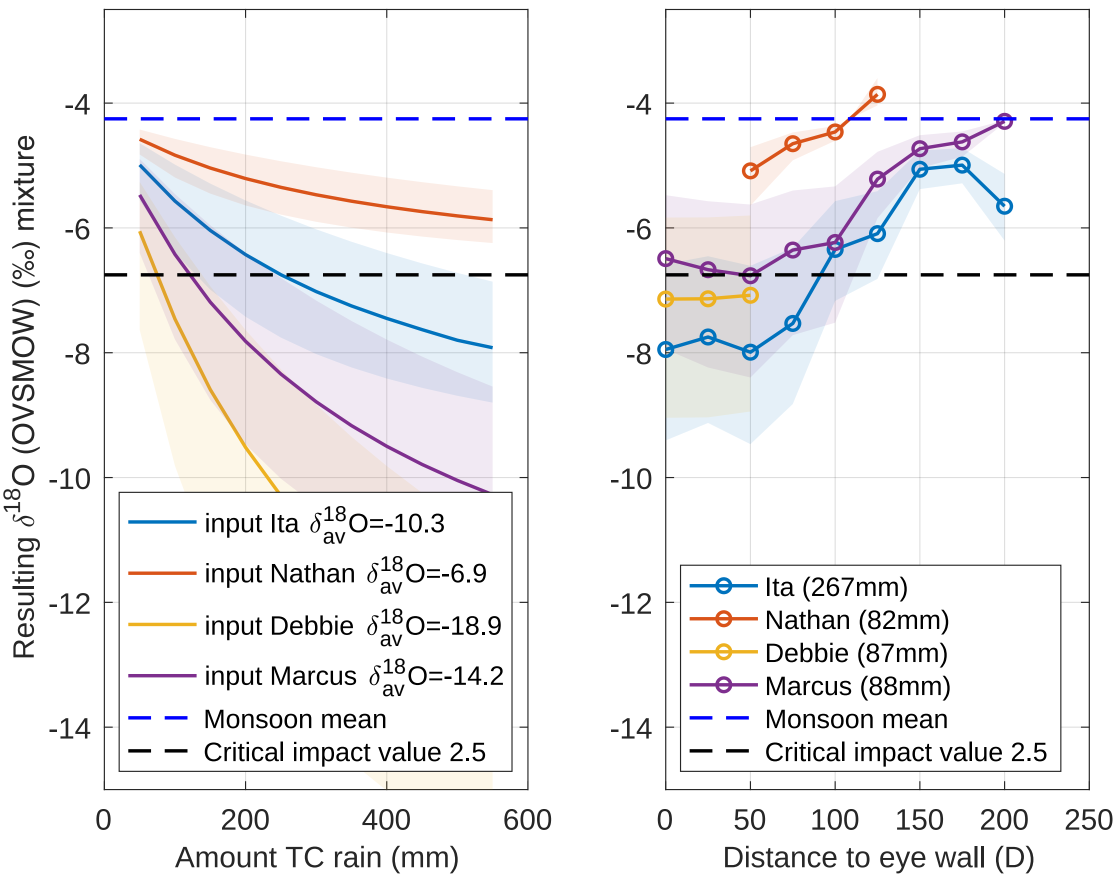

Figure 6.7: Different mixing curves showing resulting δ^{18}O in reservoir for Ita (green), Nathan (yellow) and Debbie (red). Reservoir defined as one month average wet season rainfall (360 mm) with initial δ^{18}O=-4.25 ‰, indicated by dashed blue line. Critical impact value=-2.5 ‰ as defined by Nott et al. [107]. Mixing curves were calculated using the spreadsheet developed by Faghihi et al. [136]. Shaded areas lower and upper boundaries indicate one month or full wet season rainfall amounts respectively.

for rainfall amounts exceeding 150 mm.

Figure 6.4 illustrates that the distance to the eye wall determines, to a large extent, TC rainfall $\delta^{18}O$ values.

Scenario 2

Rainfall amount of TCs was set to the observed amount during the measurement period and $\delta^{18}O$ values of each TC were averaged over 25 km intervals away from the observation sites.

The data (see Fig. 6.7) shows that, for the most diluted scenario (upper boundary of shaded areas, large initial reservoir size 725 mm) no TC/soil water mixture shows $\delta^{18}O$ value well below the critical impact level and TCs would most likely not be detected. The effect of TC Nathan was too small to lower mixture $\delta^{18}O$ values below the critical impact level. Figure 6.7 also shows that, too have enough effect, TCs need to pass in relative close proximity to the site (≈125 km) even in the least diluted scenario. An exception to this may be TC Debbie, however, no measurements further than 50 km to the eye wall were available to confirm this.

6.4 Conclusions

Negative $\delta^{18}O$ excursions in rainfall in Cairns, north east Australia were associated with the presence of the monsoon trough and low OLR values, indicating that large scale organised convection drives depletion events in this region. Furthermore, there was a clear seasonality in $\delta^{18}O$ values indicating that seasonal chronologies can potentially be retrieved from natural archives in this region, such as tree rings, lake sediments or speleothems. Seasonality was also apparent in d-excess values, reflecting a change in moisture source regions and/or conditions between wet and dry seasons. This, and the observed positive relationship the meridional wind vector and d-excess suggests that may be used as in indicator of the strength and duration of wet season conditions and as a proxy for trade wind strength.

TC rain $\delta^{18}O$ values showed a larger range (≈-21 – ≈-2 ‰) than that of multi season daily rainfall sample $\delta^{18}O$ values (≈-11 – 0 ‰). TC rainfall $\delta^{18}O$ showed a strong correlation with distance of the TC eyewall to the measurement sites. Two out of four TCs produced rainfall $\delta^{18}O$ values that were significantly lower than the wet season rainfall $\delta^{18}O$ distribution. Two mixing scenarios were evaluated and demonstrated that three out of the four TCs can potentially effect a large enough perturbation in the the calcite $\delta^{18}O$ record to be detected as TC. Providing the reservoir size equalled one month of average rainfall amount and the TC eyewall would pass the site at a distance of $\approx$100 km. One TC would most likely go undetected in a stable isotope record located in both in the wetter coastal zone and semi wet interior.

Chapter 7

Holocene monsoon hydroclimate from a lacustrine *n*-alkane δ^{2}H record, Girraween Lagoon, northern Australia.

Costijn Zwart[1,2] Cassandra R. Rowe[1,2], Niels C. Munksgaard[1,2], Christopher M. Wurster[1,2], Dirk Sachse[3], Michael Brand[1,2], Michael I. Bird[1,2]

[1] *Centre for Tropical Environmental and Sustainability Science, School of Earth and Environmental Science, James Cook University, Cairns, 4870 QLD, Australia.*
[2] *ARC Centre of Excellence for Australian Biodiversity and Heritage*
[3] *Affiliation*

Submitted to Quaternary Science Reviews.

Abstract

We present higher plant derived *n*-alkane hydrogen isotope proxy record spanning the Holocene preserved in Girraween Lagoon sediments, near Darwin in northern Australia. Comparatively high and variable δ^{2}H values during the early Holocene (11–8.5 ka) are interpreted as a period of increased variability in rainfall type and amount, seasonality, and, as a result of stronger evaporative demand. A decrease in δ^{2}H values from 8.5 ka to a broad minimum around 6–4 ka suggests more regular rainfall and the occurrence of an active monsoon phase, associated with widespread regional convection and large stratiform rainfall areas. An increase in δ^{2}H values was observed from 4–3 ka, and marginally thereafter, is interpreted as a decrease in annual rainfall and/or increased seasonality and change in rainfall type. Corroboration of this interpretation is provided by an aquatic pollen record spanning the Holocene from Girraween Lagoon and time series of hydrogen isotope composition of both daily and monthly regional rainfall from local lake waters. The differences between the identified periods are well explained by changes in ENSO activity and sea level. In general, the timing of ENSO activity deduced from this record matches well with other proxy records from this region. Differences between records most likely reflect locations of these records relative to the spatial structure of the north Australian monsoon system.

7.1 Introduction

Climate has varied substantially in the past and this variability is archived in a variety of palaeoenvironmental proxy records [3]. In tropical monsoon regions, these records potentially provide insight into the range of hydroclimate variability in the past and insight into the interactions between the range of processes driving monsoon hydroclimate [8, 3]. In these regions, the major sources of proxy hydroclimate information are the oxygen isotope ($\delta^{18}O$) composition of speleothem carbonate [60] and the hydrogen isotope ($\delta^{2}H$) composition of *n*-alkanes preserved in sedimentary archives (e.g. [137, 14]).

On glacial-interglacial timescales in the IASM-EASM region, speleothem isotope records have demonstrated that Milankovitch forcing drives changes in monsoon hydroclimate [3], ultimately through changing solar insolation, as well as through control of sea level and thereby the area of ocean available for evaporation across the maritime continent [138]. Insolation changes on orbital timescales lead to changes in monsoon strength manifest in latitudinal shifts in the position of the Inter-tropical convergence zone (ITCZ), and therefore the position of highest seasonal rainfall in the IASM region [e.g. 138].

While there are multiple speleothem isotope records of monsoon hydroclimate variability through the Holocene available for the EASM [e.g. 139] and equatorial maritime continent regions [e.g. 140], there are comparatively few records available from northern Australia. Speleothem records that span the Holocene are limited to those that comprise the composite KNI-51 record from a cave near Kununurra in Western Australia [67], with some data available from the late Holocene [85] and the early to mid- Holocene from Ball Gown Cave [141] and Cape Range [142], both also in Western Australia. To the north, in Southern Indonesia, there is a Holocene speleothem record from Liang Luar on the island of Flores [143]. During the Holocene, these speleothem isotope records have demonstrated substantial decadal to millennial scale variability in monsoon hydroclimate related to dynamic interactions between the AISM and EASM modulated by other coupled atmosphere-ocean phenomena.

Other information on Holocene hydroclimate in the region, generally of lower temporal resolution, has been derived from palynological [e.g. 144, 145, 146] and geomorphic [147, 148, 149] records onshore as well as inferred from geochemical measures thought to reflect changing runoff intensity derived from marine sediment records from offshore Western Australia [150], the Timor Sea [151], south of Java [152] and between Flores and Sumba [153].

Collectively, all records of Holocene hydroclimate change in the southern AISM region show both similarities and differences in trends, timing and magnitude of changes, and in the interpretation of the mechanisms driving inferred hydroclimatic change through the Holocene.

The hydrogen isotope composition of plant waxes (long chain alkanes and fatty acids) have shown considerable potential for reconstruction of changes in tropical hydroclimate [e.g. 14]), Despite this potential, there are few *n*-alkane hydrogen-isotope records from the AISM region and none from northern Australia. A long chain fatty acid hydrogen isotope records for the AISM region has been developed from the sediments in Lake Towuti [27], on Sulawesi in Indonesia, and a marine *n*-alkane hydrogen isotope record from the Indian Ocean off Java [154]. Here we present the first *n*-alkane hydrogen isotope record spanning the Holocene derived from sediments preserved in Girraween lagoon, near Darwin in northern Australia. We compared our results with the aquatic pollen record from Girraween Lagoon [155] to derive a record of hydroclimate change in the region. We then compared this record with other published proxies of Holocene hydroclimate change from the southern IASM region.

7.2 Methods

7.2.1 Study area

Girraween lagoon (-12.517656 °S 131.080747 °E; 25 masl) is a perennial waterbody, located on the outskirts of Darwin, Northern Territory, Australia. The site is currently ≈30 km from the open ocean, but estuaries under tidal influence extend to within ≈15 km of the site. The modern environment and Holocene evolution of the lagoon has previously been described in detail by [155]. In brief, the lagoon has a small catchment of 917 ha exhibiting little relief. The lagoon itself has a surface area of 45 ha, and at the deepest point is about 4.5 m in the dry season. There is a wet season increase of ≈1–2 m in water depth, with the lake surface in the wet season roughly coincident with the local water groundwater table.

The region experiences a strongly seasonal climate, encompassed within Köppen-Geiger's 'Tropical Savanna' classification subtype Aw [157]. The mean annual temperature maximum is 32.6 °C (minimum 23.2 °C). In the strongly seasonal climate that characterises the study area, potential evaporation exceeds 1,800 mm in most years [7] compared to mean annual regional rainfall of 1731 mm (Bureau of Meteorology Station 014015, Darwin Airport), with 90% of rain falling in the wet season between November and April (Charles et al., 2016). Monsoon conditions are characterized by west to north-westerly winds whereas winds in the dry season are dominated by east to south-easterlies. The region is subject to Tropical Cyclones with records from 1964 to 2015 including 32 severe cyclone landfalls (categories 3, 4 or 5 on the Australian scale, [103]).

Modern vegetation around the site is Eucalyptus-dominated tropical open forest savanna and/or savanna woodland (dominant overstory species *Eucalyptus tetrodonta, Eucalyptus miniata, Corymbia polycarpa*) with a grassy understorey (*Sorgum* spp.) [155]. Variable transition communities dominated by *Lophostemon* spp. and *Melaleuca* spp. and broad-leaf herbs occur on approach to the water. The lagoon itself incorporates a wetland fringe, with zonations in vegetation close to the lagoon edge determined by depth of open water and extent of onshore soil waterlogging. *Melaleuca* form partly floating woodlands in the shallow waters and on waterlogged soils. A well defined ring dominated by sedges rings the lagoon in shallow/seasonally flooded areas with *Nymphaea* and other submerged taxa occupying permanent open water.

Girraween Lagoon was cored using a floating platform with hydraulic coring-

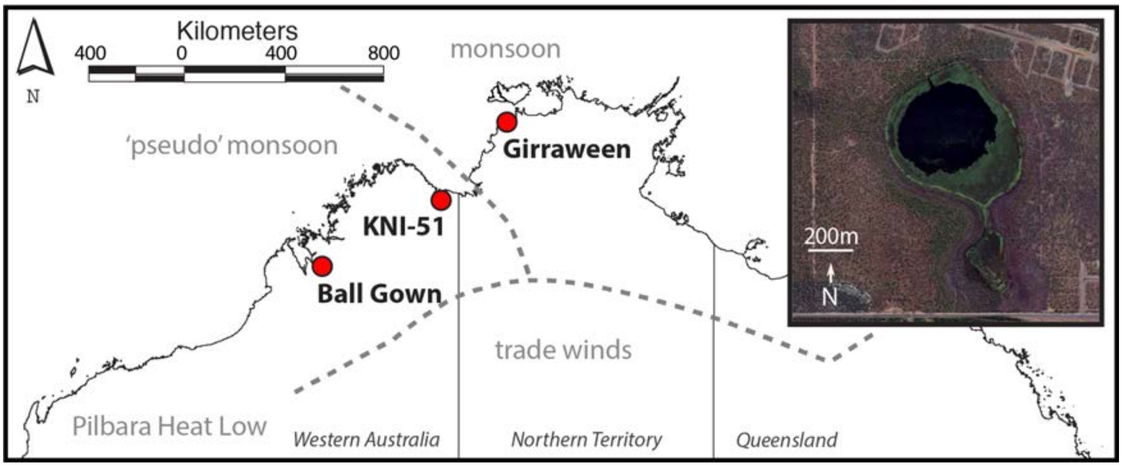

Figure 7.1: Location of Girraween lagoon, other locations mentioned in the text and monsoon wind classification scheme of [156]. Inset: satellite image of Girraween Lagoon.

rig. A 19.4 m core in 1 m sections was collected (to the point of bedrock). The focus of this paper is the upper 5 m of this core. Each 1 m section was collected in plastic tubing and sealed in the field for transport. Core sections were split in half, described and sub-sampled at 5 or 10 cm intervals (dependent on the changing nature of sediments). The upper 5 m that are the focus of this paper represent relatively uniform organic-rch peats grading to organic-rich sediment with a higher proportion of fine clay below ≈4 m depth [155]. The chronology of the core is constrained by six radiocarbon dates indicating the sediments under investigation cover the last ≈12,500 calendar years, with no breaks in sedimentation [155]. We use the chronological framework and some of the palynological data from [155] to underpin and complement the interpretation of the *n*-alkane result presented here.

7.2.2 Water isotope sampling and analysis

Accumulated 24-hourly rainfall was collected from through 2017 near Charles Darwin University (12.37 °S 130.86 °E), 28 km northwest of Girraween Lagoon, and stable isotope results have previously been reported by [42]. Lake water from 30 cm depth was sampled monthly through 2017 into 50 ml Falcon plastic centrifuge tubes. Stable isotope analysis was carried out using Picarro L2120i and L2130i instruments and autosampler connected to a diffusion sampler device [see 30]. Measurements were scaled relative to the Vienna Standard Mean Ocean (V-SMOW) water scale using three secondary water standards whose composition were determined relative to the certified isotope standards Vienna Standard Mean Ocean Water (V-SMOW), Standard Light Antarctic Precipitation (SLAP), and Greenland Ice Sheet Precipitation (GISP) by multiple analyses using Isotope Ratio Infrared Spectrometry and Isotope Ratio Mass Spectrometry at three laboratories. Precision is typically ± 0.1‰ and ± 0.5‰ for δ^2H and δ^{18}O respectively (1σSD).

7.2.3 Lipid extraction and analysis

The lipids were extracted and column chromatography was performed at the James Cook University Advanced Analytical Centre, in Cairns Australia. A ≈5 cm aliquot of lake sediment was sampled at every 20 cm along the Holocene section of the Girraween sediment core, freeze dried and homogenised using a ring mill. Lipids were solvent extracted using a MARS in a dichloromethane/methanol (9:1) mixture from ≈1.5–10 g subsamples depending on the amount of organic carbon in the sample. The *n*-alkanes were separated from the total extract using SPE columns, filled with 1.5 g of activated silica gel (0.040–0.063 micron), on a vacuum block with elution using 10 ml of hexane. Compounds were identified and quantified in the Organic Surface Geochemistry Lab at the German Research Centre for Geosciences in Potsdam, Germany (using a GC-FID/MSD Agilent 7890A GC, 5975C MSD, Agilent Technologies, Palo Alto, USA). For quantification, an internal standard (5α-androstane) and external *n*-alkane mixture was used. Some samples required extra clean up on silver nitrate columns after which all samples showed separated base line peaks.

Alkane hydrogen isotope (δ^2H_{wax}) values were determined by running samples in duplicate using a Thermo Scientific Delta V^{PLUS}, coupled to a Trace 1310GC and Isolink operated at 1420 °C. Typical standard deviations were ≤3 ‰. nC27 and nC29 displayed continuous clean signals in all samples and chosen as representative δ^2H_{wax} values. The H_3^+ factor was evaluated every measurement sequence and was constant throughout the measurement period.

7.3 Results

Modern rainfall, lake water depth and δ^2H variations all illustrate the strong seasonality of north Australia's climate (Figure 7.2). Strong rainfall events with daily rainfall amounts up to ≈185 mm occurred during the months Jan–Apr while little to no rain was recorded outside this period. The absence of rainfall in the dry season, while evapotranspiration fluxes were similar (or higher, see Figure 7.2), resulted in a ≈1 metre decrease in lake water level and, in turn, to a progressive increase of δ^2H lake water values (30 ‰). Highest lake water δ^2H values were recorded in November, before the following wet season. Rainfall δ^2H showed large variation during the wet season and varied from ≈-90 ‰ to ≈0 ‰ lowest values were observed during monsoonal outbreaks in January, consistent with results from previous studies in the region Zwart et al. [42].

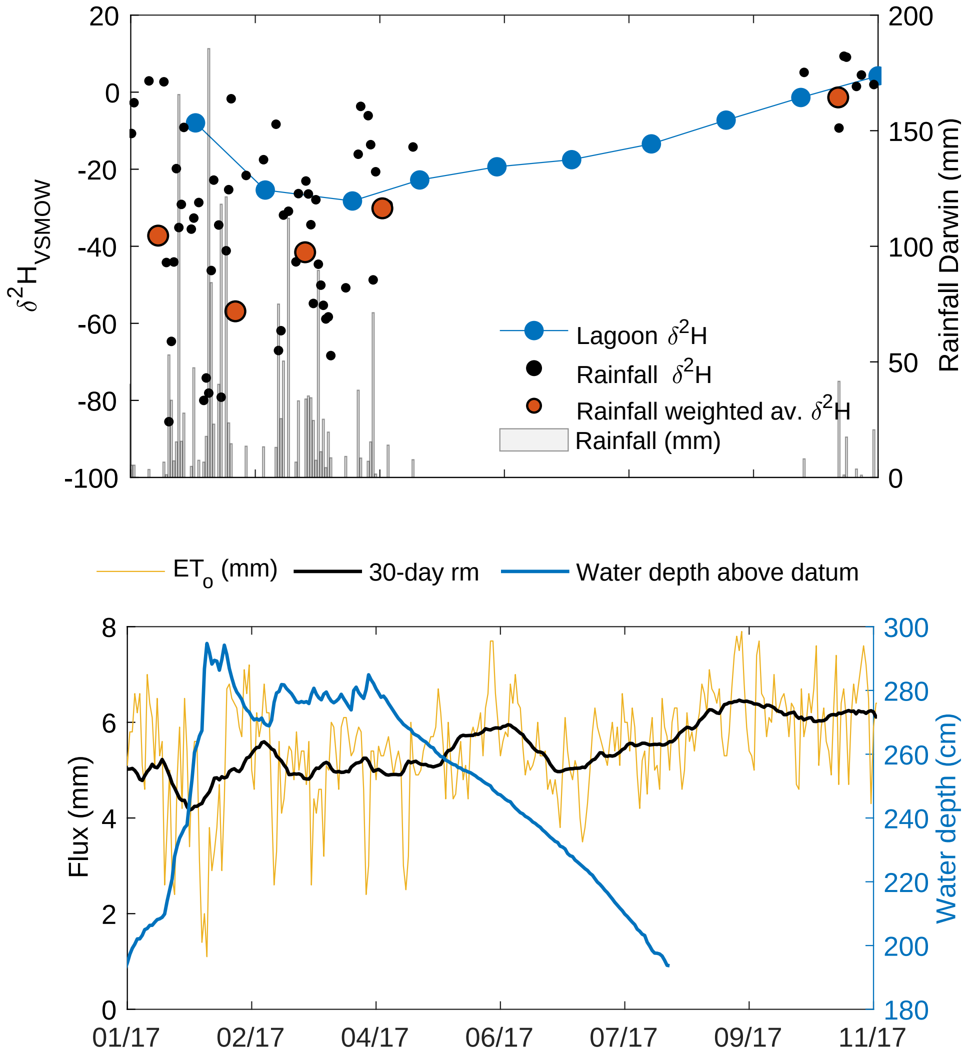

Figure 7.2: Lagoon δ^2H values (blue dots), Rainfall δ^2H (black dots) and amount weighted δ^2H (red dots) and rainfall amount (indicated by grey bars, upper panel). Evaporative flux in mm (yellow), 30-day mean evaporative flux (black) and Water depth (blue, lower panel)

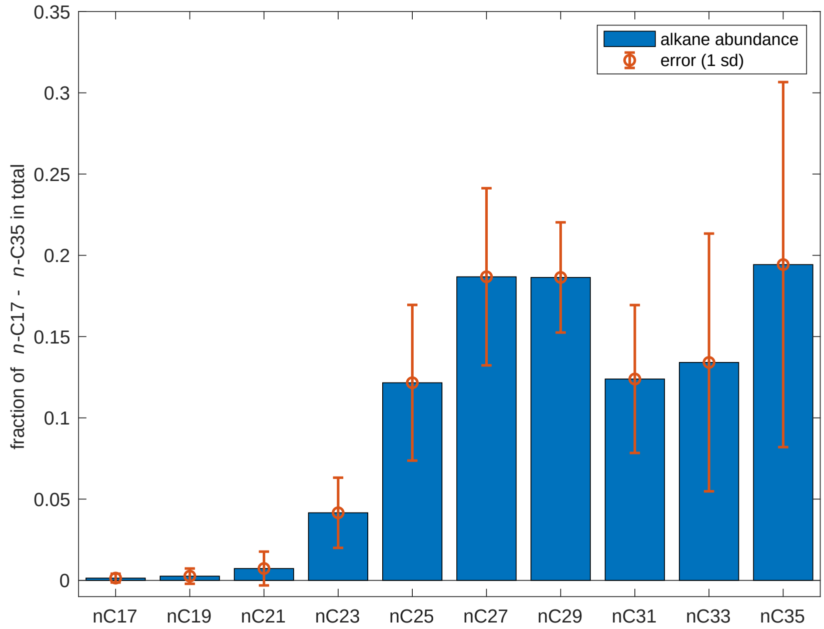

Figure 7.3: Mean proportion of each odd chain length alkane from n-C17 to n-C35, relative to the total odd chain length alkanes from n-C17 to n-C35. Error bars are standard deviation of values for all samples.

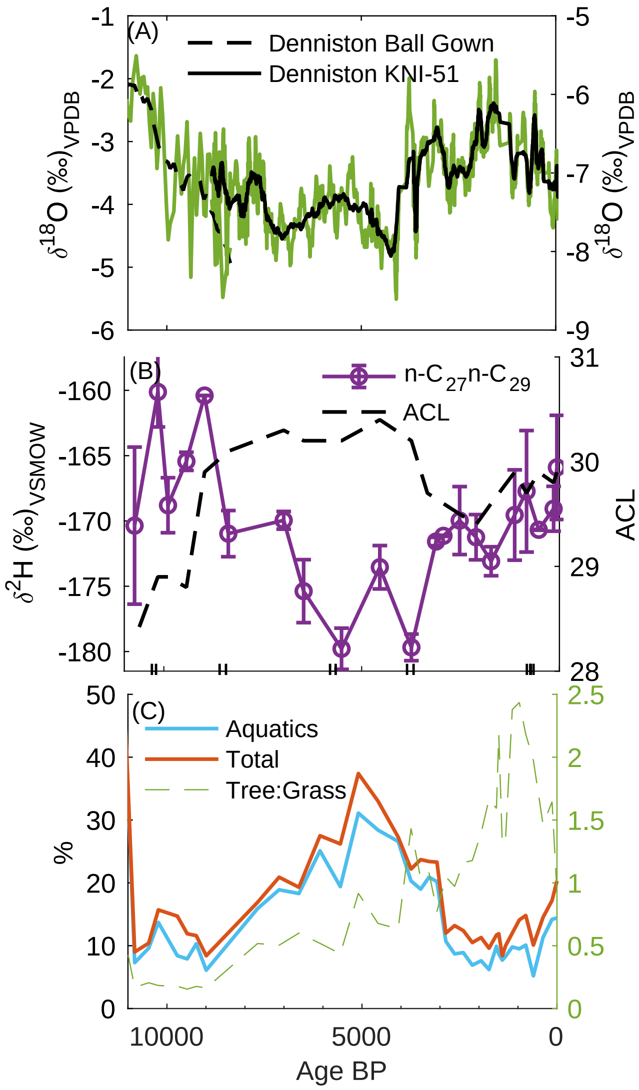

Figure 7.4: : (a) Speleothem $\delta^{18}O$ records, raw data (green line) and moving average (black), (b) δ^2H_{wax} and ACL_{odd} record from Girraween Lagoon, black vertical lines on x-axis indicate location of ^{14}C ages and uncertainty, (c) Pollen record for Girraween Lagoon from Rowe et al. [155].

The n-alkane distributions from the Girraween lagoon samples indicate a dominant higher plant source, with minor contributions from alkanes with a carbon number < n-C23, increasing to a peak in relative abundance at n-C27 and/or n-C29 (Supplementary Table 1). The abundances of n-C31 and n-C33 are lower than n-C29. There is a second peak in abundance at n-C35, for mid-Holocene samples between 3,500 and 7,000 Cal BP in age, where the n-C35 represents >31% of the total alkanes in the samples (Figure 7.3). Following Bush and McInerney [158], we calculate the average chain length of odd-numbered terrestrially derived leaf waxes from n-C27 to n-C33 (ACL_{odd} Supplementary Table 1). ACL_{odd} values are the lowest in the record (<29.0) before 8,500 cal BP, but increase rapidly thereafter to values consistently between 30.0 and 30.5 until 3,500 cal BP. After 3,500 cal BP, ACL_{odd} values decrease to 29.5 by 2,000 cal BP and then increase marginally to 30.0 toward the present. Based on the consistently high abundance of n-C27 and n-C29 in all samples (neither ever <12% and both up to 30%, of total alkanes) and the fact that these compounds clearly represent higher plant waxes of known provenance, we present the hydrogen isotope record for Girraween Lagoon as the average of the two alkanes at each depth. Deviation from the mean of those analyses represents the measure of uncertainty we adopt.

The Holocene plant wax n-alkane isotope (δ^2H_{wax}) record for n-C27 and n-C29 from Girraween is shown in Figure 7.4(b) indicating initially high δ^2H_{wax} values ($\geq$-170 ‰), decreasing from $\approx$9 ka to values $\leq$-170 ‰ between 4 and 6 ka, thereafter increasing to values between -165 and -170 ‰ toward the present. Where comparison is possible across these broad temporal periods, the other alkanes above n-C23 mirror these broad trends. The n-alkane data also exhibits relatively larger fluctuations in δ^2H_{wax} values in the period before $\approx$4 ka compared to the period towards the present.

7.4 Discussion

7.4.1 Interpreting alkane records in tropical seasonal environments

In addition to the factors governing the isotope composition of rainfall [42], the δ^2H_{wax} record is also subject to variability associated several other factors that should be considered in interpreting the record [159]. These include (i) potential evaporation of the water in the environment prior to biosynthate production, leading to an increase in the δ^2H value of the water, and (ii) a number of climate-, species-, and therefore location-specific variables that govern the apparent water-alkane isotope fractionation factor (ε_{alk}).

In the strongly seasonal climate that characterises the study area, potential evaporation exceeds 1,800 mm in most years [7] compared to mean annual regional rainfall of 1731mm (Bureau of Meteorology Station 014015, Darwin Airport), with 90% of rain falling in the wet between November and April [7]. Thus surface and soil water is subject to an extended period where evaporation can lead to a significant increase in the δ^2H value of the remaining water. This is evident in the seasonal increase of 20–30 ‰ in the δ^2H value of the water in Girraween Lagoon (Figure 7.2) and this will be reflected in the δ^2H_{wax} values of aquatic vascular plants in the lagoon [160, 137, 161].

Likewise, in the Darwin region, soil water in the upper soil layers in the dry season can be increased by 20–30 ‰ compared to wet season values in the Darwin region [162], a phenomenon that is characteristic of at least seasonally dry environments [161, 163]. To a greater degree than deeper-rooted trees, this difference will be reflected more in the shallow-rooted grasses, particularly the perennial grasses that live into the dry season. In aggregate this suggests that evaporative effects on δ^2H_{wax} will be important for alkanes originating from aquatic plants and grasses, but possibly be of less important to alkanes derived from trees.

Liu et al. [161] calculate a relatively constant global apparent ε_{alk} of -116 ± 5 ‰

(n = 941) for plants and -125 ± 6 ‰ (n=460) for modern sediments, with the lower sediment value attributed to aquatic plants contributing *n*-alkanes with generally low δ^2H_{wax} values to lake sediments. Sachse et al. [61] previously demonstrated that, in more detail, C3 dicots, primarily trees (average ε_{alk} = -113 ‰) fractionate hydrogen isotopes during the production of *n*-alkanes to a lesser degree than C4 monocots, primarily grasses (average ε_{alk} = -134 ‰). Liu et al. [161] have further demonstrated that the difference between dicots and monocots is decreased at low latitudes with a dicot apparent ε_{alk} of -115 ‰ and monocot apparent ε_{alk} of -132 ‰.

While these differences are not large, this means δ^2H_{wax} values will vary as the proportion of trees and grass vary over time, and tree to grass ratio varies substantially through the Holocene at Girraween Lagoon (Figure 7.4 panel d). Further, whereas factionation in C4 plants is not sensitive to rainfall (aridity) fractionation in C3 plants changes as rainfall changes. On an aridity transect that includes the location of this study Kahmen et al. [162] found that the C3 tree species that form the major tree component of the vegetation through the Holocene in this study - *Eucalyptus* and *Corymbia* spp. - decreased by ≈50 ‰ in δ^2H_{wax} on a rainfall gradient from 278 mm in Alice Springs to 1700 mm in Darwin. This rainfall gradient is much larger than the rainfall extremes likely over the Holocene in the study (80 year range in annual Darwin rainfall = 1025–2777 mm). Nonetheless, changing tree to grass ratio can be expected to have exerted some control over apparent ecosystem ε_{alk} over the Holocene in the Girraween record.

Vogts et al. [14] report near constant hydrogen isotope fractionation (ε_a) between precipitation and alkane (C29, C31, C33) of -109 ± 5 ‰ from marine surface sediment receiving input from adjacent terrestrial environments ranging from forest to grassland along the west coast of Africa, possibly partly due to the opposing effects of changing apparent ecosystem fractionation factors as tree to grass ratio changes with increasing aridity. Tree to grass ratio (Figure 7.4) is not correlated with variations in δ^2H_{wax} values (pearson ρ=-0.19, p-value=0.40) and in combination with the discussion above, we conclude that changing tree to grass ratio in the Holocene is unlikely to be a major driver of variations observed in the δ^2H_{wax} record.

A corollary of this conclusion is that the observed variability in *n*-alkane δ^2H record is best explained by changes in rainfall type, amount and/or the seasonality of rainfall. Thus, periods of lower rainfall and/or longer dry season provides more opportunity for dry season evaporative increase in the δ^2H values of soil water [162], lake water (Figure 7.2) and, to a lesser degree, groundwater which tends to be recharged mainly by intense rainfall events of generally lower δ^2H values [e.g. 164]. During periods of high rainfall and/or lower seasonality evaporative increases in δ^2H values are more muted.

7.4.2 Interpretation of the Girraween *n*-alkane record

From this analysis we conclude that in general terms, δ^2H_{wax} values whether aquatic- or terrestrially-derived can be interpreted as providing a combined measure of water availability and evaporative demand. Thus low δ^2H_{wax} values should indicate relatively wetter periods/less seasonality, while high δ^2H_{wax} values indicate drier periods/more seasonality. Corroboration of this conclusion is provided by the record of aquatic pollen in the lagoon (Figure 7.4; panel d). Lake surface area, and hence area available for photosynthesis, increases rapidly as water level increases due to the topography of the catchment (Fig 7.1). We interpret periods of increased aquatic pollen as times of higher lake level and therefore more effective precipitation, and the aquatic pollen record is in close accord with the major changes in the δ^2H_{wax} record.

Three periods are clearly distinguishable in the δ^2H_{wax} record from Girraween Lagoon (Figure 7.4). From the beginning of the record (11ka) until ≈8.5 ka, δ^2H_{wax} values were comparatively high and variable implying periods of low and higher rainfall different types of convection over the region. Lower rainfall is also likely a simple response to the fact that sea level at 12 ka was 40–50 m below presence and hence the coastline was 100 km further away from the site [165]. Currently mean annual rainfall decreases by 100–200 mm 100 km inland relative to the rainfall on the coast [7] and a similar effect is likely throughout the Holocene. In addition, it has been proposed that the Early Holocene was a period of increased ENSO activity [166] and this may also have led to increased inter-annual variability in rainfall and/or increased seasonality, as is currently observed in the region [7].

From 8.5 ka, δ^2H_{wax} values consistently decease to a broad minimum between ≈6 ka and ≈4 ka. This period, interpreted as indicating more regular and higher monsoonal rainfall, coincides with sea level slightly above modern in the area, with the coast ≤20 km distant from the site [167]. This period is recognized in northern Australia as a relatively wet period [67] and globally as a period of reduced ENSO variability [168, 169, 170]. δ^2H_{wax} values increase again from 4–3 ka, and thereafter increase marginally toward the present with no marked rapid changes. This trend suggests decreased annual rainfall and/or increased seasonality relative to the mid-Holocene attributed to increased ENSO variability manifest today in interannual-decadal variability in rainfall amount and change in wet season length [7]. The inference and timing of the change to increased ENSO variability correlates well with other records in northern Australia and elsewhere, which are generally placed between 4 and 3 ka [171, 67, 172, 170]. Lower rainfall may also reflect a northward contraction of the ITCZ at this time, as a sustained increase in rainfall is inferred from both the Liang Luar speleothem record [143] and a marine record from the nearby Lombok Basin [153] at around 3 ka.

7.4.3 Regional context

Two speleothem-based oxygen isotope records of Holocene hydroclimate have been published from the region. Denniston et al. [67, 141] published a high resolution Holocene record from a cave in Western Australia ≈400 km SW (KNI-51), and from Ball Gown Cave ≈850 km SW of Girraween Lagoon (Figure 7.1). Both of these speleothem-based stable isotope proxies record changes in the IASM in northern Australia and should be sensitive to similar factors driving climate variability at Girraween Lagoon. Under suitable cave conditions (i.e high humidity, limited potential for kinetic fractionation) isotope fractionation factors are well known [107, 85].

In those cases, speleothem records represent a reasonably direct and immediate measure of local rainfall $\delta^{18}O$ value, integrated over a relatively short time period and encoded in a carbonate mineral through precipitation reactions. They also provide a high resolution archive, that is precisely dateable by U-series techniques. Interpretation of these records is based on the premise that the $\delta^{18}O$ values of speleothem carbonate in the tropics predominantly records an 'amount effect' with lower $\delta^{18}O$ values reflecting 'intense' monsoon or cyclone-derived rain, although although it is also likely that part of the signal can be attributable to changes in moisture source [42, 13].

As discussed above, the alkane isotope record provides an integrated measure of relative changes in available moisture and seasonality, at lower resolution. Despite these caveats the alkane and speleothem records display remarkable general coherence. The δ^2H_{wax} values exhibits a total range through the Holocene of $\approx$20 ‰, which is similar to the total range of δ^2H values calculated from the speleothem $\delta^{18}O$ values via the relationship derived from the Global Meteoric Water Line ($\delta^2H = 8*\delta^{18}O+10$). The speleothem records exhibit the same general structure with lower $\delta^{18}O$ values in the mid-Holocene relative to earlier and later times. The trends in these records have been interpreted as indicating an early Holocene intensification of the monsoon followed by pronounced shifts in monsoon intensity, related to factors such as the position of the ITCZ and ENSO modulated changes in monsoon intensity and cyclone frequency from at least the mid Holocene [66, 67, 173]. This interpretation is in broad accord with the interpretation based on the Girraween δ^2H_{wax} record.

In detail, the speleothem and alkane records differ. The inferred trend to wetter conditions from the early to mid-Holocene Holocene begins at 11ka in the speleothem record at Ball Gown Cave and is uni-directional, whereas the δ^2H_{wax} record and aquatic pollen representation fluctuates into the early Holocene followed by a sustained trend to wetter conditions after 9 ka. Where the δ^2H_{wax} record and KNI-51 speleothem record overlap from 8 ka, the records are similar in trend. The difference between the Ball Gown speleothem record and the δ^2H_{wax} record likely relates to the location of Ball Gown Cave clearly in the 'pseudo'-monsoon zone, under the influence of recycled anticyclonic air masses that travel over the eastern Indian Ocean, deflected westwards under the influence of the Pilbara heat low [97, 174]. In contrast, Girraween Lagoon lies in the 'true' monsoon region under the influence of cross-equatorial air flow, and KNI-51 lies close to the boundary between the two. The differences between the two zones are evident in the $\approx$2 ‰ offset in $\delta^{18}O$ values between Ball Gown and KNI-51 (Figure 7.4).

Gentilli [174] proposed that the boundary between the 'pseudo'-monsoon and monsoon shifted zonally in the Holocene as climate warmed and the influence of the Pilbara heat Low changed. Girraween lagoon would be sensitively placed to record periods in the early Holocene when rainfall at the site was derived from the two sources, of divergent $\delta^{18}O$ value, and potentially also from divergent precipitation mechanisms that lead to different $\delta^{18}O$ values [42]. In addition, in the modern environment, the western Australian coast is subjected to a greater proportion of tropical cyclone landfalls (9.2–12.4 per decade) than the Northern Territory coast [6.8 per decade, 175]. Tropical cyclones produce intense rainfall of relatively low $\delta^{18}O$ values [53, 85], so changes in the number of cyclones making landfall in the Girraween area due to changes in the extent of the 'pseudo' monsoon domain in the early Holocene would impact local water balance and the δ^2H_{wax} record. Thus low δ^2H_{wax} values in the early Holocene are interpreted as periods where the true monsoon dominated, and high values as periods when the 'pseudo'-monsoon regime extended eastwards over the site as the monsoon fully established over the region.

In the last two thousand years, the KNI-51 speleothem $\delta^{18}O$ values decrease, while δ^2H_{wax} values do not, although there is a slight increase in aquatic pollen representation implying a slight increase in water balance at Girraween (Figure 7.4). This relatively minor divergence may have multiple causes. The divergence might be due to relative changes in the total amount of precipitation resulting from a long term increase in monsoon strength and associated precipitation, a phenomenon observed over the last 200 years [176]. It might also be due to the relative proportion of different precipitation modes at the two sites [177, 42], including changing cyclone incidence [67, 85], either of which can modify the $\delta^{18}O$ values of rainfall . In either case the changes could be driven by interactions between the multiple potential controls on rainfall in northern Australia [178, 179, 180, 181].

7.5 Conclusions

We present the first molecular isotope paleohydrological record for monsoonal tropical Australia. The observed record of change in δ^2H_{wax} values over the course of the Holocene in the Girraween record is best explained by changes in rainfall type, amount and the seasonality of rainfall in the past. A record of aquatic pollen representation for the same site is in close accord with the major changes in δ^2H_{wax} values, which provided evidence for the interpretation of changes in δ^2H_{wax} values the result of combinations of changing rainfall and evaporative demand. The Girraween δ^2H_{wax} record also displays a remarkable general coherence with speleothem records in this region. Trends in these records have been interpreted as indicating early Holocene intensification of the monsoon followed by pronounced shifts in monsoon intensity, related to factors such as the position of the ITCZ and ENSO-modulated changes in monsoon intensity and cyclone frequency from at least the mid Holocene. Differences between the *n*-alkane and speleothem records are attributed to a difference in location between the lake and speleothem record relative to the 'pseudo' and 'true' monsoon regions in north Australia. Combining speleothem and *n*-alkane isotope records provides a powerful tool for providing a more nuanced view of changes in hydroclimate in the past.

sample	depth (m)	Age (cal BP)	nC17 (µg/g dry weight)	nC17 fraction of total	nC19 (µg/g dry weight)	nC19 fraction of total	nC21 (µg/g dry weight)	nC21 fraction of total	nC23 (µg/g dry weight)	nC23 fraction of total	nC25 (µg/g dry weight)	nC25 fraction of total	nC27 (µg/g dry weight)	nC27 fraction of total	nC29 (µg/g dry weight)	nC29 fraction of total	nC31 (µg/g dry weight)	nC31 fraction of total	nC33 (µg/g dry weight)	nC33 fraction of total	nC35 (µg/g dry weight)	nC35 fraction of total	ACL odd (nC17 to nC33)
'A12'	0.12	64	0.85	0.01	2.37	0.01	5.69	0.03	8.94	0.05	17.61	0.11	22.45	0.14	24.32	0.15	18.82	0.11	21.50	0.13	42.82	0.26	29.9
'A16'	0.16	147	0.75	0.01	2.19	0.02	4.73	0.03	8.44	0.06	16.89	0.12	21.69	0.15	22.78	0.16	16.47	0.11	17.83	0.12	34.21	0.23	29.8
'A34'	0.34	523	0.00	0.00	0.00	0.00	0.49	0.01	2.05	0.04	4.98	0.11	6.89	0.15	7.54	0.16	5.24	0.11	6.78	0.14	13.46	0.28	29.9
'A52'	0.52	831	0.55	0.01	0.79	0.01	1.92	0.02	7.14	0.07	16.09	0.16	20.97	0.21	22.08	0.22	13.94	0.14	16.15	0.16	0.00	0.00	29.7
'A72'	0.72	1131	0.54	0.01	0.00	0.00	0.66	0.01	4.04	0.05	9.25	0.12	11.80	0.15	12.83	0.16	9.26	0.12	10.95	0.14	19.93	0.25	29.9
'B13'	1.13	1727	0.00	0.00	0.53	0.01	1.15	0.01	5.82	0.06	13.33	0.14	16.90	0.18	18.09	0.19	12.88	0.14	10.70	0.11	14.65	0.16	29.6
'B33'	1.33	2107	0.00	0.00	0.50	0.01	1.04	0.01	5.27	0.06	12.61	0.14	17.83	0.20	17.96	0.20	11.18	0.12	9.37	0.10	14.76	0.16	29.4
'B53'	1.53	2522	0.00	0.00	0.51	0.01	1.08	0.01	4.60	0.05	12.12	0.13	18.39	0.19	19.60	0.20	11.94	0.12	10.68	0.11	17.06	0.18	29.5
'B73'	1.73	2932	0.00	0.00	0.00	0.00	0.38	0.01	1.77	0.03	5.68	0.10	10.24	0.19	11.29	0.21	6.44	0.12	7.42	0.14	11.05	0.20	29.6
B82'	1.82	3337	0.58	0.01	0.00	0.00	0.57	0.01	2.40	0.03	7.41	0.09	13.83	0.17	15.61	0.20	8.72	0.11	11.63	0.15	19.01	0.24	29.7
'C13'	2.13	3742	0.00	0.00	0.00	0.00	0.00	0.00	2.51	0.02	11.86	0.08	19.78	0.13	22.60	0.15	12.96	0.09	29.91	0.20	51.80	0.34	30.2
'C33'	2.33	4540	0.00	0.00	0.00	0.00	0.00	0.00	1.61	0.02	6.72	0.08	10.16	0.12	11.46	0.14	7.23	0.09	17.34	0.21	28.50	0.34	30.4
'C54'	2.54	5508	0.00	0.00	0.00	0.00	0.00	0.00	1.35	0.02	6.09	0.09	10.00	0.14	11.24	0.16	5.48	0.08	14.40	0.20	21.87	0.31	30.2
'C74'	2.74	6466	0.00	0.00	0.00	0.00	0.00	0.00	1.26	0.02	5.29	0.08	8.74	0.14	10.34	0.16	5.05	0.08	13.23	0.21	20.54	0.32	30.2
'C84'	2.84	6970	0.00	0.00	0.00	0.00	0.00	0.00	1.29	0.01	6.98	0.07	12.83	0.13	15.78	0.16	7.75	0.08	22.13	0.22	34.03	0.34	30.3
'D12'	3.12	8370	0.00	0.00	0.00	0.00	0.00	0.00	1.71	0.03	6.12	0.11	12.32	0.23	10.85	0.20	5.26	0.10	14.92	0.27	3.47	0.06	30.1
'D33'	3.33	8970	0.00	0.00	0.00	0.00	0.00	0.00	0.13	0.03	0.53	0.12	0.97	0.21	0.79	0.17	0.60	0.13	0.92	0.20	0.63	0.14	29.9
'D53'	3.53	9430	0.00	0.00	0.00	0.00	0.00	0.00	0.17	0.03	0.75	0.12	1.65	0.26	1.63	0.26	1.20	0.19	0.00	0.00	0.94	0.15	28.8
'D73'	3.73	9895	0.00	0.00	0.00	0.00	0.00	0.00	0.23	0.03	0.84	0.12	1.97	0.28	1.78	0.25	1.75	0.25	0.00	0.00	0.55	0.08	28.9
'D84'	3.84	10151	0.00	0.00	0.00	0.00	0.00	0.00	0.24	0.06	0.73	0.20	0.97	0.26	0.80	0.22	0.84	0.23	0.00	0.00	0.13	0.04	28.9
'E10'	4.1	10740	0.00	0.00	0.00	0.00	0.00	0.00	0.12	0.10	0.36	0.29	0.38	0.31	0.27	0.21	0.13	0.10	0.00	0.00	0.00	0.00	28.3
average			0.001	0.001	0.003	0.003	0.01	0.01	0.04	0.04	0.12	0.12	0.19	0.19	0.19	0.19	0.12	0.12	0.13	0.13	0.19	0.19	29.7
(1σ)			0.003	0.003	0.005	0.005	0.01	0.01	0.02	0.02	0.05	0.05	0.05	0.05	0.03	0.03	0.05	0.05	0.08	0.08	0.11	0.11	0.5

alkane	average fraction of C17-C35 in total	error (1S)
nC17	0.0014	0.0027
nC19	0.0026	0.0047
nC21	0.0073	0.0104
nC23	0.0416	0.0216
nC25	0.1216	0.0479
nC27	0.1868	0.0545
nC29	0.1864	0.0339
nC31	0.1239	0.0455
nC33	0.1341	0.0793
nC35	0.1943	0.1123

Calibrated age 95% probability range (cal BP)	Calibrated age (median probability)
654–724	676
737–823	796
3687–3852	3766
5656–5798	5762
8429–8590	8512
10,197–10,302	10252
15,188–15,740	15453

Supplementary Table 1. n -alkane distributions from the Girraween Lagoon. ^{14}C Radiocarbon age uncertainty data from Rowe et al. [155]

Chapter 8

Discussion

Several factors need to be considered when interpreting a stable isotope proxy record of paleohydrological conditions such as the leaf wax record derived in this thesis (Figure 7.3, chapter 7). First, Chapters 3, 4, 5 and 6 demonstrated that rather than a 'simple linear' interpretation such as that implied by the classical amount effect, there are higher order controls resulting from local meteorology and circulation patterns that strongly influence the interpretation of the rainfall isotopic signal that flow directly into the inference of past climatic conditions. Secondly, modifications to the rainwater isotopic signal after rain has entered the terrestrial biosphere and potential fraction effects associated with the incorporation and preservation of a rainfall signal in a proxy record, can significantly impact interpretation, as discussed in Chapter 7. The major inferences that can be drawn from the previous chapters are discussed below.

8.1 Modern drivers of variability in monsoon rainfall isotopic composition

Water stable isotope signatures preserved in a range of natural archives in tropical regions have long been used as a simple wet-dry proxy, with high $\delta^{18}O$ or $\delta^{2}H$ values used to infer 'dry' periods and low values used to infer 'wet' periods. While this often holds true at the general level and on longer timescales, the data presented in this thesis clearly demonstrates that drivers of isotopic variation are more complex and can lead to results opposite to those that would be inferred by assuming a simple 'amount effect'.

In contrast to earlier studies in this region [76], rainfall isotope measurements across all the studies comprising this thesis (n=847) showed weak correlations with rainfall amount at the measurement sites. This indicates that the microphysical based frame work proposed by Dansgaard [15] (Rayleigh distillation and isotopic exchange) alone, cannot fully explain observed rainfall isotopic variation in northern Australia (and beyond).

At a regional level, rainfall amount and $\delta^{18}O$ values showed a strong relationship, during single rainfall events comprising several days, across several seasons and at different locations (see for example Table 3.1, Figures 3.4 and 4.1). Spectral analysis (Figure 4.3) showed similar periodicities for both parameters indicating that they share a common driver and this observation does suggest that the stable isotope record encoded in archives such as speleothems and lake sediments at annual to millennial resolution can be used as a proxy for longer-term change in wet season precipitation amount.

Analysis of satellite imagery and strong statistical correlations further strengthened the inference that regional processes play an important role in driving $\delta^{18}O$ variability. Periods of low $\delta^{18}O$ values were associated with the presence of large convective systems (Mesoscale Convective Systems) in the region. Typical of these MCSs is the presence of large (stratiform) cloud decks and the subsidence of vapour from higher altitudes. This vapour from aloft is generally depleted in ^{18}O and ^{2}H and, as a result, its condensate produces precipitation with low $\delta^{18}O$ values. Consequently, the presence of MCSs will lower the overall vapour and rainfall $\delta^{18}O$ values in a region, especially when these systems are located upwind of the measurement station. The magnitude of this recycling effect increases when vapour is recycled through multiple systems (see Figure 3.4a).

Moisture recycling in large convective systems also plays a significant role in modulating rainfall isotopic composition variability as illustrated by the strong correlation between $\delta^{18}O$ and accumulated rainfall along air parcel trajectories during two monsoonal events (chapter 3). Parcels that were subject to more rainfall events along the track showed stronger depletion and vice versa. This means that the periods of low $\delta^{18}O$ values in the proxy record may be associated with periods of enhanced large convective system activity in the region.

Five circulation regimes (classified using lower tropospheric wind and humidity profiles) dominated the weather during multiple seasons in Darwin (Chapter 4). These weather types each produced a specific range of $\delta^{18}O$ values. High resolution radar data suggested several explanations for these findings, such as distinct convective/stratiform rainfall fractions, reflectivities, raining area and cloud height distributions.

Typical monsoon-break conditions (easterly winds, trades and see breeze) were associated with intense convection. Radar pixels showed high convective reflectivities indicating intense convection (strong updrafts) and high cloud top heights, relatively smaller stratiform areas and higher $\delta^{18}O$ values. This convection was usually short lived. Convective cells during the active monsoon regime (westerlies) are often less intense and embedded in large mesoscale stratiform decks [105]. This accords with the relatively lower estimated cloud top heights during the DW regimes and associated lower convective reflectivities.

Possible explanations for the relatively high $\delta^{18}O$ values of rain originating from such convective cells are: (a) A relatively short life time of these cells, providing insufficient time for a recycling process [19] to take effect. (b) Cloud microphysics in convective cells producing different $\delta^{18}O$ values than stratiform clouds [41], and in addition, larger raindrops being less sensitive to isotopic exchange [15] after formation in convective conditions.

Rainfall in tropical regions is a mixture of convective and stratiform contributions as stratiform clouds are essentially older convective cells where strong updrafts have ceased to exist [106]. So, rainfall isotope composition represents a mix of these two cloud components. Multi-year meteorological and rainfall isotope data presented in chapter 4 showed that, different weather types, each with their associated type of convection, produced a specific range of $\delta^{18}O$ values. However rainfall amounts were often similar. This suggests that, in addition to the amount effect and moisture recycling, the type of convection and associated clouds and rainfall is a driver of $\delta^{18}O$ variability. Thus, rainfall $\delta^{18}O$ should be interpreted as a proxy for weather type rather than just rainfall amount. CPOL radar data at sub-daily timescales potentially enables monitoring convective cells on a raindrop size resolution and thereby tracking the evolution of convective cells and their rainfall isotopic development real-time. This can provide further insights regarding the relative contributions of different processes driving rainfall isotope composition.

8.2 The influence of TCs on the proxy record

TC rain can make a large contribution to vadose zone water that serves as the source for water influenced stable isotope proxy records. Numerous studies in the northern hemisphere (mainly in the US) have found that TC rain is often more depleted of the heavy water isotopes (^{18}O and ^{2}H) than regular (summer/monsoon) rainfall. This, in combination with high resolution chronologies, enables reconstructions of past TC activity. However, while Australia is home to such proxy records, no in situ isotopic measurements of TC- and monsoon rain have been available to test this hypothesis and examine the relationship between TC- and monsoon rainfall isotopic composition.

In this thesis, four TCs were sampled for their rainfall (and in some cases, vapour) isotopic content using a mobile specialised 4wd vehicle and network of volunteers. In addition, rainfall sampling stations were established near a speleothem -stable isotope- proxy site in northeast Australia to provide a multiple season rainfall isotopic baseline. This section will briefly discuss the isotopic composition of TC rain and its potential influence on the isotopic signal in the proxy record.

8.2.1 TC rainfall isotopic composition

In general, results from the four TCs observed during the course of this study confirmed findings reported elsewhere, that the $\delta^{18}O$ values of TC rainfall are relatively low. However, in some cases observed $\delta^{18}O$ values were comparable to, and in the range of, $\delta^{18}O$ values observed during 'normal' monsoon rainfall events. While the processes governing rainfall isotope composition of TC and monsoon rainfall are broadly similar, the extreme meteorological conditions and structures that are characteristic of TCs make the interpretation of TC rainfall isotope composition quite complex. For example, strong winds near the eye wall generate large amounts of sea spray. This has been reported to recharge the TC with heavy water isotopes increase the $\delta^{18}O$ values of vapour and rain near the eye wall. In contrast, rain bands outside the eye wall form effective fractionation chambers, leading to progressive rain out of heavy isotopes resulting in a decrease in $\delta^{18}O$ values towards the eye wall. In addition, fluctuations in TC intensity can also lead to changes in rainfall isotopic composition. A sudden decrease in updrafts, caused by, for example, landfall or an eye wall replacement cycle, may result in a downward flush of ice particles from aloft resulting in rainfall with low $\delta^{18}O$ values. A progressive lowering of TC rainfall $\delta^{18}O$ values towards the eye wall and over time has been attributed to rainout after making landfall and disconnecting from (relatively enriched) oceanic source water [182].

Data presented in this thesis proved valuable in assessing TC isotope dynamics. Chapter 5 demonstrated that the spatial structure of a landfalling TC remained fairly constant and exhibited a clear radial distribution, in line with observations elsewhere. Combined data from all four TC's combined showed a strong relationship with distance to the measurement sites, suggesting that rainfall isotopic composition can be used to estimate the distance to a nearby TC. In other aspects this data set differs from earlier studies; TC intensity has been reported to correlate negatively with speleothem $\delta^{18}O$ values [84, 107], suggesting that larger, more intense TC produce more negative $\delta^{18}O$ rainfall values. While this seems intuitive as larger, more intense TCs would exhibit larger stratiform cloud decks and stronger more efficient recycling as discussed above, the data presented in this thesis did not confirm this hypothesis. On the contrary, low $\delta^{18}O$ values were observed across a range of intensities from category 2 to category 4 TCs. Modelling done by Gedzelman et al. [115] suggested that tropical rain systems develop lowest $\delta^{18}O$ values long before reaching hurricane strength, which could explain our observations. This means that a strongly depleted rainfall signal is not exclusive to large TC systems. I also note that the complex meteorological processes governing rainfall isotopic composition in TCs operate on timescales much smaller than resolved in the available observational data (≈ 3–6–12 hours), and am therefore cautious to over-interpret this dataset. Based on the data available and accepting its limitations, I conclude that the amplitude of $\delta^{18}O$ values are only indicative of distance between TCs and measurement locations.

8.2.2 Post rainfall isotopic changes of TC rain

Several processes affect the isotopic composition of rainwater once in a (karst or surface) reservoir. First, kinetic fractionation effects during evaporation of surface waters could potentially lead to an increase in $\delta^{18}O$ values, especially if the water is exposed to the atmosphere for prolonged periods of time. This effect is clearly seen in Figure 7.2 , chapter 7, which illustrates evaporative enrichment in heavy isotopes of lake water during the the dry season. Secondly, mixing of TC rain with soil water will dilute the TC rainfall isotopic signature as the soil water most likely has a different precipitation history and may also have been subject to evaporation. Thirdly, as the rainwater percolates through the epikarst it is subject to isotopic exchange with the limestone bedrock that it dissolves. Kinetic fractionation during deposition of the secondary carbonate can also change the isotopic composition of its final deposit that forms the speleothem.

Nott et al. [107] observed alternating ochre and white layers along the stalagmite's growth axis, representing the wet and dry season respectively in Chillagoe, north-east Australia. The ochre layer was interpreted as the start of the wet season rains flushing organics and clays. Park Rangers also reported short lag times (personal communication), suggesting a relatively short water residence time that would reduce the potential enrichment in heavy isotopes of the surface water and reduced isotopic exchange within the epikarst system. Monitoring of cave temperatures, humidity levels and intra layer analysis of $\delta^{18}O$ values of the speleothem in Chillagoe [107] and [85] indicated equilibrium conditions in the cave at time of deposition. This indicates that changes in rain water isotope composition before it precipitates as calcite are most likely relatively small, and kinetic fractionation did not occur during the precipitation of the calcium carbonate [107] . Therefore, changes in isotope composition of the speleothem are expected to be mostly driven by changes of the isotopic composition of the waters in the vadose zone, which in turn, are driven by the input of monsoon- and TC rainfall.

A change in speleothem $\delta^{18}O$ values of more than 2.5 ‰ has been attributed to the presence of TC's for this site and mainly depends on isotopic composition of the water in the vadose zone [107]. This, as discussed above, fluctuates as input of TC rain water with relatively low $\delta^{18}O$ values mixes with the water in the vadose zone water. The potential rate of change in isotopic composition of the vadose zone water due to the influx of TC rainwater was evaluated using two moving scenarios and this demonstrated that, for the observed amount of TC rainfall, the 'isotopic impact' of TCs diminishes very quickly with increasing distance to the eyewall. For distances larger than ≈100 km, none of the observed TCs would cause a large enough perturbation in the isotopic composition of the speleothem at this location, and this is likely a general finding.

8.3 Leafwax *n*-alkane record

In addition to the isotopic composition of rainfall, discussed in Chapters 3, 4 and 6, the isotopic composition of leaf wax *n*-alkanes are determined by several others factors in the ecosystem that should be considered in interpreting the record [159]. These include (i) potential evaporation of water in the environment prior to biosynthesis of the *n*-alkanes, leading to an increase in the δ^2H value of the water, and (ii) a number of climate-, species-, and therefore location-specific variables that govern the apparent water-alkane isotope fractionation factor (ε_{alk}).

Thus surface and soil water is subject to an extended period where evaporation can lead to a significant increase in the δ^2H value of the remaining water. This is evident in the seasonal increase of 20–30 ‰ in the δ^2H value of the water in Girraween Lagoon (Figure 7.2) and this will be reflected in the δ^2H_{alk} values of aquatic vascular plants in the lagoon [160, 137, 161]. This enrichment is likely to effect shallow-rooted grasses and is possibly of less significance to deeper rooted trees.

In addition, fractionation factors during the production of n-alkanes are different for particular vegetation types (trees or grasses). For example, Sachse et al. [61] demonstrated that C3 dicots, primarily trees, fractionate hydrogen isotopes to a lesser degree than C4 monocots, primarily grasses. At lower latitudes however, these differences decrease [161]. While these differences are small, it is expected that vegetation type will exert some control on δ^2H_{alk}. Furthermore, fractionation in C4 plants is not sensitive to rainfall (aridity) while fractionation in C3 plants changes as rainfall changes [162].

However, Vogts et al. [14] reported near constant hydrogen isotope fractionation between precipitation and alkane (C29, C31, C33) of -109 $\pm$ 5 ‰ from marine surface sediment receiving input from adjacent terrestrial environments ranging from forest to grassland along the west coast of Africa, possibly partly due to the opposing effects of changing apparent ecosystem fractionation factors as tree:grass ratio changes with increasing aridity. As the in this thesis shows no correlation between tree-grass ratio and variations in δ^2H_{alk} it is unlikely that changing tree-grass ratio in the Holocene was a major driver of variations observed in the δ^2H_{alk} record.

This leads to the conclusion that the observed variability in the Girraween Lagoon n-alkane δ^2H record is best explained by changes in rainfall type, amount and or the seasonality of rainfall and that δ^2H_{alk} can best be interpreted as providing a combined measure of water availability and evaporative demand. Thus low δ^2H_{alk} values should indicate relatively wetter periods/less seasonality which high δ^2H_{alk} values indicate drier periods/more seasonality. This conclusion is supported by the aquatic pollen record of Girraween Lagoon [155] which is in close accord with the major changes in the δ^2H_{alk} record.

Three periods were clearly distinguishable in the δ^2H_{alk} record from Girraween Lagoon. In the first period (from 11ka until ≈8.5 ka), δ^2H_{alk} were relatively high and variable implying periods of low and higher rainfall and variability in the type of convection over the region. At 12 ka the sea level was 40–50 m below present and hence the coastline was 100 km further away from the site [165], potentially resulting in lower rainfall compared to the coast as is the case today [7]. In addition, the Early Holocene has been proposed to be a period of increased ENSO activity [166] which may have to to increased inter-annual variability in rainfall and seasonality as is currently observed in the region [7].

δ^2H_{alk} reach a broad minimum in the second period (between ≈6ka and ≈4 ka), δ^2H_{alk}. This period was interpreted as a time when the monsoon was intensified and prolonged (longer periods of typical deep westerly winds) and coincides with slightly higher sea levels than modern and the coast ≤20 km distant from the site [167]. Others have interpreted this region as a relative wet period for Australia [67] and globally as a period of reduced ENSO [168, 169, 170]. δ^2H_{alk} values increase again in the third period (from 4–3 ka), and thereafter increase marginally towards the present with no marked rapid changes. This trend suggests decreased annual rainfall and or increased seasonality relative to the mid-Holocene and is likely due to increased ENSO variability, illustrated by interannual decadal variability in rainfall amount and change in wet season length [7].

The inference and timing of increased ENSO variability in the Girraween Lagoon δ^2H_{alk} correspond well with other records in this region [171, 67, 172, 170]. There was also a remarkable general coherence with speleothem records from western Australia, despite the δ^2H_{alk} record being of lower resolution and less precisely dated. Differences that do exist between the speolethem and Girraween lagoon records may be due to a different location in regards to the position of the monsoon trough. The speleothem records are placed within the 'pseudo'-monsoon zone, under influence of recycled anti cyclonic airmasses that travel over the Indian Ocean, deflected westwards under the influence of the Pilbara heat low [97, 174]. In contrast, Girraween

Lagoon lies in the ‘true’ monsoon region under the influence of cross-equatorial air flow.

Chapter 9

Summary and future directions

This thesis takes an important step towards a better understanding of factors that control isotopic composition of natural archives in tropical Australia. Extensive measurement campaigns covered 'all' types of modern tropical rainfall, during dry and wet seasons (Chapters 3 and 4), and extreme events such as Tropical Cyclones (Chapters 5 and 6).

The data and associated analysis effectively contributed to filling a knowledge gap in relation to the inconsistencies of the 'amount effect' when measuring on short timescales that has been highlighted by numerous previous studies on this topic and during the IAEA Coordinated Research Project (CRP) entitled 'Stable isotopes in precipitation and paleoclimatic archives in tropical areas to improve regional hydrological and climatic impact models' (2013–2016). While great progress has been made and pan-tropical datasets of daily rainfall isotopic composition are now available [183] there are still challenges and opportunities that remain. The results of each Chapter in this thesis and recommendations for future research are summarised below.

Two monsoon rainfall events (see Chapter 3) in Darwin were closely (every 12 hrs) monitored to capture their evolution in rainfall isotopic composition. Possible drivers of rainfall isotopic variation were investigated, using remote sensing and local meteorological data. The main drivers of isotopic variation in precipitation on these intra-seasonal timescales were found to be (i) integrated precipitation history along air mass trajectories and (ii) the spatial extent and organisation of convective activity in the region. A local amount effect was not statistically significant on 12 hourly timescales. This indicated that the 'amount effect', which was until then the benchmark of rainfall isotopic variability interpretations, may not be main driver of rainfall isotopic variation in north Australia. This Chapter also showed that the larger scale atmospheric state was related to isotopic data from a single measurement location.

The measurement campaign described in Chapter 4 was the first of its kind in Australia. It combined multiple seasons of daily rainfall isotope, radar and weather balloon data and effectively combined the fields of meteorology and geochemistry to systematically investigate drivers of rainfall isotopic variation. The data showed that rainfall isotopic composition was related to different weather types that constitute the Australian monsoon. Rainfall isotopic variability was not related to local rainfall amount but to the properties of convection that are linked to large scale circulation regimes. Positive isotopic anomalies were associated with shallow westerly and easterly regimes when stratiform rainfall fractions were relatively small. The largest negative anomalies were recorded during the active monsoon regime (deep west) and were associated with the passage of the MJO. This suggests that isotopic proxy records in north Australia record the frequency with which these typical wet season regimes occur.

The Tropical Cyclone specific field campaign undertaken in north east Australia has led to some important insights in regards to the use of water stable isotopes in this specific region. Due to its geographical location, this area receives rain all year round and the local climatology (trade wind versus monsoon weather) were clearly visible in the rainfall stable isotope composition. This means that seasonal chronologies can potentially be retrieved from natural archives in this region such as tree rings, lake sediments or speleothems. This seasonality was also apparent in d-excess values. Furthermore a positive relationship with the meridional wind vector suggested that d-excess may be used as an indicator of duration and strength of monsoon conditions and proxy for trade wind strength.

Hypothetical mixing scenarios with data collection from four TCs and monsoon rainfall data demonstrated that some TCs would most likely go undetected in a stable isotope proxy record in this region. Furthermore, detectability of TCs in the stable isotope record was found to be strongly dependant on the distance of the TC eye wall to a potential proxy site, the data suggested that the limit for detection was around ≈100 km. This leads us to the question how representative one particular speleothem is for a region. Perhaps comprehensive statistical analysis, combined with the collection of potentially more speleothems throughout the region or combined analysis with other proxy records might shed more light on these matters.

These results add considerable nuance to the interpretation of stable isotope paleo climatic proxy records. While the 'amount' effect provides a simple wet-dry proxy, the results from Chapters 3 and 4 allow for a more comprehensive analysis of past rainfall, cloud and climatic conditions. Furthermore, these results also have important implications for other fields of research that use water stable isotopes, for example, ground water studies (hydrology) or climate/weather modelling that can use these results to improve cloud system parameterisations.

Until now, rainfall stable isotope composition has often been interpreted on relatively long time scales (monthly data), using averages and statistical relationships. However, processes that affect water stable isotope ratios in clouds and rainfall operate on very short time scales of seconds, minutes and hours). Resolving stable isotope composition on cloud-scale level is a big challenge. While the physics of stable isotope behaviour is relatively well understood, there is a lack of in-situ data to verify the theoretical framework and determine the relative importance/dominance of each driving parameter, under different weather conditions, at different sites. Progress has been made in regards to collecting data on shorter time scales, however, the real challenge is to combine this with in-situ high resolution weather data. Without the weather data, many interpretations are still based on 'best guess' estimates of micro meteorology processes.

An important step towards the reconstruction of hydro climate in this region was made with the start of reconstructing the first leaf wax climate record in north Australia (see Chapter 7). While the sampling resolution at this stage was still relatively low, results are promising and show remarkable coherence with other proxy records from this region. There were clear general trends in this record that have been interpreted as changes in monsoon regimes, water availability, and most likely related to factors such as the ITCZ and ENSO. The results of this core shows potential for leaf wax based climate reconstruction beyond the LGM. This, and resampling the Holocene part of this core at higher resolution was beyond the scope of this thesis and will be part of future research. The results of this thesis and future research will ultimately contribute to unravelling the natural and human drivers of change in northern Australia's climate and biodiversity.

Bibliography

[1] Alexandra Edelman, Andrea Gelding, Elena Konovalov, Rodney McComiskie, Anne Penny, Nicholas Roberts, Shelley Templeman, Dennis Trewin, Mark Ziembicki, Blair Trewin, et al. State of the Tropics 2014 report. 2014.

[2] Michael I Bird, Jordahna Haig, Xennephone Hadeen, Maria Rivera-Araya, Christopher M Wurster, and Costijn Zwart. Stable isotope proxy records in tropical terrestrial environments. *Palaeogeography, Palaeoclimatology, Palaeoecology*, 538:109445, 2020.

[3] Pin Xian Wang, Bin Wang, Hai Cheng, John Fasullo, ZhengTang Guo, Thorsten Kiefer, and ZhengYu Liu. The global monsoon across time scales: Mechanisms and outstanding issues. *Earth-Science Reviews*, 174:84–121, 2017.

[4] Karl-Heinz Wyrwoll, Zhengyu Liu, Guangshan Chen, John E Kutzbach, and Xiaodong Liu. Sensitivity of the Australian summer monsoon to tilt and precession forcing. *Quaternary Science Reviews*, 26(25-28):3043–3057, 2007.

[5] Garry D Cook and Richard G Heerdegen. Spatial variation in the duration of the rainy season in monsoonal Australia. *International Journal of Climatology: A Journal of the Royal Meteorological Society*, 21(14):1723–1732, 2001.

[6] M.C Wheeler and J.L Bride. *Intraseasonal Variability in the Atmosphere-Ocean Climate System*. Praxis Publishing, 2005.

[7] S Charles, C Petheram, A Berthet, G Browning, G Hodgson, M Wheeler, A Yang, S Gallant, J Vaze, B Wang, et al. Climate data and their characterisation for hydrological and agricultural scenario modelling across the Fitzroy, Darwin and Mitchell catchments. Technical report, A technical report to

the Australian Government from the CSIRO Northern Australia Sustainable Yields Project, 2016.

[8] Thibaut Caley, Bruno Malaizé, Marie Revel, Emmanuelle Ducassou, Karine Wainer, Mohamed Ibrahim, Dina Shoeaib, Sébastien Migeon, and Vincent Marieu. Orbital timing of the Indian, East Asian and African boreal monsoons and the concept of a 'global monsoon'. *Quaternary Science Reviews*, 30(25-26): 3705–3715, 2011.

[9] Rosanne D'Arrigo, Patrick Baker, Jonathan Palmer, Kevin Anchukaitis, and Garry Cook. Experimental reconstruction of monsoon drought variability for Australasia using tree rings and corals. *Geophysical Research Letters*, 35(12), 2008.

[10] Anthony S Kiem, Fiona Johnson, Seth Westra, Albert van Dijk, Jason P Evans, Alison O'Donnell, Alexandra Rouillard, Cameron Barr, Jonathan Tyler, Mark Thyer, et al. Natural hazards in Australia: droughts. *Climatic Change*, 139(1):37–54, 2016.

[11] Raktima Dey, Sophie C Lewis, Julie M Arblaster, and Nerilie J Abram. A review of past and projected changes in Australia's rainfall. *Wiley Interdisciplinary Reviews: Climate Change*, 10(3):e577, 2019.

[12] W Mook and Kazimierz Rozanski. Environmental isotopes in the hydrological cycle. *IAEA Publish*, 39, 2000.

[13] BL Konecky, DC Noone, and KM Cobb. The Influence of Competing Hydroclimate Processes on Stable Isotope Ratios in Tropical Rainfall. *Geophysical Research Letters*, 46(3):1622–1633, 2019.

[14] Angela Vogts, Tanja Badewien, Jürgen Rullkötter, and Enno Schefuß. Near-constant apparent hydrogen isotope fractionation between leaf wax n-alkanes and precipitation in tropical regions: Evidence from a marine sediment transect off SW Africa. *Organic geochemistry*, 96:18–27, 2016.

[15] Willi Dansgaard. Stable isotopes in precipitation. *Tellus*, 16(4):436–468, 1964.

[16] Gabriel J Bowen, Zhongyin Cai, Richard P Fiorella, and Annie L Putman. Isotopes in the Water Cycle: Regional-to Global-Scale Patterns and Applications. *Annual Review of Earth and Planetary Sciences*, 47, 2019.

[17] Roberto Gonfiantini, Michel-Alain Roche, Jean-Claude Olivry, Jean-Charles Fontes, and Gian Maria Zuppi. The altitude effect on the isotopic composition of tropical rains. *Chemical Geology*, 181(1-4):147–167, 2001.

[18] Kazimierz Rozanski, Luis Araguás-Araguás, and Roberto Gonfiantini. Isotopic patterns in modern global precipitation. *Climate change in continental isotopic records*, pages 1–36, 1993.

[19] Naoyuki Kurita. Water isotopic variability in response to mesoscale convective system over the tropical ocean. *Journal of Geophysical Research: Atmospheres*, 118(18):10376–10390, 2013.

[20] Naoyuki Kurita, Kimpei Ichiyanagi, Jun Matsumoto, Manabu D Yamanaka, and Tetsuo Ohata. The relationship between the isotopic content of precipitation and the precipitation amount in tropical regions. *Journal of Geochemical Exploration*, 102(3):113–122, 2009.

[21] Jessica L Conroy, David Noone, Kim M Cobb, Jessica W Moerman, and Bronwen L Konecky. Paired stable isotopologues in precipitation and vapor: A case study of the amount effect within western tropical Pacific storms. *Journal of Geophysical Research: Atmospheres*, 121(7):3290–3303, 2016.

[22] Ricardo Sánchez-Murillo, Christian Birkel, Kristen Welsh, Germain Esquivel-Hernández, J Corrales-Salazar, Jan Boll, E Brooks, Olivier Roupsard, O Sáenz-Rosales, Irina Katchan, et al. Key drivers controlling stable isotope variations in daily precipitation of Costa Rica: Caribbean Sea versus Eastern Pacific Ocean moisture sources. *Quaternary Science Reviews*, 131:250–261, 2016.

[23] C Zwart, NC Munksgaard, N Kurita, and MI Bird. Stable isotopic signature of Australian monsoon controlled by regional convection. *Quaternary Science Reviews*, 151:228–235, 2016.

[24] Mary Moore, Zhiming Kuang, and PN Blossey. A moisture budget perspective of the amount effect. *Geophysical Research Letters*, 41(4):1329–1335, 2014.

[25] Pradeep K Aggarwal, Oleg A Alduchov, Klaus O Froehlich, Luis J Araguas-Araguas, Neil C Sturchio, and Naoyuki Kurita. Stable isotopes in global precipitation: A unified interpretation based on atmospheric moisture residence time. *Geophysical Research Letters*, 39(11), 2012.

[26] Bronwen L Konecky, James M Russell, Thomas C Johnson, Erik T Brown, Melissa A Berke, Josef P Werne, and Yongsong Huang. Atmospheric circulation patterns during late Pleistocene climate changes at Lake Malawi, Africa. *Earth and Planetary Science Letters*, 312(3-4):318–326, 2011.

[27] Bronwen Konecky, James Russell, and Satria Bijaksana. Glacial aridity in central Indonesia coeval with intensified monsoon circulation. *Earth and Planetary Science Letters*, 437:15–24, 2016.

[28] Satrio A Wicaksono, James M Russell, Ann Holbourn, and Wolfgang Kuhnt. Hydrological and vegetation shifts in the Wallacean region of central Indonesia since the Last Glacial Maximum. *Quaternary Science Reviews*, 157:152–163, 2017.

[29] Luis Araguás-Araguás, Klaus Froehlich, and Kazimierz Rozanski. Stable isotope composition of precipitation over southeast Asia. *Journal of Geophysical Research: Atmospheres*, 103(D22):28721–28742, 1998.

[30] Niels C Munksgaard, Chris M Wurster, and Michael I Bird. Continuous analysis of δ18O and δD values of water by diffusion sampling cavity ring-down spectrometry: a novel sampling device for unattended field monitoring of pre-

cipitation, ground and surface waters. *Rapid Communications in Mass Spectrometry*, 25(24):3706–3712, 2011.

[31] Françoise Vimeux, Guillaume Tremoy, Camille Risi, and Robert Gallaire. A strong control of the South American SeeSaw on the intra-seasonal variability of the isotopic composition of precipitation in the Bolivian Andes. *Earth and Planetary Science Letters*, 307(1):47–58, 2011.

[32] Naoyuki Kurita, David Noone, Camille Risi, Gavin A Schmidt, Hiroyuki Yamada, and Kunio Yoneyama. Intraseasonal isotopic variation associated with the Madden-Julian Oscillation. *Journal of Geophysical Research: Atmospheres (1984–2012)*, 116(D24), 2011.

[33] Jessica W Moerman, Kim M Cobb, Jess F Adkins, Harald Sodemann, Brian Clark, and Andrew A Tuen. Diurnal to interannual rainfall δ^{18}O variations in northern Borneo driven by regional hydrology. *Earth and Planetary Science Letters*, 369:108–119, 2013.

[34] PR Lekshmy, M Midhun, R Ramesh, and RA Jani. ^{18}O depletion in monsoon rain relates to large scale organized convection rather than the amount of rainfall. *Scientific Reports*, 4:5661, 2014.

[35] Didier Gastmans, Vinícius Santos, Juliana Aparecida Galhardi, João Felipe Gromboni, Ludmila Vianna Batista, Konrad Miotlinski, Hung Kiang Chang, and José Silvio Govone. Controls over spatial and seasonal variations on isotopic composition of the precipitation along the central and eastern portion of Brazil. *Isotopes in environmental and health studies*, 53(5):518–538, 2017.

[36] S He, N. Goodkin, D. Jackisch, and M.R. Ong. Continuous real-time analysis of isotopic composition of precipitation during tropical rain events: insight into tropical convections. *in prep.*, 2018.

[37] Alexander Rohrmann, Manfred R Strecker, Bodo Bookhagen, Andreas Mulch, Dirk Sachse, Heiko Pingel, Ricardo N Alonso, Taylor F Schildgen, and Carolina

Montero. Can stable isotopes ride out the storms? The role of convection for water isotopes in models, records, and paleoaltimetry studies in the central Andes. *Earth and Planetary Science Letters*, 407:187–195, 2014.

[38] Camille Risi, Sandrine Bony, and Françoise Vimeux. Influence of convective processes on the isotopic composition (δ18O and δD) of precipitation and water vapor in the tropics: 2. Physical interpretation of the amount effect. *Journal of Geophysical Research: Atmospheres (1984–2012)*, 113(D19), 2008.

[39] Stanley David Gedzelman, James R Lawrence, James WC White, and Daniel Smiley. The isotopic composition of precipitation at Mohonk Lake, New York: the amount effect. *Journal of Geophysical Research: Atmospheres*, 92(D1): 1033–1040, 1987.

[40] Tyler B Coplen, Paul J Neiman, Allen B White, and F Martin Ralph. Categorisation of northern California rainfall for periods with and without a radar brightband using stable isotopes and a novel automated precipitation collector. *Tellus B: Chemical and Physical Meteorology*, 67(1):28574, 2015.

[41] Pradeep K Aggarwal, Ulrike Romatschke, Luis Araguas-Araguas, Dagnachew Belachew, Frederick J Longstaffe, Peter Berg, Courtney Schumacher, and Aaron Funk. Proportions of convective and stratiform precipitation revealed in water isotope ratios. *Nature Geoscience*, 9(8):624–629, 2016.

[42] C Zwart, NC Munksgaard, A Protat, N Kurita, D Lambrinidis, and M I Bird. The isotopic signature of monsoon conditions, cloud modes, and rainfall type. *Hydrological processes*, 32(15):2296–2303, 2018.

[43] Harmon Craig and Louis Irwin Gordon. Deuterium and oxygen 18 variations in the ocean and the marine atmosphere. 1965.

[44] Liliane Merlivat and Jean Jouzel. Global climatic interpretation of the deuterium-oxygen 18 relationship for precipitation. *Journal of Geophysical Research: Oceans*, 84(C8):5029–5033, 1979.

[45] Marion Benetti, Gilles Reverdin, Catherine Pierre, Liliane Merlivat, Camille Risi, Hans Christian Steen-Larsen, and Françoise Vimeux. Deuterium excess in marine water vapor: Dependency on relative humidity and surface wind speed during evaporation. *Journal of Geophysical Research: Atmospheres*, 119(2):584–593, 2014.

[46] Stephan Pfahl and Harald Sodemann. What controls deuterium excess in global precipitation? *Climate of the Past*, 10(2):771, 2014.

[47] Michael I Bird, Michael Brand, Aaron F Diefendorf, Jordahna L Haig, Lindsay B Hutley, Vladimir Levchenko, Peter V Ridd, Cassandra Rowe, James Whinney, Christopher M Wurster, et al. Identifying the 'savanna'signature in lacustrine sediments in northern Australia. *Quaternary Science Reviews*, 203: 233–247, 2019.

[48] Camille Risi, Sandrine Bony, Francoise Vimeux, Michel Chong, and Luc Descroix. Evolution of the stable water isotopic composition of the rain sampled along Sahelian squall lines. *Quarterly Journal of the Royal Meteorological Society*, 136(S1):227–242, 2010.

[49] Richard P Fiorella, Christopher J Poulsen, and Ashley M Matheny. Seasonal patterns of water cycling in a deep, continental mountain valley inferred from stable water vapor isotopes. *Journal of Geophysical Research: Atmospheres*, 123(14):7271–7291, 2018.

[50] K Froehlich, JJ Gibson, and PK Aggarwal. Deuterium excess in precipitation and its climatological significance. Technical report, 2002.

[51] George Hoffmann, Jean Jouzel, and Valerie Masson. Stable water isotopes in atmospheric general circulation models. *Hydrological Processes*, 14(8):1385–1406, 2000.

[52] Ricardo Sánchez-Murillo, Ana M Durán-Quesada, Christian Birkel, Germain Esquivel-Hernández, and Jan Boll. Tropical precipitation anomalies and d-

excess evolution during El Niño 2014-16. *Hydrological Processes*, 31(4):956–967, 2017.

[53] Niels C Munksgaard, Costijn Zwart, Naoyuki Kurita, Adrian Bass, Jon Nott, and Michael I Bird. Stable Isotope Anatomy of Tropical Cyclone Ita, North-Eastern Australia, April 2014. *PloS one*, 10(3):e0119728, 2015.

[54] Eugeni Barkan and Boaz Luz. High precision measurements of 17O/16O and 18O/16O ratios in H2O. *Rapid Communications in Mass Spectrometry: An International Journal Devoted to the Rapid Dissemination of Up-to-the-Minute Research in Mass Spectrometry*, 19(24):3737–3742, 2005.

[55] Joseph Galewsky, Hans Christian Steen-Larsen, Robert D Field, John Worden, Camille Risi, and Matthias Schneider. Stable isotopes in atmospheric water vapor and applications to the hydrologic cycle. *Reviews of Geophysics*, 54(4):809–865, 2016.

[56] JJ Gibson, SJ Birks, and TWD Edwards. Global prediction of δA and δ2H-δ18O evaporation slopes for lakes and soil water accounting for seasonality. *Global Biogeochemical Cycles*, 22(2), 2008.

[57] Brice Tchakam Kamtchueng, Wilson Yetoh Fantong, Mengnjo Jude Wirmvem, Rosine Edwige Tiodjio, Alain Fouépé Takounjou, Kazuyoshi Asai, Serges L Bopda Djomou, Minoru Kusakabe, Takeshi Ohba, Gregory Tanyileke, et al. A multi-tracer approach for assessing the origin, apparent age and recharge mechanism of shallow groundwater in the Lake Nyos catchment, Northwest, Cameroon. *Journal of Hydrology*, 523:790–803, 2015.

[58] Pedro Villegas, Vanesa Paredes, Teresita Betancur, Jean D Taupin, and Luis E Toro. Groundwater evolution and mean water age inferred from hydrochemical and isotopic tracers in a tropical confined aquifer. *Hydrological processes*, 32(14):2158–2175, 2018.

[59] Scott Jasechko and Richard G Taylor. Intensive rainfall recharges tropical groundwaters. *Environmental Research Letters*, 10(12):124015, 2015.

[60] Matthew S Lachniet. Climatic and environmental controls on speleothem oxygen-isotope values. *Quaternary Science Reviews*, 28(5):412–432, 2009.

[61] Dirk Sachse, Isabelle Billault, Gabriel J Bowen, Yoshito Chikaraishi, Todd E Dawson, Sarah J Feakins, Katherine H Freeman, Clayton R Magill, Francesca A McInerney, Marcel TJ Van der Meer, et al. Molecular paleohydrology: interpreting the hydrogen-isotopic composition of lipid biomarkers from photosynthesizing organisms. *Annual Review of Earth and Planetary Sciences*, 40:221–249, 2012.

[62] Jessica M Reeves, Timothy T Barrows, Timothy J Cohen, Anthony S Kiem, Helen C Bostock, Kathryn E Fitzsimmons, John D Jansen, Justine Kemp, Claire Krause, Lynda Petherick, et al. Climate variability over the last 35,000 years recorded in marine and terrestrial archives in the Australian region: an OZ-INTIMATE compilation. *Quaternary Science Reviews*, 74:21–34, 2013.

[63] A Nele Meckler, Stéphane Affolter, Yuri V Dublyansky, Yves Krüger, Nadia Vogel, Stefano M Bernasconi, Martin Frenz, Rolf Kipfer, Markus Leuenberger, Christoph Spötl, et al. Glacial–interglacial temperature change in the tropical West Pacific: A comparison of stalagmite-based paleo-thermometers. *Quaternary Science Reviews*, 127:90–116, 2015.

[64] Robin W Twaddle, Sean Ulm, Jane Hinton, Christopher M Wurster, and Michael I Bird. Sclerochronological analysis of archaeological mollusc assemblages: methods, applications and future prospects. *Archaeological and Anthropological Sciences*, pages 1–21, 2015.

[65] Stacy A Carolin, Kim M Cobb, Jean Lynch-Stieglitz, Jessica W Moerman, Judson W Partin, Syria Lejau, Jenny Malang, Brian Clark, Andrew A Tuen, and Jess F Adkins. Northern Borneo stalagmite records reveal West Pacific

hydroclimate across MIS 5 and 6. *Earth and Planetary Science Letters*, 439: 182–193, 2016.

[66] Julian P Sachs, Dirk Sachse, Rienk H Smittenberg, Zhaohui Zhang, David S Battisti, and Stjepko Golubic. Southward movement of the Pacific intertropical convergence zone AD 1400–1850. *Nature Geoscience*, 2(7):519–525, 2009.

[67] Rhawn F Denniston, Karl-Heinz Wyrwoll, Victor J Polyak, Josephine R Brown, Yemane Asmerom, Alan D Wanamaker, Zachary LaPointe, Rebecca Ellerbroek, Michael Barthelmes, Daniel Cleary, et al. A Stalagmite record of Holocene Indonesian–Australian summer monsoon variability from the Australian tropics. *Quaternary Science Reviews*, 78:155–168, 2013.

[68] L Araguás-Araguás, K Froehlich, and K Rozanski. Deuterium and oxygen-18 isotope composition of precipitation and atmospheric moisture. *Hydrological Processes*, 14(8):1341–1355, 2000.

[69] Stephen P Good, Derek V Mallia, John C Lin, and Gabriel J Bowen. Stable isotope analysis of precipitation samples obtained via crowdsourcing reveals the spatiotemporal evolution of Superstorm Sandy. *PloS one*, 9(3):e91117, 2014.

[70] NC Munksgaard, CM Wurster, A Bass, and MI Bird. Extreme short-term stable isotope variability revealed by continuous rainwater analysis. *Hydrological Processes*, 26(23):3630–3634, 2012.

[71] Sandrine Bony, Camille Risi, and Francoise Vimeux. Influence of convective processes on the isotopic composition (δ18O and δD) of precipitation and water vapor in the tropics: 1. Radiative-convective equilibrium and Tropical Ocean–Global Atmosphere–Coupled Ocean-Atmosphere Response Experiment (TOGA-COARE) simulations. *Journal of Geophysical Research: Atmospheres*, 113(D19), 2008.

[72] Guillaume Tremoy, Françoise Vimeux, Salifou Soumana, Ide Souley, Camille Risi, Guillaume Favreau, and Monique Oï. Clustering mesoscale convective systems with laser-based water vapor δ18O monitoring in Niamey (Niger). *Journal of Geophysical Research: Atmospheres*, 119(9):5079–5103, 2014.

[73] Hélène Celle-Jeanton, Roberto Gonfiantini, Yves Travi, and Bernard Sol. Oxygen-18 variations of rainwater during precipitation: application of the Rayleigh model to selected rainfalls in Southern France. *Journal of Hydrology*, 289(1):165–177, 2004.

[74] A. J. Troup. Variations in the upper tropospheric flow associated with the onset of the Australian summer monsoon. *Indian journal of meteorology and geophysics*, 12:217–230, 1961.

[75] JL McBride. Satellite observations of the southern hemisphere monsoon during Winter MONEX. *Tellus A*, 35(3):189–197, 1983.

[76] Jianrong Liu, Guobin Fu, Xianfang Song, Stephen P Charles, Yinghua Zhang, Dongmei Han, and Shiqin Wang. Stable isotopic compositions in Australian precipitation. *Journal of Geophysical Research: Atmospheres*, 115(D23), 2010.

[77] George J Huffman, David T Bolvin, Eric J Nelkin, David B Wolff, Robert F Adler, Guojun Gu, Yang Hong, Kenneth P Bowman, and Erich F Stocker. The TRMM multisatellite precipitation analysis (TMPA): Quasi-global, multiyear, combined-sensor precipitation estimates at fine scales. *J. Hydrometeor.*, 8(1): 38–55, 2007.

[78] B. Liebmann and C. A. Smith. Description of a Complete (Interpolated) Outgoing Longwave Radiation Dataset. *Bull. Amer. Meteor. Soc.*, 77:1275–1277, 1996.

[79] Robert F. Adler, George J. Huffman, Alfred Chang, Ralph Ferraro, Ping-Ping Xie, John Janowiak, Bruno Rudolf, Udo Schneider, Scott Curtis, David Bolvin,

Arnold Gruber, Joel Susskind, Philip Arkin, and Eric Nelkin. The Version-2 Global Precipitation Climatology Project (GPCP) Monthly Precipitation Analysis (1979–Present). *J. Hydrometeor.*, 4(6):1147–1167, 2015/01/19 2003. doi: 10.1175/1525-7541(2003)004⟨1147:TVGPCP⟩2.0.CO;2.

[80] R. R. Draxler and G. D. Hess. Description of the HYSPLIT 4 modeling system. NOAA Tech. Memo ERL ARL-224, NOAA Air Resources Laboratory, Silver Spring, 1997.

[81] Harmon Craig. Variations in Meteoric Waters. *Science, New Series*, 133(3465): 1702–1703, May 1961.

[82] BoM. Monthly Weather Review. Technical report, Northern Territory Climate Services Centre, 2013.

[83] BoM. Soundings. http://www.bom.gov.au/aviation/observations/aerological-diagrams/, January-April 2013. URL `http://www.bom.gov.au/aviation/observations/aerological-diagrams/`.

[84] Amy Benoit Frappier, Dork Sahagian, Scott J Carpenter, Luis A González, and Brian R Frappier. Stalagmite stable isotope record of recent tropical cyclone events. *Geology*, 35(2):111–114, 2007.

[85] Jordahna Haig, Jonathan Nott, and Gert-Jan Reichart. Australian tropical cyclone activity lower than at any time over the past 550–1,500 years. *Nature*, 505(7485):667, 2014.

[86] James Robert Lawrence, Stanley David Gedzelman, Darielle Dexheimer, Hye-Khung Cho, Gordon D Carrie, Robert Gasparini, Casey R Anderson, Kenneth P Bowman, and Mike I Biggerstaff. Stable isotopic composition of water vapor in the tropics. *Journal of Geophysical Research: Atmospheres (1984–2012)*, 109(D6), 2004.

[87] P Treble, W Budd, P Hope, and P Rustomji. Synoptic-scale climate patterns

associated with rainfall δ18O in southern Australia. *Journal of Hydrology*, 302 (1-4):270282, 2005. ISSN 0022-1694. doi: 10.1016/j.jhydrol.2004.07.003.

[88] José L Corrales, Ricardo Sánchez-Murillo, Germain Esquivel-Hernández, Esteban Herrera, and Jan Boll. Tracking the water fingerprints of Cocos Island: a stable isotope analysis of precipitation, surface water, and groundwater. *Revista de Biología Tropical/International Journal of Tropical Biology and Conservation*, 64(1):105–120, 2016.

[89] Lucas A. Cernusak and Nathan B. English. Beyond tree-ring widths: stable isotopes sharpen the focus on climate responses of temperate forest trees. *Tree Physiology*, 35(1):1–3, 2015.

[90] Wasyl Drosdowsky. Variability of the Australian summer monsoon at Darwin: 1957–1992. *Journal of Climate*, 9(1):85–96, 1996.

[91] Mick Pope, Christian Jakob, and Michael J Reeder. Regimes of the north Australian wet season. *Journal of Climate*, 22(24):6699–6715, 2009.

[92] Alain Protat, Julien Delanoë, PT May, J Haynes, C Jakob, E O'Connor, M Pope, and MC Wheeler. The variability of tropical ice cloud properties as a function of the large-scale context from ground-based radar-lidar observations over Darwin, Australia. *Atmospheric Chemistry and Physics*, 11(16):8363–8384, 2011.

[93] Vickal V Kumar, Alain Protat, Peter T May, Christian Jakob, Guillaume Penide, Sushil Kumar, and Laura Davies. On the effects of large-scale environment and surface types on convective cloud characteristics over Darwin, Australia. *Monthly Weather Review*, 141(4):1358–1374, 2013.

[94] Guillaume Penide, Vickal V Kumar, Alain Protat, and Peter T May. Statistics of drop size distribution parameters and rain rates for stratiform and convective precipitation during the North Australian wet season. *Monthly Weather Review*, 141(9):3222–3237, 2013.

[95] Gareth J Berry and Michael J Reeder. The Dynamics of Australian Monsoon Bursts. *Journal of the Atmospheric Sciences*, 73(1):55–69, 2016.

[96] Sugata Narsey, Michael J Reeder, Duncan Ackerley, and Christian Jakob. A Midlatitude Influence on Australian Monsoon Bursts. *Journal of Climate*, 30 (14):5377–5393, 2017.

[97] R Suppiah. The Australian summer monsoon: a review. *Progress in Physical Geography*, 16(3):283–318, 1992.

[98] David B Wolff, David A Marks, and Walter A Petersen. General application of the relative calibration adjustment (RCA) technique for monitoring and correcting radar reflectivity calibration. *Journal of Atmospheric and Oceanic Technology*, 32(3):496–506, 2015.

[99] Robert A Warren, Alain Protat, Steven T Siems, Hamish A Ramsay, Valentin Louf, Michael J Manton, and Thomas A Kane. Calibrating ground-based radars against TRMM and GPM. *Journal of Atmospheric and Oceanic Technology*, 35(2):323–346, 2018.

[100] Vickal V Kumar, Christian Jakob, Alain Protat, Peter T May, and Laura Davies. The four cumulus cloud modes and their progression during rainfall events: AC-band polarimetric radar perspective. *Journal of Geophysical Research: Atmospheres*, 118(15):8375–8389, 2013.

[101] Matthias Steiner, Robert A Houze Jr, and Sandra E Yuter. Climatological characterization of three-dimensional storm structure from operational radar and rain gauge data. *Journal of Applied Meteorology*, 34(9):1978–2007, 1995.

[102] Michael Schulz and Manfred Mudelsee. REDFIT: estimating red-noise spectra directly from unevenly spaced paleoclimatic time series. *Computers & Geosciences*, 28(3):421–426, 2002.

[103] BoM. Weather and Climate data online. URL `http://www.bom.gov.au/climate/data/index.shtml`.

[104] Harry H Hendon and Brant Liebmann. The intraseasonal (30–50 day) oscillation of the Australian summer monsoon. *Journal of the Atmospheric Sciences*, 47(24):2909–2924, 1990.

[105] Brian Mapes and Robert A Houze. An integrated view of the 1987 Australian monsoon and its mesoscale convective systems. I: Horizontal structure. *Quarterly Journal of the Royal Meteorological Society*, 118(507):927–963, 1992.

[106] Robert A Houze Jr. Stratiform precipitation in regions of convection: A meteorological paradox? *Bulletin of the American Meteorological Society*, 78 (10):2179–2196, 1997.

[107] Jonathan Nott, Jordahna Haig, Helen Neil, and David Gillieson. Greater frequency variability of landfalling tropical cyclones at centennial compared to seasonal and decadal scales. *Earth and Planetary Science Letters*, 255(3-4): 367–372, 2007.

[108] Zheng-Hua Li, Nicole Labbé, Steven G Driese, and Henri D Grissino-Mayer. Micro-scale analysis of tree-ring δ18O and δ13C on α-cellulose spline reveals high-resolution intra-annual climate variability and tropical cyclone activity. *Chemical Geology*, 284(1-2):138–147, 2011.

[109] Dana L Miller, Claudia I Mora, Henri D Grissino-Mayer, Cary J Mock, Maria E Uhle, and Zachary Sharp. Tree-ring isotope records of tropical cyclone activity. *Proceedings of the National Academy of Sciences*, 103(39):14294–14297, 2006.

[110] Robert James Lawrence and David Stanley Gedzelman. Low stable isotope ratios of tropical cyclone rains. *Geophysical Research Letters*, 23(5):527–530, 1996.

[111] James R Lawrence. Isotopic spikes from tropical cyclones in surface waters: opportunities in hydrology and paleoclimatology. *Chemical Geology*, 144(1-2): 153–160, 1998.

[112] James R Lawrence, Stanley David Gedzelman, John Gamache, and Michael Black. Stable isotope ratios: hurricane Olivia. *Journal of Atmospheric Chemistry*, 41(1):67–82, 2002.

[113] H Fudeyasu, Kimpei Ichiyanagi, A Sugimoto, Kei Yoshimura, A Ueta, MD Yamanaka, and K Ozawa. Isotope ratios of precipitation and water vapor observed in Typhoon Shanshan. *Journal of Geophysical Research: Atmospheres*, 113(D12), 2008.

[114] Kevin E Trenberth, Christopher A Davis, and John Fasullo. Water and energy budgets of hurricanes: Case studies of Ivan and Katrina. *Journal of Geophysical Research: Atmospheres*, 112(D23), 2007.

[115] Stanley Gedzelman, James Lawrence, John Gamache, Michael Black, Edward Hindman, Robert Black, Jason Dunion, Hugh Willoughby, and Xiaoping Zhang. Probing hurricanes with stable isotopes of rain and water vapor. *Monthly Weather Review*, 131(6):1112–1127, 2003.

[116] Luis Gimeno, Andreas Stohl, Ricardo M Trigo, Francina Dominguez, Kei Yoshimura, Lisan Yu, Anita Drumond, Ana María Durán-Quesada, and Raquel Nieto. Oceanic and terrestrial sources of continental precipitation. *Reviews of Geophysics*, 50(4), 2012.

[117] BoM. http://www.bom.gov.au/cyclone/. Accessed April 2014, November 2014.

[118] JTWC. https://www.metoc.navy.mil/jtwc/jtwc.html?southern-hemisphere. Accessed April 2014, November 2014.

[119] TRMM. http://trmm.gsfc.nasa.gov/. Accessed April 2014, November 2014.

[120] BoM. http://www.bom.gov.au/products/IDR193.loop.shtml. Accessed April 2014, November 2014.

[121] Picarro. http://www.picarro.com. Accessed November 2014, November 2014.

[122] AIMS. http://data.aims.gov.au/aimsrtds/station.xhtml?station=1166. Accessed April 2014, November 2014.

[123] N Kurita, BD Newman, LJ Araguas-Araguas, and P Aggarwal. Evaluation of continuous water vapor [delta] D and [delta] 18O measurements by off-axis integrated cavity output spectroscopy. *Atmospheric Measurement Techniques*, 5(8):2069, 2012.

[124] Ayataka Ebita, Shinya Kobayashi, Yukinari Ota, Masami Moriya, Ryoji Kumabe, Kazutoshi Onogi, Yayoi Harada, Soichiro Yasui, Kengo Miyaoka, Kiyotoshi Takahashi, et al. The Japanese 55-year reanalysis JRA-55: an interim report. *Sola*, 7:149–152, 2011.

[125] NOAA. https://ready.arl.noaa.gov/gdas1.php. Accessed July 2014, November 2014.

[126] BoM. http://www.bom.gov.au/qld/observations/qldall.shtml. Accessed April 2014, November 2014.

[127] Manuel Lonfat, Frank D Marks Jr, and Shuyi S Chen. Precipitation distribution in tropical cyclones using the Tropical Rainfall Measuring Mission (TRMM) microwave imager: A global perspective. *Monthly Weather Review*, 132(7):1645–1660, 2004.

[128] Dieter H Ehhalt and H Göte Östlund. Deuterium in Hurricane Faith 1966: preliminary results. *Journal of Geophysical Research*, 75(12):2323–2327, 1970.

[129] Juske Horita and David J Wesolowski. Liquid-vapor fractionation of oxygen and hydrogen isotopes of water from the freezing to the critical temperature. *Geochimica et Cosmochimica Acta*, 58(16):3425–3437, 1994.

[130] Jean Jouzel, Gilles Delaygue, Amaëlle Landais, Valérie Masson-Delmotte, Camille Risi, and Françoise Vimeux. Water isotopes as tools to document oceanic sources of precipitation. *Water Resources Research*, 49(11):7469–7486, 2013.

[131] Joel R Gat. Oxygen and hydrogen isotopes in the hydrologic cycle. *Annual Review of Earth and Planetary Sciences*, 24(1):225–262, 1996.

[132] Jung-Eun Lee and Inez Fung. 'Amount effect' of water isotopes and quantitative analysis of post-condensation processes. *Hydrological Processes*, 22(1): 1–8, 2008.

[133] Ingo Heinrich, Kathrin Weidner, Gerhard Helle, Heinz Vos, and John CG Banks. Hydroclimatic variation in Far North Queensland since 1860 inferred from tree rings. *Palaeogeography, Palaeoclimatology, Palaeoecology*, 270(1-2): 116–127, 2008.

[134] FM Peerdeman, PJ Davies, AR Chivas, et al. The stable oxygen isotope signal in shallow-water, upper-slope sediments off the Great Barrier Reef (Hole 820A). In *Proceedings of the Ocean Drilling Program, Scientific Results*, volume 133, pages 163–173, 1993.

[135] Arnold Peter Kershaw. Climatic change and Aboriginal burning in north-east Australia during the last two glacial/interglacial cycles. *Nature*, 322(6074):47, 1986.

[136] V Faghihi, HAJ Meijer, and M Gröning. A thoroughly validated spreadsheet for calculating isotopic abundances (2H, 17O, 18O) for mixtures of waters with different isotopic compositions. *Rapid Communications in Mass Spectrometry*, 29(15):1351–1356, 2015.

[137] Yannick Garcin, Valérie F Schwab, Gerd Gleixner, Ansgar Kahmen, Gilbert Todou, Olivier Séné, Jean-Michel Onana, Gaston Achoundong, and Dirk Sachse. Hydrogen isotope ratios of lacustrine sedimentary n-alkanes as proxies of tropical African hydrology: insights from a calibration transect across Cameroon. *Geochimica et Cosmochimica Acta*, 79:106–126, 2012.

[138] Michael L Griffiths, Russell Neil Drysdale, MK Gagan, J-x Zhao, LK Ayliffe, John Charles Hellstrom, WS Hantoro, Silvia Frisia, Y-x Feng, Ian Cartwright,

et al. Increasing Australian–Indonesian monsoon rainfall linked to early Holocene sea-level rise. *Nature Geoscience*, 2(9):636, 2009.

[139] Sang Chen, Sharon S Hoffmann, David C Lund, Kim M Cobb, Julien Emile-Geay, and Jess F Adkins. A high-resolution speleothem record of western equatorial Pacific rainfall: Implications for Holocene ENSO evolution. *Earth and Planetary Science Letters*, 442:61–71, 2016.

[140] Jennifer B Wurtzel, Nerilie J Abram, Sophie C Lewis, Petra Bajo, John C Hellstrom, Ulrike Troitzsch, and David Heslop. Tropical Indo-Pacific hydroclimate response to North Atlantic forcing during the last deglaciation as recorded by a speleothem from Sumatra, Indonesia. *Earth and Planetary Science Letters*, 492:264–278, 2018.

[141] Rhawn F Denniston, Yemane Asmerom, Victor J Polyak, AD Wanamaker Jr, Caroline C Ummenhofer, William F Humphreys, John Cugley, David Woods, and Stephanie Lucker. Decoupling of monsoon activity across the northern and southern Indo-Pacific during the Late Glacial. *Quaternary Science Reviews*, 176:101–105, 2017.

[142] Rhawn F Denniston, Yemane Asmerom, Matthew Lachniet, Victor J Polyak, Pandora Hope, Ni An, Kristyn Rodzinyak, and William F Humphreys. A Last Glacial Maximum through middle Holocene stalagmite record of coastal Western Australia climate. *Quaternary Science Reviews*, 77:101–112, 2013.

[143] Linda K Ayliffe, Michael K Gagan, Jian-xin Zhao, Russell N Drysdale, John C Hellstrom, Wahyoe S Hantoro, Michael L Griffiths, Heather Scott-Gagan, Emma St Pierre, Joan A Cowley, et al. Rapid interhemispheric climate links via the Australasian monsoon during the last deglaciation. *Nature communications*, 4:2908, 2013.

[144] James Shulmeister and Brian G Lees. Pollen evidence from tropical Australia

for the onset of an ENSO-dominated climate at c. 4000 BP. *The Holocene*, 5 (1):10–18, 1995.

[145] Hamish McGowan, Samuel Marx, Patrick Moss, and Andrew Hammond. Evidence of ENSO mega-drought triggered collapse of prehistory Aboriginal society in northwest Australia. *Geophysical Research Letters*, 39(22), 2012.

[146] Emily Field, Hamish A McGowan, Patrick T Moss, and Samuel K Marx. A late Quaternary record of monsoon variability in the northwest Kimberley, Australia. *Quaternary International*, 449:119–135, 2017.

[147] Karl-Heinz Wyrwoll and Gifford H Miller. Initiation of the Australian summer monsoon 14,000 years ago. *Quaternary International*, 83:119–128, 2001.

[148] R Wasson, P Bayliss, and S Clelland. River flow and climate in the ‘top end’of Australia for the last 1000 years, and the Asian-Australian monsoon. In *Kakadu National Park Landscape Symposia Series*, volume 2009, pages 15–31, 2007.

[149] Jan-Hendrik May, Frank Preusser, and Luke Andrew Gliganic. Refining late Quaternary plunge pool chronologies in Australia’s monsoonal’Top End’. *Quaternary Geochronology*, 30:328–333, 2015.

[150] Takeshige Ishiwa, Yusuke Yokoyama, Lars Reuning, Cecilia M McHugh, David De Vleeschouwer, and Stephen J Gallagher. Australian Summer Monsoon variability in the past 14,000 years revealed by IODP Expedition 356 sediments. *Progress in Earth and Planetary Science*, 6(1):17, 2019.

[151] Wolfgang Kuhnt, Ann Holbourn, Jian Xu, Bradley Opdyke, Patrick De Deckker, Ursula Röhl, and Manfred Mudelsee. Southern Hemisphere control on Australian monsoon variability during the late deglaciation and Holocene. *Nature communications*, 6(1):1–7, 2015.

[152] Mahyar Mohtadi, Delia W Oppo, Stephan Steinke, Jan-Berend W Stuut, Ricardo De Pol-Holz, Dierk Hebbeln, and Andreas Lückge. Glacial to Holocene

swings of the Australian–Indonesian monsoon. *Nature Geoscience*, 4(8):540–544, 2011.

[153] Stephan Steinke, Mahyar Mohtadi, Matthias Prange, Vidya Varma, Daniela Pittauerova, and Helmut W Fischer. Mid-to late-Holocene Australian–Indonesian summer monsoon variability. *Quaternary Science Reviews*, 93: 142–154, 2014.

[154] Yanming Ruan, Mahyar Mohtadi, Sander van der Kaars, Lydie Dupont, Dierk Hebbeln, Ellen Hopmans, Stefan Schouten, and Enno Schefuß. Evolution of Fire Regimes in East Java Since the Last Glacial. In *29th International Meeting on Organic Geochemistry*, volume 2019, pages 1–2. European Association of Geoscientists & Engineers, 2019.

[155] Cassandra Rowe, Michael Brand, Lindsay B Hutley, Christopher Wurster, Costijn Zwart, Vlad Levchenko, and Michael Bird. Holocene savanna dynamics in the seasonal tropics of northern Australia. *Review of Palaeobotany and Palynology*, 267:17–31, 2019.

[156] J Gentilli. Dynamics of the Australian troposphere. *World Survey of Climatology*, pages 53–118, 1971.

[157] Murray C Peel, Brian L Finlayson, and Thomas A McMahon. Updated world map of the Köppen-Geiger climate classification. *Hydrology and earth system sciences discussions*, 4(2):439–473, 2007.

[158] Rosemary T Bush and Francesca A McInerney. Leaf wax n-alkane distributions in and across modern plants: implications for paleoecology and chemotaxonomy. *Geochimica et Cosmochimica Acta*, 117:161–179, 2013.

[159] Jinzhao Liu and Zhisheng An. A hierarchical framework for disentangling different controls on leaf wax δDn-alkane values in terrestrial higher plants. *Quaternary Science Reviews*, 201:409–417, 2018.

[160] Ines Mügler, Dirk Sachse, Martin Werner, Baiqing Xu, Guangjian Wu, Tandong Yao, and Gerd Gleixner. Effect of lake evaporation on δD values of lacustrine n-alkanes: A comparison of Nam Co (Tibetan Plateau) and Holzmaar (Germany). *Organic Geochemistry*, 39(6):711–729, 2008.

[161] Weiguo Liu, Huanye Wang, Qin Leng, Hu Liu, Huan Zhang, Meng Xing, Yunning Cao, and Hong Yang. Hydrogen isotopic compositions along a precipitation gradient of Chinese Loess Plateau: Critical roles of precipitation/evaporation and vegetation change as controls for leaf wax δD. *Chemical Geology*, 528:119278, 2019.

[162] Ansgar Kahmen, Bernd Hoffmann, Enno Schefuß, Stefan K Arndt, Lucas A Cernusak, Jason B West, and Dirk Sachse. Leaf water deuterium enrichment shapes leaf wax n-alkane δD values of angiosperm plants II: Observational evidence and global implications. *Geochimica et Cosmochimica Acta*, 111: 50–63, 2013.

[163] Yangyang Li, Shiling Yang, Pan Luo, and Shangfa Xiong. Aridity-controlled hydrogen isotope fractionation between soil n-alkanes and precipitation in China. *Organic Geochemistry*, 133:53–64, 2019.

[164] Suzanne E Hollins, Catherine E Hughes, Jagoda Crawford, Dioni I Cendón, and Karina M Meredith. Rainfall isotope variations over the Australian continent–Implications for hydrology and isoscape applications. *Science of the Total Environment*, 645:630–645, 2018.

[165] Alan N Williams, Sean Ulm, Tom Sapienza, Stephen Lewis, and Chris SM Turney. Sea-level change and demography during the last glacial termination and early Holocene across the Australian continent. *Quaternary Science Reviews*, 182:144–154, 2018.

[166] Da Shao, Yanjun Mei, Zhongkang Yang, Yuhong Wang, Wenqing Yang, Yuesong Gao, Lianjiao Yang, and Liguang Sun. Holocene ENSO variabil-

ity in the South China Sea recorded by high-resolution oxygen isotope records from the shells of Tridacna spp. *Scientific reports*, 10(1):1–10, 2020.

[167] Stephen E Lewis, Craig R Sloss, Colin V Murray-Wallace, Colin D Woodroffe, and Scott G Smithers. Post-glacial sea-level changes around the Australian margin: a review. *Quaternary Science Reviews*, 74:115–138, 2013.

[168] HV McGregor, Mathew J Fischer, MK Gagan, David Fink, Steven J Phipps, H Wong, and CD Woodroffe. A weak El Niño/Southern Oscillation with delayed seasonal growth around 4,300 years ago. *Nature Geoscience*, 6(11): 949, 2013.

[169] ND Leonard, KJ Welsh, JM Lough, Y-x Feng, JM Pandolfi, TR Clark, and J-x Zhao. Evidence of reduced mid-Holocene ENSO variance on the Great Barrier Reef, Australia. *Paleoceanography*, 31(9):1248–1260, 2016.

[170] Sarah M White, A Christina Ravelo, and Pratigya J Polissar. Dampened El Niño in the Early and Mid-Holocene Due To Insolation-Forced Warming/Deepening of the Thermocline. *Geophysical Research Letters*, 45(1):316–326, 2018.

[171] Colin D Woodroffe and Michael K Gagan. Coral microatolls from the central Pacific record late Holocene El Nino. *Geophysical Research Letters*, 27(10): 1511–1514, 2000.

[172] C Barr, J Tibby, MJ Leng, JJ Tyler, ACG Henderson, JT Overpeck, GL Simpson, JE Cole, SJ Phipps, JC Marshall, et al. Holocene el Niño–southern Oscillation variability reflected in subtropical Australian precipitation. *Scientific reports*, 9(1):1627, 2019.

[173] Anthony J Forsyth, Jonathan Nott, and Mark D Bateman. Beach ridge plain evidence of a variable late-Holocene tropical cyclone climate, North Queensland, Australia. *Palaeogeography, Palaeoclimatology, Palaeoecology*, 297(3-4): 707–716, 2010.

[174] J Gentilli. Holocene Climates of the Northern Australian Region. *Journal of Coastal Research*, pages 119–121, 1995.

[175] Richard A Dare, Noel E Davidson, and John L McBride. Tropical cyclone contribution to rainfall over Australia. *Monthly Weather Review*, 140(11): 3606–3619, 2012.

[176] David Gallego, Ricardo García-Herrera, Cristina Peña-Ortiz, and Pedro Ribera. The steady enhancement of the Australian Summer Monsoon in the last 200 years. *Scientific reports*, 7(1):16166, 2017.

[177] Jennifer L Catto, Christian Jakob, and Neville Nicholls. The influence of changes in synoptic regimes on north Australian wet season rainfall trends. *Journal of Geophysical Research: Atmospheres*, 117(D10), 2012.

[178] Michael J Murphy Jr, Steven T Siems, and Michael J Manton. Regional variation in the wet season of northern Australia. *Monthly Weather Review*, 144(12):4941–4962, 2016.

[179] Cassandra Denise Wilks Rogers and Jason Beringer. Describing rainfall in northern Australia using multiple climate indices. *Biogeosciences*, 14(3):597–615, 2017.

[180] Roohi PS Ghelani, Eric CJ Oliver, Neil J Holbrook, Matthew C Wheeler, and Philip J Klotzbach. Joint Modulation of Intraseasonal Rainfall in Tropical Australia by the Madden-Julian Oscillation and El Niño-Southern Oscillation. *Geophysical Research Letters*, 44(20):10–754, 2017.

[181] CJC Reason. Variability in rainfall over tropical Australia during summer and relationships with the Bilybara High. *Theoretical and applied climatology*, 132 (1-2):313–326, 2018.

[182] James Robert Lawrence, Stanley David Gedzelman, Xiaoping Zhang, and Robert Arnold. Stable isotope ratios of rain and vapor in 1995 hurricanes. *Journal of Geophysical Research: Atmospheres*, 103(D10):11381–11400, 1998.

[183] Niels C Munksgaard, Naoyuki Kurita, Ricardo Sánchez-Murillo, Nasir Ahmed, Luis Araguas, Dagnachew L Balachew, Michael I Bird, Supriyo Chakraborty, Nguyen Kien Chinh, Kim M Cobb, et al. Data Descriptor: Daily observations of stable isotope ratios of rainfall in the tropics. *Scientific reports*, 9(1):1–7, 2019.